Politecnico di Torino

FACOLTÀ DI INGEGNERIA
Corso di Laurea Magistrale in Ingegneria Aerospaziale

TESI DI LAUREA

Optimal Control of Low-Thrust Satellite Formation-Flying Reconfiguration using a LQR

considering Collision Avoidance and Fuel Balancing issues.

Candidato:
Matteo Paolo Clemente

Relatore:
Prof.ssa Manuela Battipede

Correlatore:
Prof. Jaemyung Ahn

Sessione di Laurea: Aprile 2020

Contents

1 Introduction **4**
1.1 Introduction to Formation Flying for small satellites 4
1.1.1 General introduction 4
1.1.2 Formation Flying methods classification 5
1.1.3 Formation Flying Control Techniques 6
1.2 Thesis workflow overview 7

2 Mean Relative Orbital Elements (ROE) System for Formation Relative Motion **9**
2.1 Introduction to ROE State Transition Matrix 9
2.1.1 Introduction 9
2.1.2 State Vector definition 10
2.1.3 Eccentricity/Inclination vector separation 11
2.2 Quasi-Nonsingular State Transition Matrix formulation 15
2.2.1 Derivation Methodology 15
2.2.2 Relative motion due to STM 18
2.3 Control Matrix 20
2.3.1 Definition 20
2.3.2 ΔV lower bound for impulsive maneuvers 21

3 Linear Quadratic Regulator Overview and Implementation **23**
3.1 Theoretical Overview 23
3.1.1 Introduction to Continuous-Time LQR 23
3.1.2 State and Costate Equations 24
3.1.3 Finite-Horizon derivation methodology 24
3.1.4 Infinite-Horizon derivation methodology 25
3.1.5 Controllability Property 25
3.2 Implementation of LQR for ROE system control 26
3.2.1 Controllability assessment of ROE system 26
3.2.2 Software Implementation 27
3.3 Model testing and results 29
3.3.1 Input Data 29
3.3.2 Results 31

4 Collision Avoidance using Artificial Potential functions **36**
4.1 Mathematical Overview 36
4.1.1 Introduction 36
4.1.2 Reference Governor 36
4.1.3 Reference Governor model testing and results 37
4.1.4 Minimum distance using Eccentricity/Inclination vector separation 41
4.1.5 Artificial Potential Field for Collision Avoidance 42

4.2 Scenario for Collision Avoidance potential field testing . . . 43
4.2.1 Input Data . . . 43
4.2.2 Results . . . 45

5 Fuel Balance between satellites **52**
5.1 Fuel Balance exploiting the $\boldsymbol{R}$ matrix . . . 52
5.1.1 Basic Idea . . . 52
5.1.2 Algorithm Implementation . . . 52
5.1.3 Algorithm testing and results . . . 53
5.2 Fuel Balance through smart mission and maneuver planning . . . 60
5.2.1 Scenario 1: TanDEM-X like mission . . . 60
5.2.2 Scenario 2: Deployment of a 4-sats formation with along-track separation 67
5.2.3 Scenario 3: TanDEM-X like mission with initial fuel unbalance . . . 72

6 Model Validation using GMAT **78**
6.1 Chapter Overview . . . 78
6.1.1 Introduction . . . 78
6.1.2 Validation Procedure . . . 78
6.2 Scenario for Model Validation . . . 79
6.2.1 Scenario Introduction . . . 79
6.2.2 Model Results . . . 81
6.2.3 GMAT Simulation . . . 86
6.2.4 Conclusion . . . 87

7 Conclusions and future work **88**
7.1 Conclusions about the Model . . . 88
7.2 Future Work . . . 89

Chapter 1

Introduction

1.1 Introduction to Formation Flying for small satellites

1.1.1 General introduction

In the last century, as a result of the so-called "space race", humankind successfully started a new era of opportunities and discoveries, giving a great contribution to scientific and social progress.
Nowadays, space technologies and applications have brought many innovations in a large variety of fields, from scientific to commercial ones. As of October 2019, approximately 5290 satellites are orbiting Earth [1], providing services and applications related to communications, navigation and positioning, meteorology, Earth observation and disaster monitoring, marine exploration, and other fields [2].
Most of these achievements are based on a single satellite, which is the most classical mission concept and also the main force in applications of satellites. Nevertheless, the quick development of space technology at the present days is leading towards two different *trends* [2]:

- Increasing the weight and size of a single satellite, making its structure and functions more complex at the same time.
- Employing small satellites with various structures and simple functions, coordinated to work together in order to replace the complexity of a single large satellite.

Multiple *small satellites* can be employed instead of a much bigger and more complex conventional satellite for a large amount of different applications, such as communication services and synthetic aperture radars [3, 4]. The advantage of using multiple small satellites instead of a single one is that a comparable operativity can be achieved, but with significantly enhanced flexibility and robustness [4].
Small satellites are universally classified into different categories based on their mass:

- *Miscrosatellites* in the range 10-500 kg
- *Nanosatellites* in the range 1-10 kg
- *Picosatellites* in the range 0.1-1 kg
- *Femtosatellites* less than 100 g

A class of standardized nanosatellites, called CubeSats [5], range in size from 1U (10x10x10 cm) to 6U (30x20x10 cm), weigh between 1 and 8 kg, and are usually launched using the standardized CubeSat deployment system called Poly Picosatellite Orbital Deployer (P-POD) [6]. This

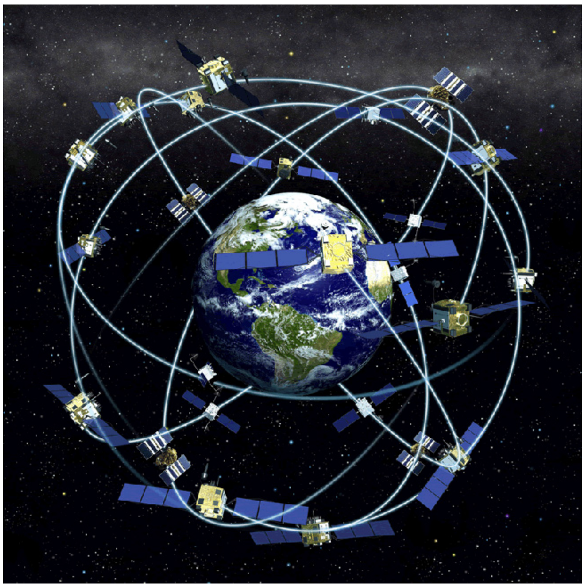

(a) GPS Constellation. Credits: *NASA*

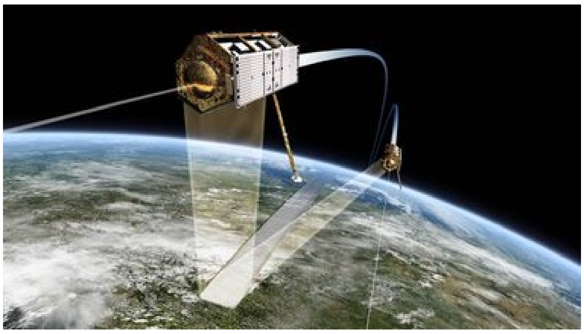

(b) TanDEM-X Formation. Credits: *DLR*

Figure 1.1: Comparison between a Constellation and a Formation.

kind of standardization makes the whole design-implementation-launch process esponentially faster and cheaper for a multitude of CubeSats than for a single complex satellite.
Multisatellite missions can be broadly divided into *two categories* [4]:

- *Formation Flying* missions, if at least one satellite tracks a desired state relative to another satellite, and its control law must depend upon the state of this satellite.
- *Constellation* missions, i.e. missions that don't satisfy the Formation Flying definition.

Constellation missions can also be subclassified into *controlled* constellation missions [4], where each satellite actively maintains its position (e.g. GPS), and *uncontrolled* constellation missions, where satellites have no active control over their position. Satellites in Formation Flying missions and controlled constellation missions must have active propulsion systems.

1.1.2 Formation Flying methods classification

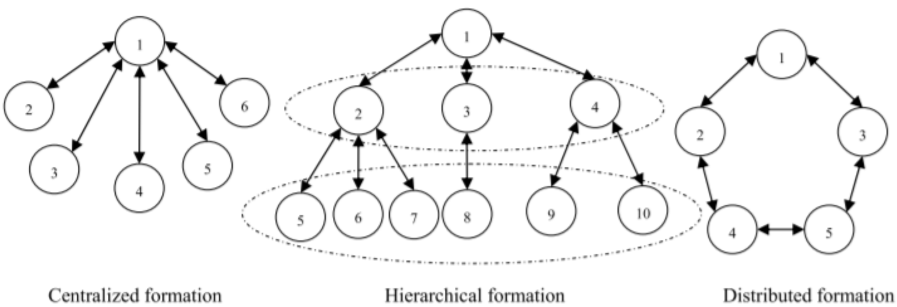

Figure 1.2: Architecture of Formation Flying coordination.[2]

The architecture of satellite formation coordination can be divided into centralized and decentralized systems in general [2], and also the decentralized structure can be subdivided into hierarchical and distributed ones, as shown in fig. 1.2.
In terms of different structures [7], formation control methods can be classified as:

- *Leader/Follower* (L/F) architecture, called also *Chief/deputy*, uses a hierarchical arrangement of individual spacecraft controllers that reduces formation control to individual tracking problems to a reference satellite. The Chief spacecraft can be single, multiple or virtual (fig. 1.3).

- *Virtual Structure*, the spacecraft behave as embedded in a larger, virtual rigid structure. In particular, the overall motion of the virtual structure and the constant, specified positions and orientations of spacecraft within it are used to generate reference trajectories for the spacecraft to track using individual spacecraft controllers.

- *Cyclic method*, a formation controller in the Cyclic architecture is formed by connecting individual spacecraft controllers. However, Cyclic differs from L/F in that the controller connections are not hierarchical but rather distributed (fig. 1.2).

- *Behavorial method*, combines the outputs of multiple controllers designed for achieving different and possibly competing behaviors. For example, an L/F algorithm plus a repulsive potential field centered on each spacecraft is a Behavioral algorithm consisting of maintain-formation and collision-avoidance behaviors.

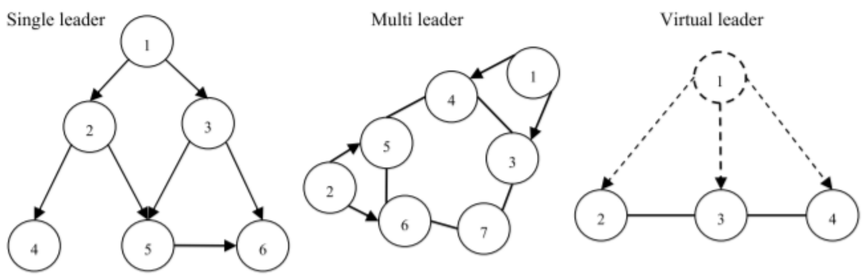

Figure 1.3: Leader/Follower architecture.[2]

1.1.3 Formation Flying Control Techniques

The first step in order to design a satellite controller for Formation Flying consists of choosing a *dynamic system* describing the relative motion of spacecraft in the formation. The most popular ones in literature are:

- *Hill-Clohessy-Wiltshire Equations*, describing the relative motion in the along-track, radial, out-of-plane space, valid only if the distance between the spacecraft is small [8]. This approach offers an easy implementation of the drag perturbance but on the other hand makes difficult the implementation of the Earth's oblateness effect.

- *Gauss' Variational Equations* (GVE), describing the variation of the 6 Keplerian orbital elements in time. This approach offers an easier implementation of the Earth's oblateness effect with respect to HCW equations, at least for the J_2 term (using Brouwer formulation [9]).

- *Mean Relative Orbital Elements* (ROE), deriving from GVEs and describing the relative motion in terms of mean relative orbital elements. This approach offers the same advantages as GVEs, but since it uses mean elements which are approximately constant during the mission time, allows the linearization of the model [10, 11].

Once the dynamic system describing the relative motion of the formation has been chosen, a control theory can be applied for the development of the tracking control law. Based on the chosen formation architecture and on the system, there are several viable options, here are some examples: H_∞ for L/F control [12], LQR control for linearized systems [13] and coupled with Deep Learning techniques to include nonlinearities [14], Lyapunov stability theory [15, 16], artificial potential fields (especially for collision avoidance algorithms [16]).

1.2 Thesis workflow overview

Low-thrust guidance and control of satellite Formation Flying relative motion is a field of study that is gaining more and more attention by researchers from every part of the world due to the recent development of more and more performing electric propulsion systems [17] and since future missions will follow the trend of miniaturizing spacecraft [18]. The challenge is to design a controller that must address limited thrusting and propellant capabilities while maintaining operational aspects, such as collision safety and time constraints [16].
For the scope of this work, a formation of satellites in LEO will be considered, employing thrusters capable of providing thrust in the order of μ-Newtons. In the first place the formation will include two spacecraft (deputy and chief), and it will be then expanded to more spacecraft once the model will have been validated. The workflow could be summarized as follows:

- Definition of a *dynamic model* for the relative motion of spacecraft in the formation;
- Definition and implementation of a *control strategy* in order to achieve an optimal (or near-optimal) tracking of the state space vector's desired configuration;
- Implementation of a method to guide the state space vector along a *reference trajectory* in order to guarantee collision avoidance (Potential Field Technique);
- Definition of a strategy to assure *fuel balance* of the whole formation, in order to avoid that one spacecraft would run out of fuel before the others;
- *Validation* of the model using an orbital propagation tool such GMAT.

See fig. 1.4 for further details.

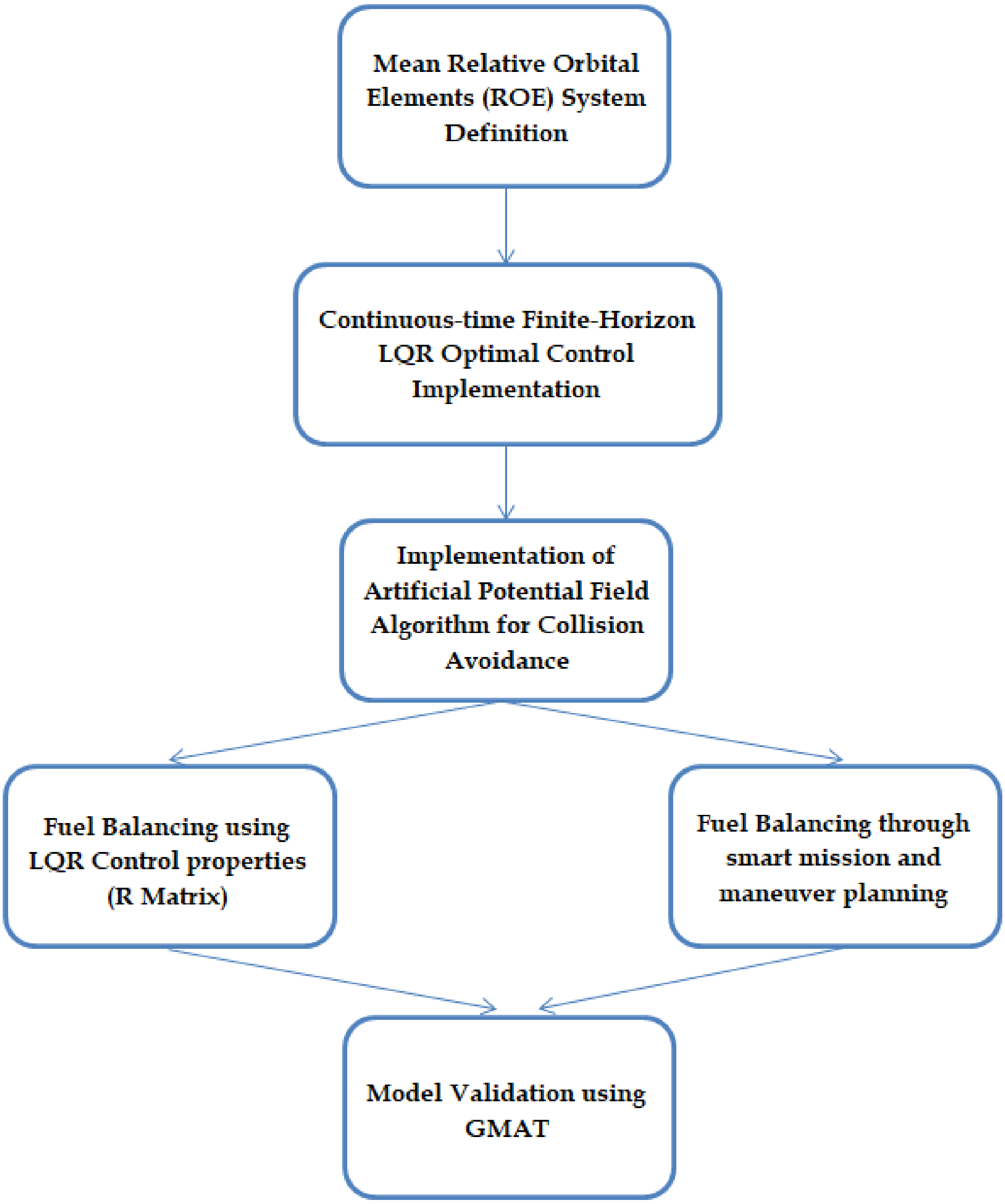

Figure 1.4: Work Flowchart

Chapter 2

Mean Relative Orbital Elements (ROE) System for Formation Relative Motion

2.1 Introduction to ROE State Transition Matrix

2.1.1 Introduction

As already said in the previous chapter, the first State Transition Matrix (STM) for spacecraft relative motion is the well-known *Hill-Clohessy-Wiltshire* STM for formations in unperturbed, near-circular orbits. The HCW STM uses a relative state defined from the relative position and velocity in a rotating frame centered about one of the spacecraft. This STM has been applied to several different missions in the past including Apollo, the Space Shuttle, and many others. The most popular models in literature involving HCW equations are the following ones [11]:

- Schweighart's and Izzo's [19, 20] models, including first-order secular effects of J_2 and differential drag;
- Yamanaka-Ankersen's [21] model, which includes no perturbations, but has been formulated for linear propagation of relative position and velocity in *eccentric orbits*.

It can be seen that there is no state-of-the-art model involving HCW equations suitable for both eccentric and perturbed orbits.
This is the reason why recent works have derived STMs using states defined as functions of the Keplerian orbit elements of the spacecraft, hereafter called *relative orbital elements* (ROE). These states vary slowly with time and allow astrodynamics tools such as the Gauss variational equations to be leveraged to include perturbations [11]. The contributions to this kind of model came from two different sources:

- The first model originates from a STM derived by Gim and Alfriend [22], which includes first-order secular and osculating J2 effects in arbitrarily eccentric orbits;
- The second model was derived by DAmico and includes the first-order secular effects of J2 on formations in near-circular orbits [10]. This model has then been expanded to include the effect of differential drag on the relative semi-major axis, and the effect of time-varying differential drag on the relative eccentricity vector [23].

For the purpose of this work, the model proposed by Koenig and D'Amico [11] will be exploited, which includes the following features:

- STMs for three mean ROE state definitions (singular, quasi-singular, non-singular) in order to guarantee model validity for different types of orbit (near-circular, eccentric);

- Includes first-order secular effects of J_2;
- Includes the effect of differential drag thanks to an accurate Density-Free Model (DFM) that takes in account an a-priori estimate of the time derivative of the relative semi-major axis $\delta\dot{a}_{drag}$, which can be estimated in flight, and requires the State Vector to be augmented.

2.1.2 State Vector definition

As it has been said in the previous section, there are three different formulations for the State Vector. Let a, e, i, Ω, ω, M denote the classical mean Keplerian orbital elements, for a formation of two spacecraft called Chief, subscript c, and Deputy, subscript d, we have [11]:

- *Singular State Vector*

$$\delta\overline{X}_s = \begin{pmatrix} \delta a \\ \delta\lambda \\ \delta e_x \\ \delta e_y \\ \delta i_x \\ \delta i_y \end{pmatrix} = \begin{pmatrix} \frac{a_d - a_c}{a_c} \\ M_d - M_c \\ e_d - e_c \\ \omega_d - \omega_c \\ i_d - i_c \\ \Omega_d - \Omega_c \end{pmatrix} \tag{2.1}$$

  It is not uniquely defined when either spacecraft is in a circular or equatorial orbit.

- *Quasi-Nonsingular State Vector*

$$\delta\overline{X}_{qns} = \begin{pmatrix} \delta a \\ \delta\lambda \\ \delta e_x \\ \delta e_y \\ \delta i_x \\ \delta i_y \end{pmatrix} = \begin{pmatrix} \frac{a_d - a_c}{a_c} \\ (M_d + \omega_d) - (M_c + \omega_c) + (\Omega_d - \Omega_c)\cos i_c \\ e_d \cos\omega_d - e_c \cos\omega_c \\ e_d \sin\omega_d - e_c \sin\omega_c \\ i_d - i_c \\ (\Omega_d - \Omega_c)\sin i_c \end{pmatrix} \tag{2.2}$$

  The quasi-nonsingular state is not unique when the deputy is in an equatorial orbit.

- *Nonsingular State Vector*

$$\delta\overline{X}_{ns} = \begin{pmatrix} \delta a \\ \delta\lambda \\ \delta e_x^\star \\ \delta e_y^\star \\ \delta i_x^\star \\ \delta i_y^\star \end{pmatrix} = \begin{pmatrix} \frac{a_d - a_c}{a_c} \\ (M_d + \omega_d + \Omega_d) - (M_c + \omega_c + \Omega_c) \\ e_d \cos(\omega_d + \Omega_d) - e_c \cos(\omega_c + \Omega_c) \\ e_d \sin(\omega_d + \Omega_d) - e_c \sin(\omega_c + \Omega_c) \\ \tan\frac{i_d}{2}\cos\Omega_d - \tan\frac{i_c}{2}\cos\Omega_c \\ \tan\frac{i_d}{2}\sin\Omega_d - \tan\frac{i_c}{2}\sin\Omega_c \end{pmatrix} \tag{2.3}$$

  The nonsingular state is uniquely defined for all possible chief and deputy orbits.

For the purpose of this work, since almost none spacecraft has an equatorial orbit in LEO, the quasi-nonsingular state vector represents the most suitable one to the problem.
The quasi-nonsingular state is identical to D'Amicos ROE [10], whose main advantage is that they provide insight into passive safety and stability for Formation Flying design in a simple manner using eccentricity/inclination vector separation that will be discussed in the next section.

2.1.3 Eccentricity/Inclination vector separation

The *eccentricity/inclination vector separation* methodology has been initially developed for safe collocation of geostationary satellites, by Eckstein et al. [24], and then exploited and rearranged by Montenbruck [25] for Formation Flying proximity operations design and control.
Eccentricity/Inclination vector separation is a powerful methodology because it can be used to completely describe the relative motion of spacecraft flying in close formations. In the following mathematical formulation, the orbital parameters a, e, i, Ω, ω, M will be referred to an ECI (Earth Centered Inertial) coordinate frame, while the relative motion will be studied in a Radial-Tangential-Normal coordinate frame. The RTN frame (fig. 2.7) is centered on the Chief spacecraft and has the following orthogonal axes:

- R, aligned to the radial vector joining the Chief with Earth's Center, pointing towards space;
- T, tangential to the Chief's orbit, same direction as the velocity vector;
- N, normal to the orbital plane, completing the orthonormal frame.

The relative motion of spacecraft 2 (Deputy) with respect to spacecraft 1 (Chief) can be expressed in the Chief-centered RTN frame as:

$$\Delta\overline{r} = \overline{r}_2 - \overline{r}_1 = \Delta r_R \overline{e}_R + \Delta r_T \overline{e}_T + \Delta r_N \overline{e}_N \tag{2.4}$$

In contrast to an elaborate numerical integration of the orbit followed by a subsequent differencing of individual trajectories, the equation of motion for the two-body problem can directly be differenced [25]. Two assumptions are used to derive an appropriate relative motion model:

- First, the spacecraft are assumed to fly in near-circular orbits (i.e., $e \ll 1$);
- Second, they are taken sufficiently close to each other to justify the linearization of the equations of relative motion.

As a consequence, the in-plane ($\overline{e}_R$, $\overline{e}_T$) and out-of-plane ($\overline{e}_N$) relative motions are decoupled and can be expressed separately.

Relative Inclination vector and out-of-plane motion

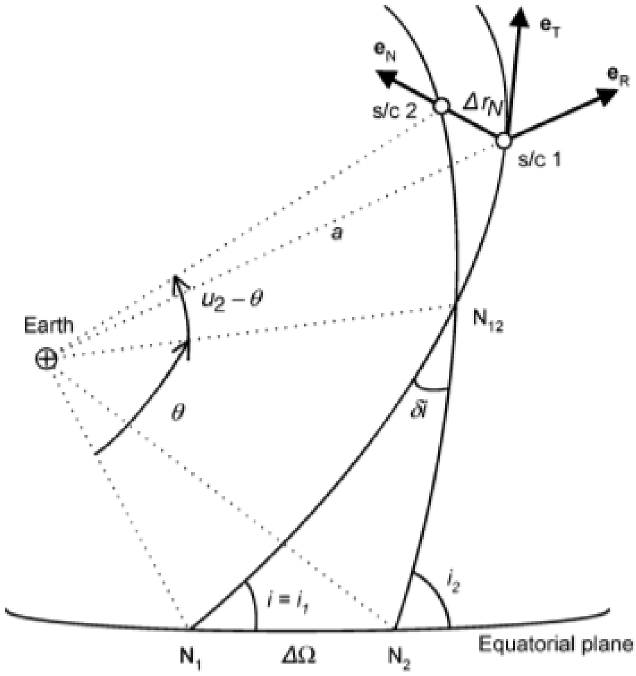

Figure 2.1: Spherical triangles for the relative inclination vector definition [25]

As showed in fig. 2.1, simple geometrical considerations suggest adopting the angle enclosed by the two orbital planes δi and the relative ascending node θ at which spacecraft 2 crosses the orbital plane of spacecraft 1 in ascending direction to define a relative inclination vector as:

$$\Delta\bar{i} = \begin{pmatrix} \Delta i_x \\ \Delta i_y \end{pmatrix} = \sin(\delta i) \begin{pmatrix} \cos\theta \\ \sin\theta \end{pmatrix} \tag{2.5}$$

Let us now consider the sphere of radius $a_1 = a_2 = a$ centered on the Earths center of mass. As it can be recognized from the law of sines and cosines for the spherical triangle with vertices N_1, N_2, and N_{12} (i.e., the absolute and relative ascending nodes), for small differences in the orbital elements definition (2.5) simplifies to:

$$\Delta\bar{i} \simeq \begin{pmatrix} \Delta i \\ \Delta\Omega \sin i \end{pmatrix} \tag{2.6}$$

i is the inclination of spacecraft 1, but can be also substituted by i_2 in the frame of first-order theory. The omission of the satellite designating subscript indicates that the orbital elements of both satellites can be used equivalently. It is possible to apply the law of sines to the spherical triangle with vertices s/c 1, s/c 2, and N_{12}, to get a first-order approximation of the relative motion in cross-track direction [25]:

$$\frac{\Delta r_N}{a} \simeq \sin(u_2 - \theta)\sin(\delta i) = -\Delta i_y \cos(u) + \Delta i_x \sin(u) \tag{2.7}$$

where $u = \omega + M$ is the mean argument of latitude.

Relative Eccentricity vector and in-plane motion

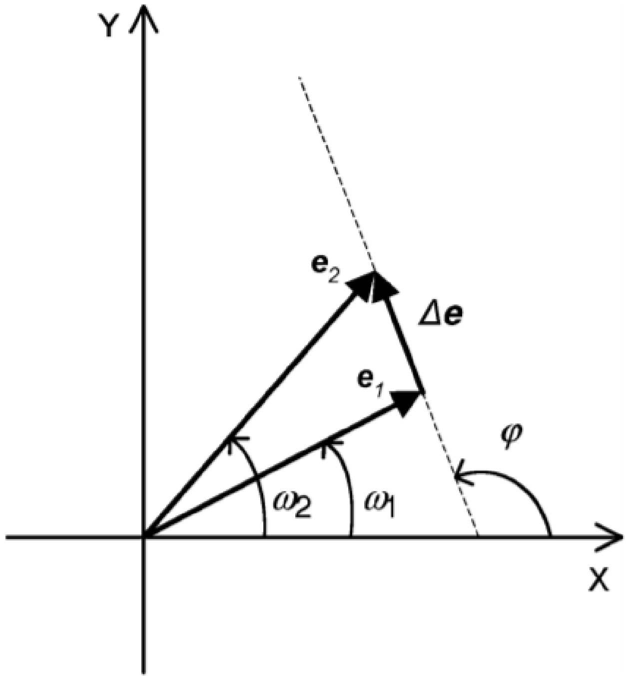

Figure 2.2: Relative eccentricity vector definition [25]

For near-circular satellite orbits, the Keplerian elements eccentricity and argument of perigee are commonly replaced by the eccentricity vector:

$$\overline{e} = \begin{pmatrix} e_x \\ e_y \end{pmatrix} = e \begin{pmatrix} \cos(\omega) \\ \sin(\omega) \end{pmatrix} \tag{2.8}$$

The relative motion of two satellites as a result of variations in the eccentricity e and argument of perigee ω (fig. 2.2) is easily described by introducing the difference:

$$\Delta\overline{e} = \overline{e}_2 - \overline{e}_1 = \begin{pmatrix} \Delta e_x \\ \Delta e_y \end{pmatrix} = \delta e \begin{pmatrix} \cos(\varphi) \\ \sin(\varphi) \end{pmatrix} \tag{2.9}$$

where φ is the relative perigee.
This so-called relative eccentricity vector characterizes the periodic relative motion within the orbital plane [25]. It can be shown that for near-circular orbits the difference between true anomaly f and mean anomaly M is given by:

$$f - M = 2e\sin(M) = -2e_y\cos(u) + 2e_x\sin(u) \tag{2.10}$$

While the radius r can be expressed as:

$$\frac{r}{a} = 1 - e\cos(M) = -e_x\cos(u) - e_y\sin(u) \tag{2.11}$$

Differencing (2.10) and (2.11) between two satellites in close proximity with identical mean argument of latitude yields to:

$$\frac{\Delta r_T}{a} = (f_2 - M_2) - (f_1 - M_1) = -2\Delta e_y\cos(u) + 2\Delta e_x\sin(u) \tag{2.12}$$

and also:

$$\frac{\Delta r_R}{a} = \frac{r_2 - r_1}{a} = -\Delta e_x\cos(u) - \Delta e_y\sin(u) \tag{2.13}$$

Eccentricity/Inclination vector separation

Let's suppose that $\Delta a = 0$, rewriting (2.7), (2.12) and (2.13) using the polar representation [25], we obtain the following:

$$\frac{\Delta r_R}{a} = -\delta e \cos(u - \varphi) \tag{2.14}$$

$$\frac{\Delta r_T}{a} = 2\delta e \sin(u - \varphi) \tag{2.15}$$

$$\frac{\Delta r_N}{a} = \delta i \sin(u - \theta) \tag{2.16}$$

The relative orbit of spacecraft 2 with respect to spacecraft 1 is an ellipse of semi-major axis $2a\delta e$ in along-track direction and semi-minor axis $a\delta e$ in radial direction (fig. 2.3).

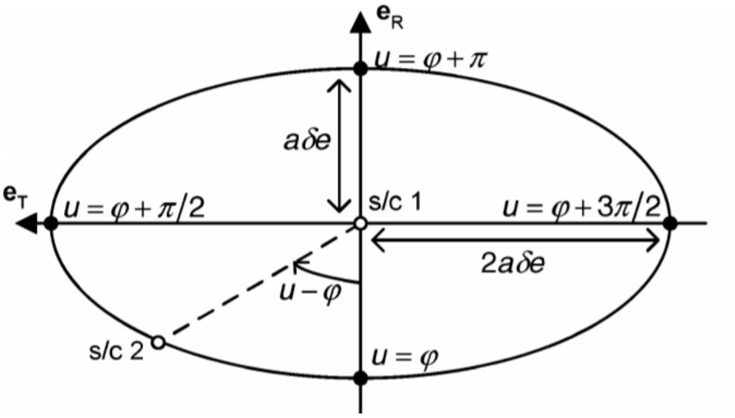

Figure 2.3: In-plane relative motion of two spacecraft with e/i vector separation [25]

Whenever the argument of latitude u equals φ, spacecraft 2 is located right below the center. As soon as $u = \varphi + \frac{\pi}{2}$, spacecraft 2 takes over and is just ahead of the Chief satellite.
In analogy with the previous concepts, the relative inclination vector is used to describe the relative motion perpendicular to the orbital plane. The cross-track relative motion is described by a harmonic oscillation of amplitude $a\delta i$ and phase angle $u - \theta$ (fig. 2.4).

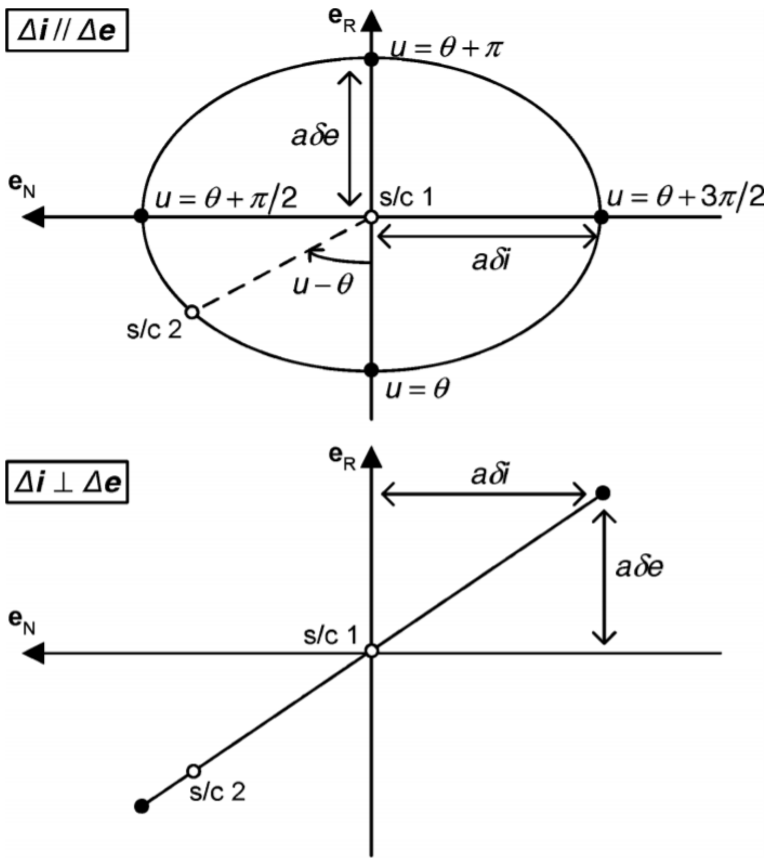

Figure 2.4: Out-of-plane relative motion of two spacecraft with parallel e/i vectors (top) and orthogonal e/i vectors (bottom) [25]

Parallel vectors $\Delta\overline{e}$ and $\Delta\overline{i}$ imply equality of the associated angles φ and θ. As in fig. 2.3, $u = \varphi + k\pi$ $(k = 0, 1, 2, ...)$ marks the positions at which the two spacecraft exhibit their maximum radial separation; instead, $u = \varphi + \left(k + \frac{1}{2}\right)\pi$ are the points of vanishing radial separation. Considering out-of-plane motion when $\varphi = \theta$ (in case of parallel vectors, fig. 2.4-top), having $\Delta\overline{e}//\Delta\overline{i}$ ensures maximum r_R when $r_N = 0$ and vice versa, maximum r_N when $r_R = 0$. In contrast to this, the radial and cross-track separation can jointly vanish $(r_R = r_N = 0)$ for orthogonal vectors $\Delta\overline{e} \perp \Delta\overline{i}$, which is risky in the presence of along-track position uncertainties (fig. 2.4-bottom).

2.2 Quasi-Nonsingular State Transition Matrix formulation

2.2.1 Derivation Methodology

In this section, an overview of the derivation methodology for the *Quasi-Nonsingular STM* will be presented, referring to Koenig's work [11].
The STM is derived using a simple method which allows inclusion of multiple perturbations in orbits of arbitrary eccentricity and admits a wide range of ROE states. The only requirement is a *closed-form expression* of the time derivatives of the relative state as a function of the absolute states of the chief and deputy. Consider a general absolute state $\overline{X}$ and relative state $\delta\overline{X}$ which include parameters to model non-conservative forces. Let the time derivatives of the relative state be given as:

$$\delta\dot{\overline{X}}\,(t) = f\left(\overline{X}_d\left(\overline{X}_c\,(t)\,, \delta\overline{X}\,(t)\right), \overline{X}_c\,(t)\,, \overline{\gamma}\right) \tag{2.17}$$

where the absolute state of the deputy is formulated explicitly as a function of the chief state and the relative state, while $\overline{\gamma}$ denotes a general set of parameters relevant to included perturbations. The STM is derived by first performing a first-order Taylor expansion on the equations of relative motion, given as:

$$\delta\dot{\overline{X}}\left(t\right) = \boldsymbol{A}\left(\overline{X}_c\left(t\right), \overline{\gamma}\right)\delta\overline{X}\left(t\right) + \mathcal{O}\left(\delta X^2\right) \tag{2.18}$$

$$\boldsymbol{A}\left(\overline{X}_c\left(t\right), \overline{\gamma}\right) = \left.\frac{\partial\delta\dot{\overline{X}}}{\partial\overline{X}_d}\right|_{\delta\overline{X}=0} \left.\frac{\partial\overline{X}_d}{\partial\delta\overline{X}}\right|_{\overline{X}_d=\overline{X}_c} \tag{2.19}$$

where the plant matrix $\boldsymbol{A}$ is computed by a simple chain rule derivative. If the terms of $\boldsymbol{A}$ are constant, the resulting system of linear differential equations is solved exactly in closed-form:

$$\delta\overline{X}\left(t_i + \tau\right) = \boldsymbol{\Phi}\left(\overline{X}_c\left(t_i\right), \overline{\gamma}, \tau\right)\delta\overline{X}\left(t_i\right) \tag{2.20}$$

where $\boldsymbol{\Phi}\left(\overline{X}_c\left(t_i\right), \overline{\gamma}, \tau\right)$ denotes the STM. However, in some cases the plant matrix cannot reasonably be treated as time-invariant. This issue is corrected by transforming the state into a modified form by a simple linear transformation provided that the relevant dynamics of the chief absolute state are known. The STM for the modified state can then be computed from the time-invariant plant matrix. In these cases, the STM for the original state can be expressed in closed-form as:

$$\boldsymbol{\Phi}\left(\overline{X}_c\left(t_i\right), \overline{\gamma}, \tau\right) = \boldsymbol{J}^{-1}\left(\overline{X}_c\left(t_i\right) + \dot{\overline{X}}_c\left(t_i\right)\tau\right)\boldsymbol{\Phi'}\left(\overline{X}_c\left(t_i\right), \overline{\gamma}, \tau\right)\boldsymbol{J}\left(\overline{X}_c\left(t_i\right)\right) \tag{2.21}$$

where $\dot{\overline{X}}_c\left(t_i\right)$ denotes the time derivative of the chief state at time t_i, $\boldsymbol{\Phi'}\left(\overline{X}_c\left(t_i\right), \overline{\gamma}, \tau\right)$ denotes the STM for the modified state, and $\boldsymbol{J}\left(\overline{X}_c\left(t_i\right)\right)$ denotes the transformation matrix to the modified state at time t.

Keplerian Dynamics

Under the assumption of a Keplerian orbit, the time derivatives of the orbit elements are given as:

$$\dot{a} = \dot{e} = \dot{i} = \dot{\Omega} = \dot{\omega} = 0 \tag{2.22}$$

$$\dot{M} = n = \frac{\sqrt{\mu}}{a^{\frac{3}{2}}} \tag{2.23}$$

Because only M is time varying, the time derivatives of all previously described ROE states are equivalent and given as:

$$\delta\dot{\overline{X}} = \begin{pmatrix} 0 \\ \dot{M}_d - \dot{M}_c \\ 0 \\ 0 \\ 0 \\ 0 \end{pmatrix} = \sqrt{\mu}\begin{pmatrix} 0 \\ a_d^{-\frac{3}{2}} - a_c^{-\frac{3}{2}} \\ 0 \\ 0 \\ 0 \\ 0 \end{pmatrix} \tag{2.24}$$

The first-order Taylor expansion of (2.24) about zero separation is given as:

$$\delta\dot{\overline{X}} = \boldsymbol{A}^{kep}\left(\overline{X}_c\right)\delta\overline{X} + \mathcal{O}\left(\delta X^2\right) \tag{2.25}$$

$$
\boldsymbol{A}^{kep}\left(\overline{X}_c\right) = \begin{bmatrix} 0 & 0 & 0 & 0 & 0 & 0 \\ -\frac{3}{2}n_c & 0 & 0 & 0 & 0 & 0 \\ 0 & 0 & 0 & 0 & 0 & 0 \\ 0 & 0 & 0 & 0 & 0 & 0 \\ 0 & 0 & 0 & 0 & 0 & 0 \\ 0 & 0 & 0 & 0 & 0 & 0 \end{bmatrix} \tag{2.26}
$$

It is evident from (2.24) that Keplerian relative motion depends only on the semi-major axes of each of the spacecraft orbits. Accordingly, the only non-zero higher order terms will be proportional to powers of δa. Thus, this relative motion model is valid for unperturbed orbits with small δa and arbitrary separation in all other state components [11].

J_2 Perturbation

The Quasi-Nonsingular Keplerian STM is generalized to include the first-order secular effects of the second-order zonal geopotential harmonic J_2. The J_2 perturbation causes secular drifts in the mean anomaly M, right ascension of the ascending node Ω, and the argument of perigee ω. These drift rates are given by Brouwer [9]:

$$
\begin{pmatrix} \dot{M} \\ \dot{\omega} \\ \dot{\Omega} \end{pmatrix} = \frac{3}{4}\frac{J_2 R_E^2 \sqrt{\mu}}{a^{\frac{7}{2}}\eta^4} \begin{pmatrix} \eta\left(3\cos^2(i) - 1\right) \\ 5\cos^2(i) - 1 \\ -2\cos(i) \end{pmatrix} \tag{2.27}
$$

The whole derivation process in the Quasi-Nonsingular state vector case is omitted, see [11] for further details. The result of the first-order Taylor expansion is the following:

$$
\boldsymbol{A}^{J_2}\left(\overline{X}_c(T)\right) = k \begin{bmatrix} 0 & 0 & 0 & 0 & 0 & 0 \\ -\frac{7}{2}EP & 0 & e_{xi}FGP & e_{yi}FGP & -FS & 0 \\ \frac{7}{2}e_{yf}Q & 0 & -\left(4e_{xi}e_{yf}G + C\right)Q & -\left(1 + 4e_{yi}e_{yf}G - D\right)Q & 5e_{yf}S & 0 \\ -\frac{7}{2}e_{xf}Q & 0 & \left(1 + 4e_{xi}e_{xf}G - D\right)Q & \left(4e_{xf}e_{yi}G - C\right)Q & -5e_{xf}S & 0 \\ 0 & 0 & 0 & 0 & 0 & 0 \\ \frac{7}{2}S & 0 & -4e_{xi}GS & -4e_{yi}GS & 2T & 0 \end{bmatrix} \tag{2.28}
$$

where $\eta_c = \sqrt{1 - e_c^2}$, $k = \frac{3}{4}\frac{J_2 R_E^2 \sqrt{\mu}}{a^{\frac{7}{2}}\eta^4}$, $e_{xi} = e_c\cos(\omega_c)$, $e_{yi} = e_c\sin(\omega_c)$, $E = 1 + \eta_c$, $C = \sin(\omega_c)$, $D = \cos(\omega_c)$, $F = 4 + 3\eta_c$, $G = \frac{1}{\eta_c^2}$, $P = 3\cos^2(i_c) - 1$, $Q = 5\cos^2(i_c) - 1$, $S = \sin(2i_c)$, $T = \sin^2(i_c)$, $\dot{\omega} = kQ$, $e_{xf}(t) = e_c\cos(\omega_c + \dot{\omega}t)$, $e_{yf}(t) = e_c\sin(\omega_c + \dot{\omega}t)$.
The range of applicability is again assessed by considering higher order terms of the Taylor expansion. It can be seen that the time derivative of the state does not depend on M or Ω, which correspond to the $\delta\lambda$ and δi_y state components. Accordingly, the model is valid for small separations in δa, δe_x, δe_y, and δi_x, but arbitrary separations in $\delta\lambda$ and δi_y. Moreover, while the quasi-nonsingular state avoids the circular orbit singularity present in the singular state, the cost of this property is that arbitrary differences in the argument of perigee are no longer allowed [11].

Density-Free Model for differential drag

It is known that the density of the atmosphere can vary widely due to solar activity and other effects, rendering development of an accurate differential drag model difficult. This problem can be mitigated by using a density-model-free formulation of the effects of differential drag on eccentric orbits [11]. This approach requires a ROE state augmented with the time derivative of the relative semi-major axis, denoted $\delta\dot{a}_{drag}$, which can be estimated by the relative navigation system in-flight. Recalling that atmospheric drag circularizes eccentric orbits, the relative dynamics must satisfy:

$$\delta\dot{e} = (1-e)\,\delta\dot{a}_{drag} \tag{2.29}$$

The result of the first-order Taylor expansion in this case is the following:

$$\begin{pmatrix} \delta\dot{\overline{X}} \\ \delta\ddot{a}_{drag} \end{pmatrix} = \boldsymbol{A}^{drag}\left(\overline{X}_c\left(t\right)\right)\begin{pmatrix} \delta\overline{X} \\ \delta\dot{a}_{drag} \end{pmatrix} \tag{2.30}$$

$$\boldsymbol{A}^{drag}\left(\overline{X}_c\left(t\right),\tau\right) = k\begin{bmatrix} 0 & 0 & 0 & 0 & 0 & 0 & \frac{1}{k} \\ 0 & 0 & 0 & 0 & 0 & 0 & 2\left(-\frac{3}{4}\frac{n_c}{k} - \frac{7}{4}EP + \frac{1}{2}e\left(1-e\right)FGP\right)\tau \\ 0 & 0 & 0 & 0 & 0 & 0 & \frac{D-e_{xf}}{k} - 2e_{yf}Q\left(-\frac{7}{4} + 2e\left(1-e\right)G\right)\tau \\ 0 & 0 & 0 & 0 & 0 & 0 & \frac{C-e_{yf}}{k} + 2e_{xf}Q\left(-\frac{7}{4} + 2e\left(1-e\right)G\right)\tau \\ 0 & 0 & 0 & 0 & 0 & 0 & 0 \\ 0 & 0 & 0 & 0 & 0 & 0 & 2S\left(\frac{7}{4} - 2e\left(1-e\right)G\right)\tau \\ 0 & 0 & 0 & 0 & 0 & 0 & 0 \end{bmatrix} \tag{2.31}$$

This model is only valid as long as the semi-major axis and eccentricity of the chief orbit and the time derivative of the relative semi-major axis can be treated as constant. Additionally, this STM require orbit eccentricities large enough that the circularization assumptions holds, this means that this model is not valid for perfectly circular orbits.

Complete model

Since the model is linearized, we can obtain the complete model by summing all the contributes analyzed previously (Keplerian, J_2, differential drag). We can write as follows:

$$\begin{pmatrix} \delta\dot{\overline{X}} \\ \delta\ddot{a}_{drag} \end{pmatrix} = \boldsymbol{A}\left(\overline{X}_c\left(t\right)\right)\begin{pmatrix} \delta\overline{X} \\ \delta\dot{a}_{drag} \end{pmatrix} \tag{2.32}$$

where $\boldsymbol{A} = \boldsymbol{A}^{kep} + \boldsymbol{A}^{J_2} + \boldsymbol{A}^{drag}$. We obtain:

$$\boldsymbol{A} = k\begin{bmatrix} 0 & 0 & 0 & 0 & 0 & 0 & \frac{1}{k} \\ -\left(\frac{3}{2}\frac{n_c}{k} + \frac{7}{2}EP\right) & 0 & e_{xi}FGP & e_{yi}FGP & -FS & 0 & 2\left(-\frac{3}{4}\frac{n_c}{k} - \frac{7}{4}EP + \frac{1}{2}e\left(1-e\right)FGP\right)\tau \\ \frac{7}{2}e_{yf}Q & 0 & -\left(4e_{xi}e_{yf}G + C\right)Q & -\left(1 + 4e_{yi}e_{yf}G - D\right)Q & 5e_{yf}S & 0 & \frac{D-e_{xf}}{k} - 2e_{yf}Q\left(-\frac{7}{4} + 2e\left(1-e\right)G\right)\tau \\ -\frac{7}{2}e_{xf}Q & 0 & \left(1 + 4e_{xi}e_{xf}G - D\right)Q & \left(4e_{xf}e_{yi}G - C\right)Q & -5e_{xf}S & 0 & \frac{C-e_{yf}}{k} + 2e_{xf}Q\left(-\frac{7}{4} + 2e\left(1-e\right)G\right)\tau \\ 0 & 0 & 0 & 0 & 0 & 0 & 0 \\ \frac{7}{2}S & 0 & -4e_{xi}GS & -4e_{yi}GS & 2T & 0 & 2S\left(\frac{7}{4} - 2e\left(1-e\right)G\right)\tau \\ 0 & 0 & 0 & 0 & 0 & 0 & 0 \end{bmatrix} \tag{2.33}$$

Let's see know what is the effect of the STM on the relative motion.

2.2.2 Relative motion due to STM

Effect of Keplerian Dynamics and J_2

First of all, the effect of Keplerian and J_2 is considered [11]:

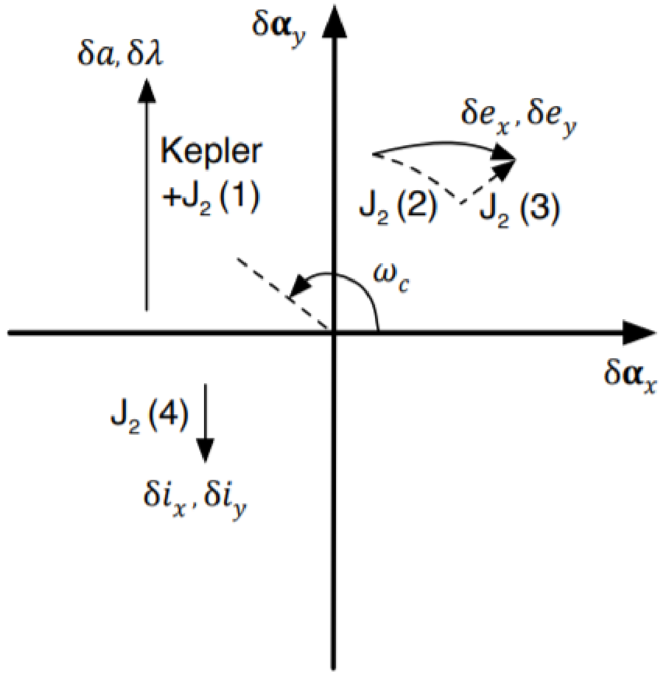

Figure 2.5: Effect of Keplerian and J_2 STMs on relative motion. [11]

As reported in fig. 2.5, the combined effects of Kepler and J_2 produce four distinct types of motion:

- 1: a constant drift of $\delta\lambda$ due to both Keplerian relative motion and J_2;
- 2: a rotation of the relative eccentricity vector due to J_2;
- 3: a secular drift of the relative eccentricity vector proportional to the chief eccentricity and orthogonal to the phase angle of the chief argument of perigee due to J_2;
- 4: a constant drift of δi_y due to J_2.

Effect of differential drag

Now, let's consider also the effect of the differential drag.

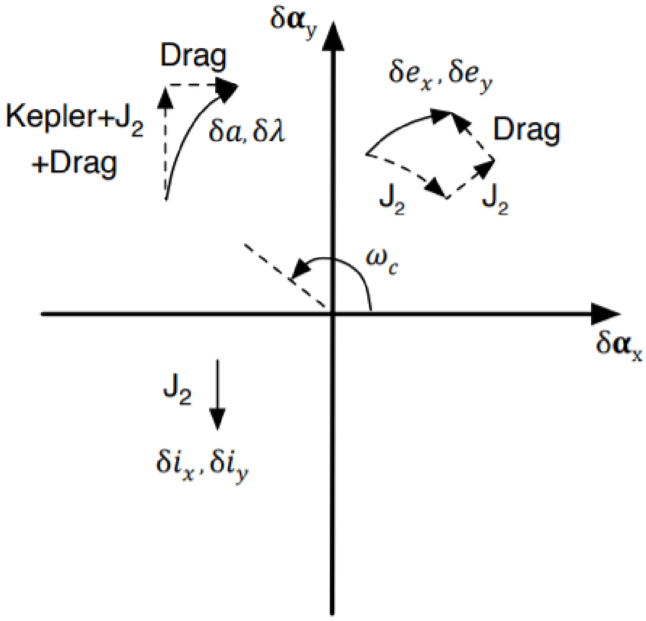

Figure 2.6: Effect of differential drag on relative motion. [11]

There are three new effects caused by differential drag (fig. 2.6):

- 1: a linear drift of δa;
- 2: a quadratic drift in $\delta\lambda$ due to the coupling between differential drag and Keplerian relative motion;
- 3: a linear drift of the relative eccentricity vector parallel to the phase angle of the chief argument of perigee.

There are also additional effects due to terms in the STM that are quadratic in time which derive from the coupling between drag and J_2, but because the secular drifts due to drag are already small and the quadratic terms are multiplied by k, these terms are generally negligible unless the propagation time is very long [11].

2.3 Control Matrix

2.3.1 Definition

Since the goal is to control the spacecraft relative motion, we need to write the dynamical system as follows:

$$\begin{pmatrix} \delta\dot{\overline{X}} \\ \delta\ddot{a}_{drag} \end{pmatrix} = \boldsymbol{A}\left(\overline{X}_c\left(t\right)\right)\begin{pmatrix} \delta\overline{X} \\ \delta\dot{a}_{drag} \end{pmatrix} + \boldsymbol{B}\left(\overline{X}_c\left(t\right)\right)\overline{u} \tag{2.34}$$

where $\boldsymbol{B}$ is the *Control Matrix* and $\overline{u}$ is the *Control Vector*.
Considering spacecraft on near-circular orbits, the chosen *control parameters* are the accelerations in the *RTN* (Radial-Tangential-Normal) directions.

Figure 2.7: RTN Frame. [25]

The Control Matrix $\boldsymbol{B}$ considering Quasi-Nonsingular STM and $\overline{u} = \begin{pmatrix} u_R \\ u_T \\ u_N \end{pmatrix}$ has been derived by Chernick and D'Amico [26]:

$$\boldsymbol{B}\left(\overline{X}_c(t)\right) = \frac{1}{a_c n_c} \begin{bmatrix} \frac{2}{\eta_c} e_c \sin(f_c) & \frac{2}{\eta_c}\left(1 + e_c \cos(f_c)\right) & 0 \\ -\frac{2\eta_c^2}{1+e_c\cos(f_c)} & 0 & 0 \\ \eta_c \sin(\omega_c + f_c) & \eta_c \frac{(2+e_c\cos(f_c))\cos(\omega_c+f_c)+e_x}{(1+e_c\cos(f_c))} & \frac{\eta_c e_y}{\tan(i_c)} \frac{\sin(\omega_c+f_c)}{1+e_c\cos(f_c)} \\ -\eta_c \cos(\omega_c + f_c) & \eta_c \frac{(2+e_c\cos(f_c))\sin(\omega_c+f_c)+e_y}{(1+e_c\cos(f_c))} & -\frac{\eta_c e_x}{\tan(i_c)} \frac{\sin(\omega_c+f_c)}{1+e_c\cos(f_c)} \\ 0 & 0 & \eta_c \frac{\cos(\omega_c+f_c)}{1+e_c\cos(f_c)} \\ 0 & 0 & \eta_c \frac{\sin(\omega_c+f_c)}{1+e_c\cos(f_c)} \\ 0 & 0 & 0 \end{bmatrix} \tag{2.35}$$

where f_c is the Chief's True Anomaly.

2.3.2 ΔV lower bound for impulsive maneuvers

It is useful to define the ΔV lower bound for RTN maneuvers, in order to compare later the total ΔVs of our continuous maneuver to this optimal value. It can be deduced from the $\boldsymbol{B}$ Matrix that [26]:

ROE Change	Direction of Maneuver	Optimal Location	ΔV Lower Bound $\frac{m}{s}$
$\Delta\delta a$	Radial	$f_c = \frac{\pi}{2}, \frac{3}{2}\pi, ...$	
	Tangential	$f_c = 0$	$\frac{\eta_c}{2(1+e_c)} n_c a_c \lvert\Delta\delta a\rvert$
$\Delta\delta\lambda$	Radial	$f_c = \frac{\pi}{2}, \frac{3}{2}\pi, ...$	$\frac{\eta_c}{3e_c\Delta M + 2\eta_c^3} n_c a_c \lvert\Delta\delta\lambda\rvert$
	Tangential	$f_c = 0$	$\frac{\eta_c}{3(1+e_c)\Delta M} n_c a_c \lvert\Delta\delta\lambda\rvert$
$\lvert\Delta\delta\bar{e}\rvert$	Radial	Anywhere	
	Tangential	$f_c = 0, \pi, 2\pi, ...$	$\frac{1}{2\eta_c} n_c a_c \lvert\Delta\delta e\rvert$
	Normal	$\omega_c + f_c = \arctan\left(\frac{\Delta\delta e_y}{\Delta\delta e_x}\right)$	
$\lvert\Delta\delta\bar{i}\rvert$	Normal	$\omega_c + f_c = \arctan\left(\frac{\Delta\delta i_y}{\Delta\delta i_x}\right)$	$\frac{1-e_c}{\eta_c} n_c a_c \lvert\Delta\delta i\rvert$

Table 2.1: ΔV lower bound in RTN directions during control interval identified by a shift of mean anomaly $\Delta M = M_f - M_0$ [26]

It can be seen that a variation of $\delta\lambda$ can be achieved through a tangential or radial ΔV which introduces the proper drift in modified relative mean longitude for the duration of the reconfiguration. Radial maneuvers provide a direct shift of $\Delta\delta\lambda = \frac{3}{\eta_c} e_c \Delta M + 2\eta_c^2$, while tangential maneuvers provide a direct shift of $\Delta\delta\lambda = \frac{3}{\eta_c} e_c \Delta M + 3\frac{3}{\eta_c}\Delta M$. As a result, tangential maneuvers are more efficient than radial maneuvers in the case that $\frac{3}{\eta_c}\Delta M \;\; > 2\eta_c^2$ or $\Delta M > \frac{2}{3}\eta_c^3$. Since $0 \leq \eta_c \leq 1$, this condition translates to a reconfiguration span of $\Delta M = [0, 38.2]$ degrees, dependent on the reference eccentricity. The limit cases are provided by a control window of zero degrees, where only radial maneuvers can affect the modified relative mean longitude, and 38.2 degrees, for a circular orbit [26].
The most general in-plane and out-of-plane ΔV lower bound for orbits of arbitrary eccentricity is given by:

$$\Delta V_{LB} = n_c a_c \eta_c \cdot max\left(\frac{|\Delta\delta a|}{2\,(1+e_c)}, \frac{|\Delta\delta\lambda|}{K\,(e_c, \Delta M)}, \frac{|\Delta\delta\bar{e}|}{2\eta_c^2} + \frac{1-e_c}{\eta_c^2}\left|\Delta\delta\bar{i}\right|\right) \tag{2.36}$$

where $K\,(e_c, \Delta M) = max\,(3e_c\Delta M + 2\eta_c^3, 3\,(1+e_c)\,\Delta M)$. It should be noted that as the mission time increases, ΔM increases and a mean longitude separation $\Delta\delta\lambda$ could be achieved with a lower ΔV_{LB}.

Chapter 3

Linear Quadratic Regulator Overview and Implementation

3.1 Theoretical Overview

3.1.1 Introduction to Continuous-Time LQR

In the theory of *Optimal Control*, the main concern is to find a way to control and operate a dynamical system at minimum cost. The case where the dynamics of a system are described by a set of linear differential equations and the cost is represented by a quadratic function, is called *LQ* problem.

A largely used method in literature to solve this kind of problems is the *Linear Quadratic Regulator*. Let's consider the following linear time-varying plant [27]:

$$\dot{\overline{x}} = \boldsymbol{A}(t)\,\overline{x} + \boldsymbol{B}(t)\,\overline{u} \tag{3.1}$$

where $\overline{x} \in \mathbb{R}^n$ is the State Vector and $\overline{u} \in \mathbb{R}^m$ is the Control Vector. In LQR theory, the quadratic cost function to be minimized is defined as follows:

$$J(t_0) = \frac{1}{2}\overline{x}^T(T)\,\boldsymbol{M}(T)\,\overline{x}(T) + \frac{1}{2}\int_{t_0}^{T}\left(\overline{x}^T\boldsymbol{Q}(t)\,\overline{x} + \overline{u}^T\boldsymbol{R}(t)\,\overline{u}\right)dt \tag{3.2}$$

The time interval over which we are interested in the behavior of the plant is $[t_0, T]$. We shall determine the control $\overline{u}^\star$ on $[t_0, T]$ that minimizes J, knowing: the initial state $\overline{x}_0$, the target final state $\overline{x}_d$, the initial and final times t_0, T.

Three different weighting matrices are present in (3.2):

- $\boldsymbol{M}$, which is symmetric and positive semi-definite in $[t_0, T]$, it is the solution of the Differential Riccati Equation and will be used later to calculate the Gain Matrix;

- $\boldsymbol{Q}$, which is also symmetric and positive semi-definite in $[t_0, T]$, it modulates the effect of the state vector in the cost function. This means that if we increase the elements in $\boldsymbol{Q}$, the error on the state vector will decrease, viceversa if we decrease the values in $\boldsymbol{Q}$ the errors in the state vector will increase.

- $\boldsymbol{R}$, which is symmetric and positive definite in $[t_0, T]$, it modulates the effect of the control vector in the cost function. This means that if we increase the elements in $\boldsymbol{R}$, we force the control parameters to be smaller, viceversa if we decrease the values in $\boldsymbol{R}$ the control parameters will be larger.

The $\boldsymbol{Q}$ and $\boldsymbol{R}$ matrices should be tuned in order to match the constraints.

3.1.2 State and Costate Equations

The *Hamiltonian* associated to the system is:

$$H(t) = \frac{1}{2}\left(\overline{x}^T \boldsymbol{Q}\overline{x} + \overline{u}^T \boldsymbol{R}\overline{u}\right) + \overline{\lambda}^T \left(\boldsymbol{A}\overline{x} + \boldsymbol{B}\overline{u}\right) \tag{3.3}$$

where $\overline{\lambda}(t) \in \mathbb{R}^n$ is a set of *costate variables*, that can be thought as a set of undetermined Lagrange multipliers associated to the state equations representing the marginal cost of violating the system constraints. The Hamiltonian itself, introduced for the first time by Lev Pontryagin, is a function used to solve a problem of optimal control for a dynamical system. It can be thought as an instantaneous increment of the Lagrangian expression of the problem that has to be optimized over a certain time horizon.
Once the Hamiltonian and the costate variables have been defined, we can write the *State and Costate Equations*:

$$\dot{\overline{x}} = \frac{\partial H}{\partial \overline{\lambda}} = \boldsymbol{A}\overline{x} + \boldsymbol{B}\overline{u} \tag{3.4}$$

$$-\dot{\overline{\lambda}} = \frac{\partial H}{\partial \overline{x}} = \boldsymbol{Q}\overline{x} + \boldsymbol{A}^T\overline{\lambda} \tag{3.5}$$

The stationarity condition should also be added:

$$0 = \frac{\partial H}{\partial \overline{u}} = \boldsymbol{R}\overline{u} + \boldsymbol{B}^T\overline{\lambda} \tag{3.6}$$

From (3.6) we can write the optimal control in terms of the costate variables:

$$\overline{u}(t) = -\boldsymbol{R}^{-1}\boldsymbol{B}^T\overline{\lambda} \tag{3.7}$$

Putting (3.7) into the state equation yields to the homogeneous *Hamiltonian System*:

$$\begin{pmatrix} \dot{\overline{x}} \\ \dot{\overline{\lambda}} \end{pmatrix} = \begin{bmatrix} \boldsymbol{A} & \boldsymbol{B}\boldsymbol{R}^{-1}\boldsymbol{B}^T \\ -\boldsymbol{Q} & -\boldsymbol{A}^T \end{bmatrix} \begin{pmatrix} \overline{x} \\ \overline{\lambda} \end{pmatrix} \tag{3.8}$$

To find the optimal control, we must take into account the boundary conditions and solve (3.8). We have two different formulations based on T:

- *Finite-Horizon* if the final time has a finite value;
- *Infinite-Horizon* if $T \to \infty$

3.1.3 Finite-Horizon derivation methodology

We can find an optimal control law in the form of a state feedback by fixing the final state at a desired final value $\overline{x}_d$, the optimal solution will also minimize the cost function defined by (3.2).
To solve the two-point boundary-value problem specified by (3.4) and (3.5), given $\overline{x}(t_0) = \overline{x}_0$ and $\overline{x}(T) = \overline{x}_d = \overline{0}$, let's assume that $\overline{x}(t)$ and $\overline{\lambda}(t)$ are related by a linear relation thanks to $\boldsymbol{M}$ as follows [27]:

$$\overline{\lambda}(t) = \boldsymbol{M}(t)\,\overline{x}(t) \tag{3.9}$$

If we can find such a matrix $\boldsymbol{M}$, then this assumption is valid. In order to find the intermediate function $\boldsymbol{M}$, let's differentiate (3.9):

$$\dot{\overline{\lambda}} = \dot{\boldsymbol{M}}\overline{x} + \boldsymbol{M}\dot{\overline{x}} = \dot{\boldsymbol{M}}\overline{x} + \boldsymbol{M}\left(\boldsymbol{A}\overline{x} - \boldsymbol{B}\boldsymbol{R}^{-1}\boldsymbol{B}^T\boldsymbol{M}\overline{x}\right) \tag{3.10}$$

Substituting the costate equation (3.5) we obtain:

$$-\dot{\boldsymbol{M}}\overline{x} = \left(\boldsymbol{A}^T\boldsymbol{M} + \boldsymbol{M}\boldsymbol{A} - \boldsymbol{M}\boldsymbol{B}\boldsymbol{R}^{-1}\boldsymbol{B}^T\boldsymbol{M} + \boldsymbol{Q}\right)\overline{x} \tag{3.11}$$

for all t. Since this holds for all state trajectories given any $\overline{x}_0$, it is necessary that:

$$-\dot{\boldsymbol{M}} = \boldsymbol{A}^T\boldsymbol{M} + \boldsymbol{M}\boldsymbol{A} - \boldsymbol{M}\boldsymbol{B}\boldsymbol{R}^{-1}\boldsymbol{B}^T\boldsymbol{M} + \boldsymbol{Q} \tag{3.12}$$

This is called *Differential Riccati Equation*, and if $\boldsymbol{M}(t)$ is its solution with final condition $\boldsymbol{M}(T)$, then (3.9) holds for all $t \leq T$. In terms of the Riccati equation's solution $\boldsymbol{M}(t)$, the optimal control is given by (3.7) and (3.9) as:

$$\overline{u}(t) = -\boldsymbol{R}^{-1}\boldsymbol{B}^T\boldsymbol{M}\overline{x}(t) = -\boldsymbol{K}(t)\overline{x} \tag{3.13}$$

where

$$\boldsymbol{K}(t) = \boldsymbol{R}^{-1}\boldsymbol{B}^T\boldsymbol{M} \tag{3.14}$$

is the *Gain Matrix*. The control (3.13) is a time-varying state feedback, since even if $\boldsymbol{A}$, $\boldsymbol{B}$, $\boldsymbol{Q}$ and $\boldsymbol{R}$ are time invariant, $\boldsymbol{K}(t)$ varies with time.

3.1.4 Infinite-Horizon derivation methodology

In the *Infinite-Horizon* case, since $T \to \infty$, we can assume that the matrix $\boldsymbol{M}$ evolves really slowly from $\boldsymbol{M}(t_0)$ to $\boldsymbol{M}(T)$:

$$\dot{\boldsymbol{M}} \simeq 0 \tag{3.15}$$

Then (3.12) is simplified as follows:

$$\boldsymbol{0} = \boldsymbol{A}^T\boldsymbol{M} + \boldsymbol{M}\boldsymbol{A} - \boldsymbol{M}\boldsymbol{B}\boldsymbol{R}^{-1}\boldsymbol{B}^T\boldsymbol{M} + \boldsymbol{Q} \tag{3.16}$$

(3.16) is called *Algebraic Riccati Equation*, and it gives $\boldsymbol{M}(t)$ as solution. The Gain matrix and the optimal control are still given by (3.13) and (3.14).

3.1.5 Controllability Property

In order to successfully control a dynamic system, it must satisfy a property called *Controllability*. A system with initial state vector $\overline{x}(t_0) = \overline{x}_0$ is *controllable* to $\overline{x}(t_1 > t_0) = \overline{x}_1$ if there exists an admissible control function $\overline{u}$ such that $\overline{x}(t_1, \overline{u}) = \overline{x}_1$.
For a *time-invariant linear system* in the form:

$$\dot{\overline{x}} = \boldsymbol{A}\overline{x}(t) + \boldsymbol{B}\overline{u}(t) \tag{3.17}$$

we can define the *Controllability Matrix* as follows:

$$\boldsymbol{C}(\boldsymbol{A}, \boldsymbol{B}) = \left[\boldsymbol{B}, \boldsymbol{A}\boldsymbol{B}, \boldsymbol{A}^2\boldsymbol{B}, ..., \boldsymbol{A}^{n-1}\boldsymbol{B}\right] \in \mathbb{R}^{n \times n \cdot m} \tag{3.18}$$

Property

- A system is *controllable* if the *Controllability Matrix* $\boldsymbol{C}$ is full-rank.

For *time-varying linear systems* we can formulate the Silverman-Meadows criteria [28], the *Controllability Matrix* is thus defined:

$$\boldsymbol{C}_v(\boldsymbol{A}, \boldsymbol{B}, t) = [\boldsymbol{P}_0, \boldsymbol{P}_1, \boldsymbol{P}_2, ..., \boldsymbol{P}_{n-1}] \in \mathbb{R}^{n \times n \cdot m} \tag{3.19}$$

where

$$\boldsymbol{P}_0 = \boldsymbol{B}(t), \boldsymbol{P}_{k+1} = -\boldsymbol{A}(t)\boldsymbol{P}_k(t) + \dot{\boldsymbol{P}}_k, k = 0, 1, ..., n-2 \tag{3.20}$$

Theorem

- The system is completely controllable if $rank(\boldsymbol{C}_v) = n$ for some $t \in [t_0, T]$;
- The system is totally controllable if and only if $rank(\boldsymbol{C}_v) = n$ $\forall t \in [t_0, T]$.

3.2 Implementation of LQR for ROE system control

3.2.1 Controllability assessment of ROE system

Let's consider our dynamic system, largely discussed in the previous chapter:

$$\begin{pmatrix} \delta\dot{\overline{X}} \\ \delta\ddot{a}_{drag} \end{pmatrix} = \boldsymbol{A}\left(\overline{X}_c(t)\right)\begin{pmatrix} \delta\overline{X} \\ \delta\dot{a}_{drag} \end{pmatrix} + \boldsymbol{B}\left(\overline{X}_c(t)\right)\overline{u} \tag{3.21}$$

where

$$\boldsymbol{A} = k\begin{bmatrix} 0 & 0 & 0 & 0 & 0 & 0 & \frac{1}{k} \\ -\left(\frac{3}{2}\frac{n_c}{k}+\frac{7}{2}EP\right) & 0 & e_{xi}FGP & e_{yi}FGP & -FS & 0 & 2\left(-\frac{3}{4}\frac{n_c}{k}-\frac{7}{4}EP+\frac{1}{2}e(1-e)FGP\right)\tau \\ \frac{7}{2}e_{yf}Q & 0 & -\left(4e_{xi}e_{yf}G+C\right)Q & -\left(1+4e_{yi}e_{yf}G-D\right)Q & 5e_{yf}S & 0 & \frac{D-e_{xf}}{k}-2e_{yf}Q\left(-\frac{7}{4}+2e(1-e)G\right)\tau \\ -\frac{7}{2}e_{xf}Q & 0 & \left(1+4e_{xi}e_{xf}G-D\right)Q & \left(4e_{xf}e_{yi}G-C\right)Q & -5e_{xf}S & 0 & \frac{C-e_{yf}}{k}+2e_{xf}Q\left(-\frac{7}{4}+2e(1-e)G\right)\tau \\ 0 & 0 & 0 & 0 & 0 & 0 & 0 \\ \frac{7}{2}S & 0 & -4e_{xi}GS & -4e_{yi}GS & 2T & 0 & 2S\left(\frac{7}{4}-2e(1-e)G\right)\tau \\ 0 & 0 & 0 & 0 & 0 & 0 & 0 \end{bmatrix} \tag{3.22}$$

and

$$\boldsymbol{B}\left(\overline{X}_c(t)\right) = \frac{1}{a_c n_c}\begin{bmatrix} \frac{2}{\eta_c}e_c\sin(f_c) & \frac{2}{\eta_c}\left(1+e_c\cos(f_c)\right) & 0 \\ -\frac{2\eta_c^2}{1+e_c\cos(f_c)} & 0 & 0 \\ \eta_c\sin(\omega_c+f_c) & \eta_c\frac{(2+e_c\cos(f_c))\cos(\omega_c+f_c)+e_x}{(1+e_c\cos(f_c))} & \frac{\eta_c e_y}{\tan(i_c)}\frac{\sin(\omega_c+f_c)}{1+e_c\cos(f_c)} \\ -\eta_c\cos(\omega_c+f_c) & \eta_c\frac{(2+e_c\cos(f_c))\sin(\omega_c+f_c)+e_y}{(1+e_c\cos(f_c))} & -\frac{\eta_c e_x}{\tan(i_c)}\frac{\sin(\omega_c+f_c)}{1+e_c\cos(f_c)} \\ 0 & 0 & \eta_c\frac{\cos(\omega_c+f_c)}{1+e_c\cos(f_c)} \\ 0 & 0 & \eta_c\frac{\sin(\omega_c+f_c)}{1+e_c\cos(f_c)} \\ 0 & 0 & 0 \end{bmatrix} \tag{3.23}$$

It can be already seen from (3.22) and (3.23) that, since the last rows of $\boldsymbol{A}$ and $\boldsymbol{B}$ are null, the *Controllability Matrix* has $rank\left(\boldsymbol{C}_v\right) \neq n \ \forall t \in [t_0, T]$. This means that we cannot control the system, since we have no way to control specifically $\delta\dot{a}_{drag}$.
In order to solve this issue, the effect of differential drag can be implemented in the model as an external disturbance. The system can be therefore written as follows:

$$\delta\dot{\overline{X}} = \boldsymbol{A}'\left(\overline{X}_c(t)\right)\delta\overline{X} + \boldsymbol{B}'\left(\overline{X}_c(t)\right)\overline{u} \tag{3.24}$$

$$\delta\overline{Y} = \boldsymbol{C}_o\left(\overline{X}_c(t)\right)\begin{pmatrix} \delta\overline{X} \\ \delta\dot{a}_{drag} \end{pmatrix} \tag{3.25}$$

where $\delta\dot{\overline{Y}}$ is the *output* state vector.

$$\boldsymbol{A}'\left(\overline{X}_c(t)\right) = k\begin{bmatrix} 0 & 0 & 0 & 0 & 0 & 0 \\ -\left(\frac{3}{2}\frac{n_c}{k}+\frac{7}{2}EP\right) & 0 & e_{xi}FGP & e_{yi}FGP & -FS & 0 \\ \frac{7}{2}e_{yf}Q & 0 & -\left(4e_{xi}e_{yf}G+C\right)Q & -\left(1+4e_{yi}e_{yf}G-D\right)Q & 5e_{yf}S & 0 \\ -\frac{7}{2}e_{xf}Q & 0 & \left(1+4e_{xi}e_{xf}G-D\right)Q & \left(4e_{xf}e_{yi}G-C\right)Q & -5e_{xf}S & 0 \\ 0 & 0 & 0 & 0 & 0 & 0 \\ \frac{7}{2}S & 0 & -4e_{xi}GS & -4e_{yi}GS & 2T & 0 \end{bmatrix} \tag{3.26}$$

$$\boldsymbol{B}'\left(\overline{X}_c(t)\right) = \frac{1}{a_c n_c}\begin{bmatrix} \frac{2}{\eta_c}e_c\sin(f_c) & \frac{2}{\eta_c}\left(1+e_c\cos(f_c)\right) & 0 \\ -\frac{2\eta_c^2}{1+e_c\cos(f_c)} & 0 & 0 \\ \eta_c\sin(\omega_c+f_c) & \eta_c\frac{(2+e_c\cos(f_c))\cos(\omega_c+f_c)+e_x}{(1+e_c\cos(f_c))} & \frac{\eta_c e_y}{\tan(i_c)}\frac{\sin(\omega_c+f_c)}{1+e_c\cos(f_c)} \\ -\eta_c\cos(\omega_c+f_c) & \eta_c\frac{(2+e_c\cos(f_c))\sin(\omega_c+f_c)+e_y}{(1+e_c\cos(f_c))} & -\frac{\eta_c e_x}{\tan(i_c)}\frac{\sin(\omega_c+f_c)}{1+e_c\cos(f_c)} \\ 0 & 0 & \eta_c\frac{\cos(\omega_c+f_c)}{1+e_c\cos(f_c)} \\ 0 & 0 & \eta_c\frac{\sin(\omega_c+f_c)}{1+e_c\cos(f_c)} \end{bmatrix} \tag{3.27}$$

$$\boldsymbol{C}_o\left(\overline{X}_c\left(t\right)\right)=\left[\boldsymbol{I}^{6\times6},\overline{0}^{6\times1}\right]+\int_t^{t+\tau}\left(\boldsymbol{A}^{drag}_{6\times7}\left(\overline{X}_c\left(t\right),\tau\right)\right)dt \tag{3.28}$$

$$\boldsymbol{C}_o\left(\overline{X}_c\left(t\right)\right)=k\begin{bmatrix}1&0&0&0&0&0&\frac{\tau}{k}\\0&1&0&0&0&0&\left(-\frac{3}{4}\frac{n_c}{k}-\frac{7}{4}EP+\frac{1}{2}e\left(1-e\right)FGP\right)\tau^2\\0&0&1&0&0&0&\frac{D-e_{xf}}{k}\tau-e_{yf}Q\left(-\frac{7}{4}+2e\left(1-e\right)G\right)\tau^2\\0&0&0&1&0&0&\frac{C-e_{yf}}{k}\tau+e_{xf}Q\left(-\frac{7}{4}+2e\left(1-e\right)G\right)\tau^2\\0&0&0&0&1&0&0\\0&0&0&0&0&1&S\left(\frac{7}{4}-2e\left(1-e\right)G\right)\tau^2\end{bmatrix} \tag{3.29}$$

where $\boldsymbol{A}^{drag}_{6\times7}$ is the $\boldsymbol{A}^{drag}$ matrix without the last row.
Using this new configuration, the system is *totally controllable* in the interval $[t_0, T]$

3.2.2 Software Implementation

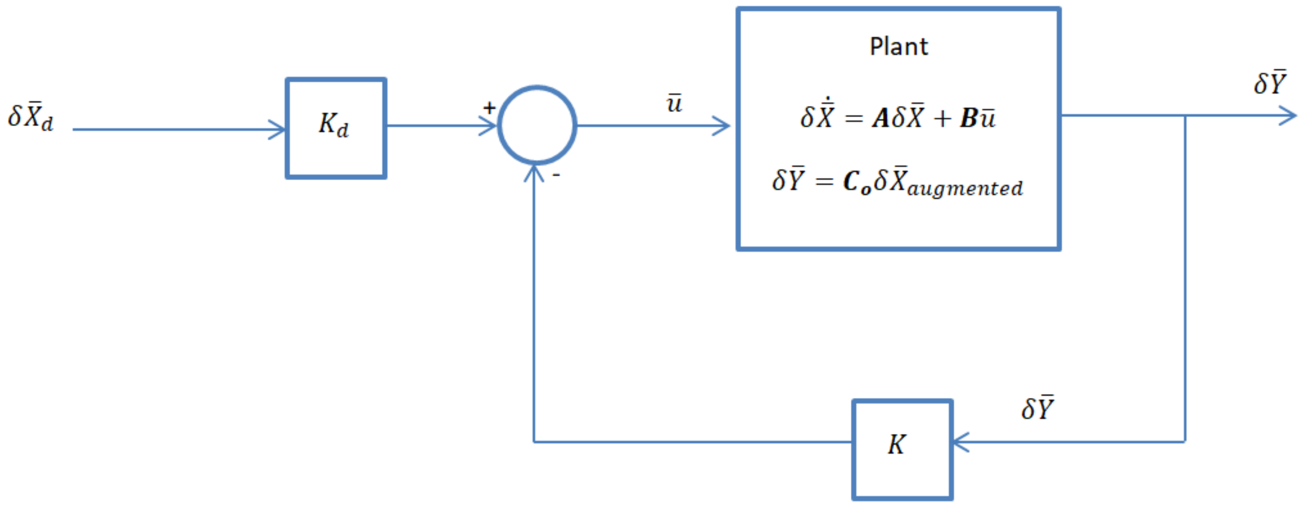

Figure 3.1: LQR Feedback Controller block scheme.

Since our controller must track the desired reference state vector $\overline{X}_d$, the control will be in the form:

$$\overline{u}\left(t\right)=-\boldsymbol{K}\delta\overline{Y}+\boldsymbol{K}_d\delta\overline{X}_d \tag{3.30}$$

where $\boldsymbol{K}_d$ is the reference Gain Matrix that takes in account steady-state errors, $\boldsymbol{K}_d=\boldsymbol{K}$ will be used in this framework.
In order to solve the *Differential Riccati Equation*, a final condition on $\boldsymbol{M}$ will be imposed as follows:

$$\boldsymbol{M}\left(T\right)=\boldsymbol{0} \tag{3.31}$$

This means that at time T, i.e. when $\overline{X}_d$ will be reached, the Gain Matrix will be $\boldsymbol{0}$ as well:

$$\boldsymbol{K}\left(T\right)=-\boldsymbol{R}^{-1}\boldsymbol{B}^T\left(T\right)\boldsymbol{M}\left(T\right)=\boldsymbol{0} \tag{3.32}$$

The cost function to be minimized is then:

$$J\left(t_0\right)=\frac{1}{2}\int_{t_0}^{T}\left(\delta\overline{x}^T\boldsymbol{Q}\left(t\right)\delta\overline{x}+\overline{u}^T\boldsymbol{R}\left(t\right)\overline{u}\right)dt \tag{3.33}$$

It can be seen that for the *Finite-Horizon* approach, a backward integration of the *Differential Riccati Equation* is needed in order to obtain $\boldsymbol{M}\left(t\right)$. Known data:

- Chief's state $\overline{X}_c$;
- Initial relative state $\delta\overline{X}_0$;
- Final relative state $\delta\overline{X}_d$;
- Initial time t_0;
- Final time T;
- $\boldsymbol{Q}$ and $\boldsymbol{R}$ matrices.

Unknown:

- Control $\overline{u}$

The model has been implemented using *MATLAB*®, where the backward integration of the Differential Riccati Equation is possible thanks to the command *ode*.

Figure 3.2: MATLAB® logo. Credits: *Mathworks*

The flowchart describing the sequence of operations performed by *MATLAB*® is showed in fig. 3.3, for both Finite-Horizon and Infinite-Horizon cases.

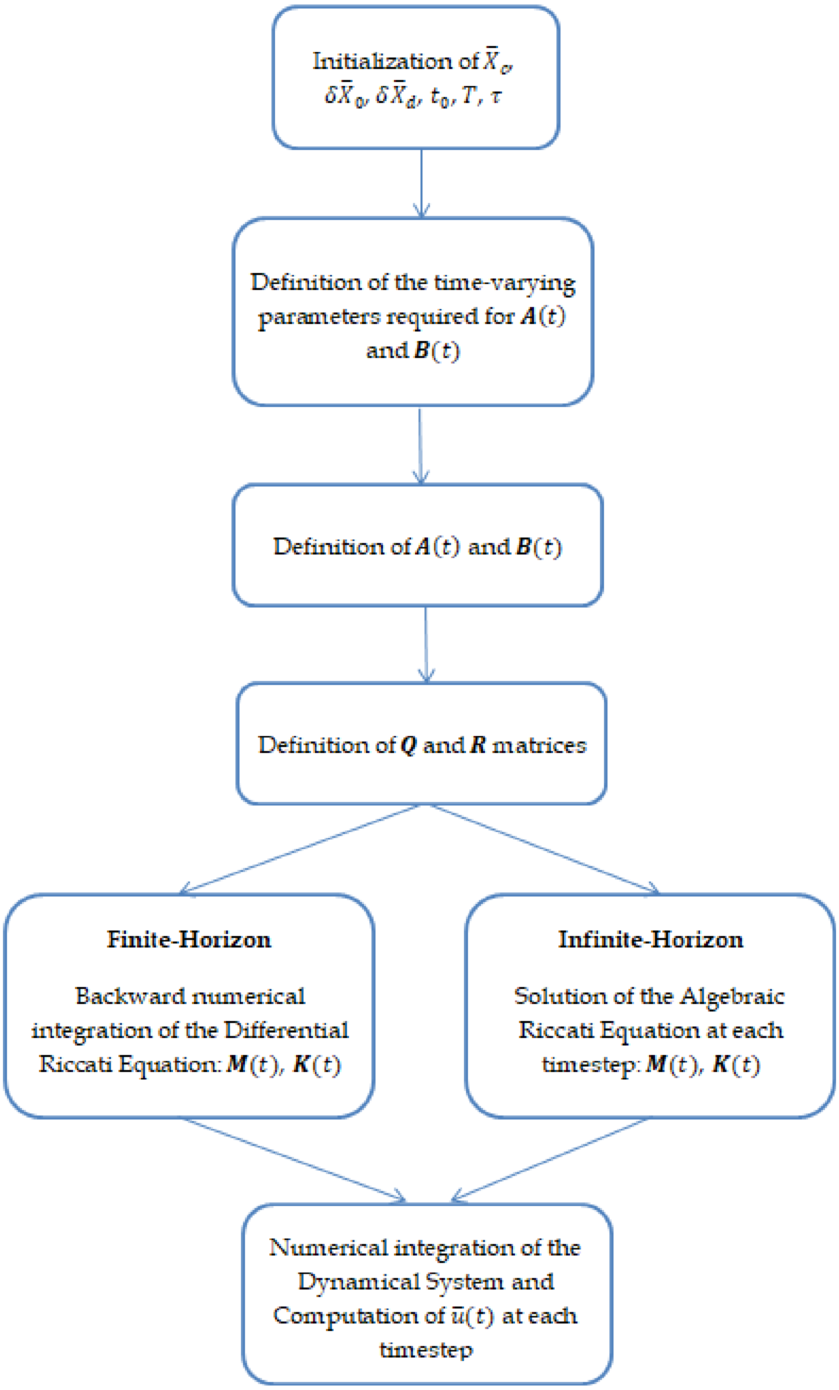

Figure 3.3: Flowchart of the algorithm.

3.3 Model testing and results

3.3.1 Input Data

Let's consider a scenario with a *Virtual Leader* and another spacecraft, the goal is to control the second spacecraft from an initial relative state with respect to the virtual leader to a final state in the given time $[t_0, T]$. The chosen Chief's reference orbit, expressed in classical orbital elements, is:

$$\overline{X}_c = \begin{pmatrix} a_c \\ e_c \\ i_c \\ \Omega_c \\ \omega_c \\ f_c \end{pmatrix} = \begin{pmatrix} 6878km \\ 0.0002 \\ 110\deg \\ 260\deg \\ 90\deg \\ 315\deg \end{pmatrix} \tag{3.34}$$

It should be noted that these elements are different from the mean orbital elements, and they vary a lot throughout the mission. In order to implement the Mean ROE model, we should convert this set of orbital parameters into mean orbital parameters; this can be done using *GMAT®*, an open-source software developed by NASA (fig. 3.4), which implements a *Brouwer-Lyddane* theory-based algorithm to compute short-term and long-term averaged orbital elements.

Figure 3.4: GMAT® logo. Credits: *NASA*

Since we will consider a mission time of one order of magnitude greater than the orbital period, the long-term average of orbital parameters will be used:

$$\overline{X}_c = \begin{pmatrix} a_c \\ e_c \\ i_c \\ \Omega_c \\ \omega_c \\ M_0 \end{pmatrix} = \begin{pmatrix} 6878km \\ 0.000935 \\ 110\deg \\ 260.5\deg \\ 310.6\deg \\ 90\deg \end{pmatrix} \tag{3.35}$$

These elements remain approximately constant throughout the mission, except for the mean anomaly that increases linearly, $M = M_0 + n_c t$.
We can compute the orbital period:

$$T_{orbit} = 2\pi\sqrt{\frac{a_c^3}{\mu}} \simeq 5677s \tag{3.36}$$

Let's set the initial and final mission times:

$$t_0 = 0 \tag{3.37}$$

$$T = 15 \cdot T_{orbit} \simeq 85152s \tag{3.38}$$

The initial and final relative states (expressed in meters) are:

ROE Variable	Initial	Final
$a_c \cdot 1000 \cdot \delta a$	$0m$	$0m$
$a_c \cdot 1000 \cdot \delta \lambda$	$800m$	$250m$
$a_c \cdot 1000 \cdot \delta e_x$	$600m$	$250m$
$a_c \cdot 1000 \cdot \delta e_y$	$600m$	$250m$
$a_c \cdot 1000 \cdot \delta i_x$	$0m$	$0m$
$a_c \cdot 1000 \cdot \delta i_y$	$500m$	$250m$

Table 3.1: Initial and final relative states.

The chosen $\boldsymbol{Q}$ and $\boldsymbol{R}$ matrices are:

$$\boldsymbol{Q} = \begin{bmatrix} 1 & 0 & 0 & 0 & 0 & 0 \\ 0 & 1 & 0 & 0 & 0 & 0 \\ 0 & 0 & 1 & 0 & 0 & 0 \\ 0 & 0 & 0 & 1 & 0 & 0 \\ 0 & 0 & 0 & 0 & 5 & 0 \\ 0 & 0 & 0 & 0 & 0 & 5 \end{bmatrix} \tag{3.39}$$

$$\boldsymbol{R} = \begin{bmatrix} 3 & 0 & 0 \\ 0 & 3 & 0 \\ 0 & 0 & 3 \end{bmatrix} \tag{3.40}$$

3.3.2 Results

State

The evolution of the spacecraft relative state with respect to the virtual chief, for both Finite-Horizon and Infinite-Horizon approaches, is showed in fig. 3.5a and fig. 3.5b.
As regards the Infinite-Horizon approach, it can be seen that δe_x and δe_y are not converging to the desired final state. This is a critical issue related to the chosen timestep τ, that should be:

- Small enough in order to consider $\boldsymbol{A}(t)$ and $\boldsymbol{B}(t)$ constant;
- Large enough in order to let the system converge to the instant solution.

Unfortunately, there is no timestep that satisfies both those conditions; therefore the conclusion is that the Infinite-Horizon approach is not suitable for this problem.
Concerning the Finite-Horizon approach, since we are considering that $\dot{\boldsymbol{M}} \neq 0$ by integrating the Differential Riccati Equation, the timestep doesn't have to satisfy the second condition anymore; therefore the system will converge to the final state, given that the timestep itself is sufficiently small.

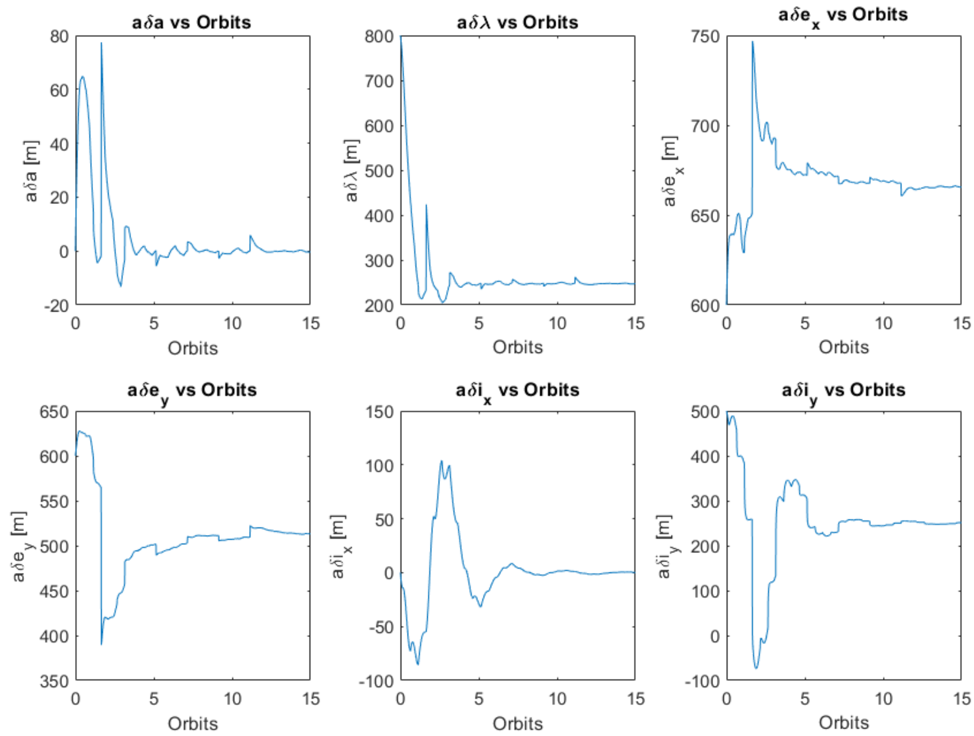

(a) Infinite-Horizon, relative state evolution.

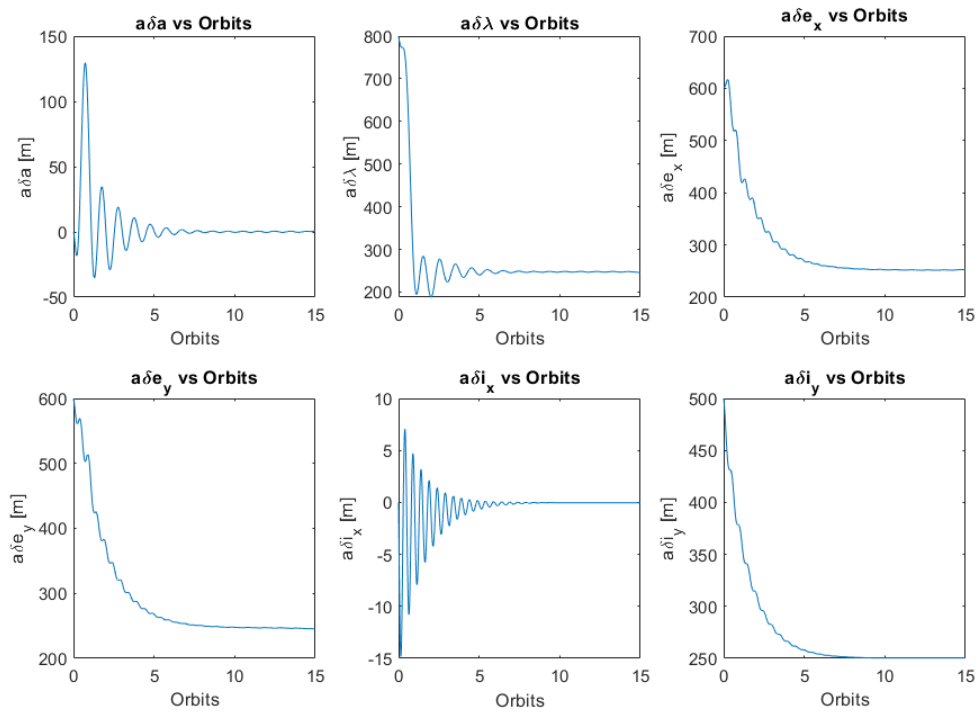

(b) Finite-Horizon, relative state evolution.

Figure 3.5: Comparison between Infinite-Horizon and Finite-Horizon relative state evolutions.

ROE Variable	Desired	Final
$a_c \cdot 1000 \cdot \delta a$	$0m$	$0.7590m$
$a_c \cdot 1000 \cdot \delta\lambda$	$250m$	$245.4m$
$a_c \cdot 1000 \cdot \delta e_x$	$250m$	$253.0m$
$a_c \cdot 1000 \cdot \delta e_y$	$250m$	$245.1m$
$a_c \cdot 1000 \cdot \delta i_x$	$0m$	$-0.03169m$
$a_c \cdot 1000 \cdot \delta i_y$	$250m$	$250.4m$

Table 3.2: Finite-Horizon: Desired and final relative states.

Control

In order to simulate a real micro-Newton thruster, a thrust range of $0.1\mu N - 2mN$ has been imposed; if the thrust level is below the minimum limit, the thruster will be turned off:

$$u\left(t_i\right) = \begin{cases} 0 \quad if\ mass \cdot u\left(t_i\right) < 0.1\mu N \\ u\left(t_i\right) \quad otherwise \end{cases} \tag{3.41}$$

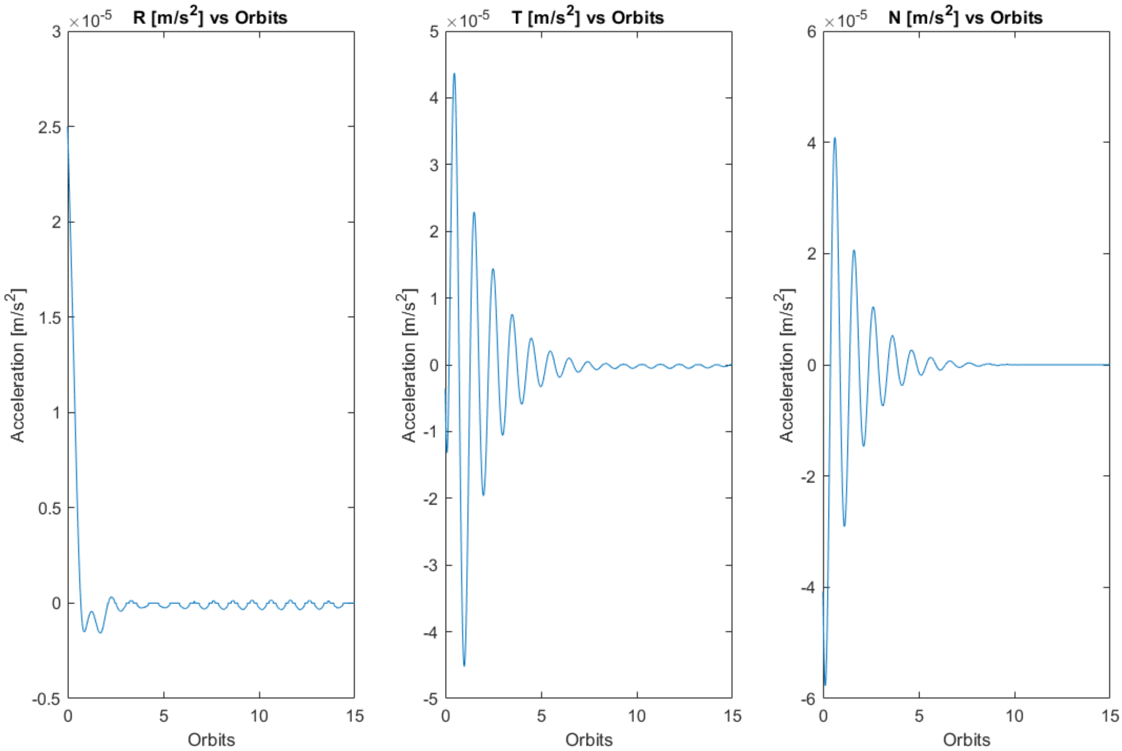

Figure 3.6: Control Accelerations in the RTN Directions.

The total acceleration magnitude can be calculated as follows:

$$u_{tot}\left(t\right) = \sqrt{u_R^2\left(t\right) + u_T^2\left(t\right) + u_N^2\left(t\right)} \tag{3.42}$$

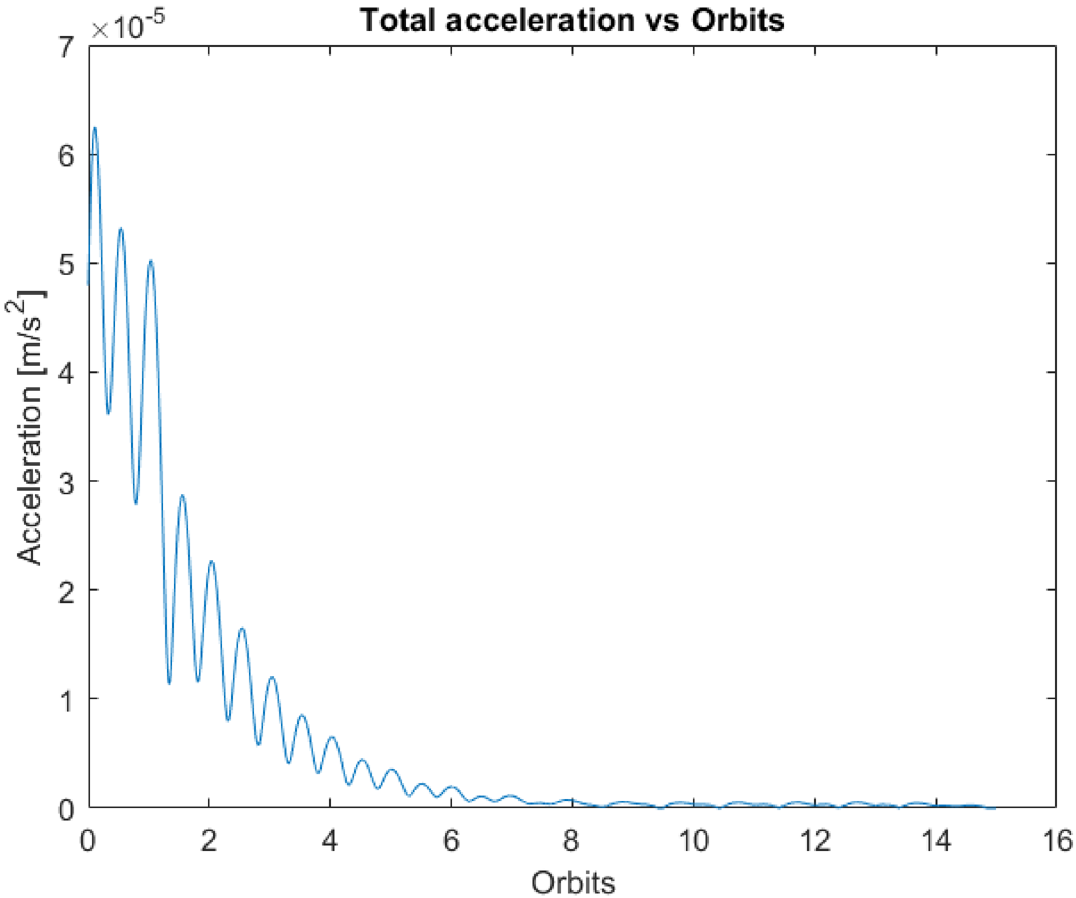

Figure 3.7: Total acceleration magnitude over time (in orbits).

ΔV

Using 2.36, the ΔV lower bound for the maneuver can be computed as:

$$\Delta V_{LB} = n_c a_c \eta_c \left(\frac{|\Delta \delta \bar{e}|}{2\eta_c^2} + \frac{1 - e_c}{\eta_c^2} \left| \Delta \delta \bar{i} \right| \right) = 0.5504 \frac{m}{s} \tag{3.43}$$

The real ΔV can be computed by integrating numerically the total acceleration magnitude profile, shown in fig. 3.7, over time. The result of this operation is shown in fig. 3.8.
The value of the real ΔV required by the maneuver can be found in 3.3, it can be seen that it is only 2.1% more than the optimal ΔV.

	Lower Bound	Real
ΔV	$0.5504 \frac{m}{s}$	$0.5619 \frac{m}{s}$

Table 3.3: Comparison between the real ΔV and the lower bound.

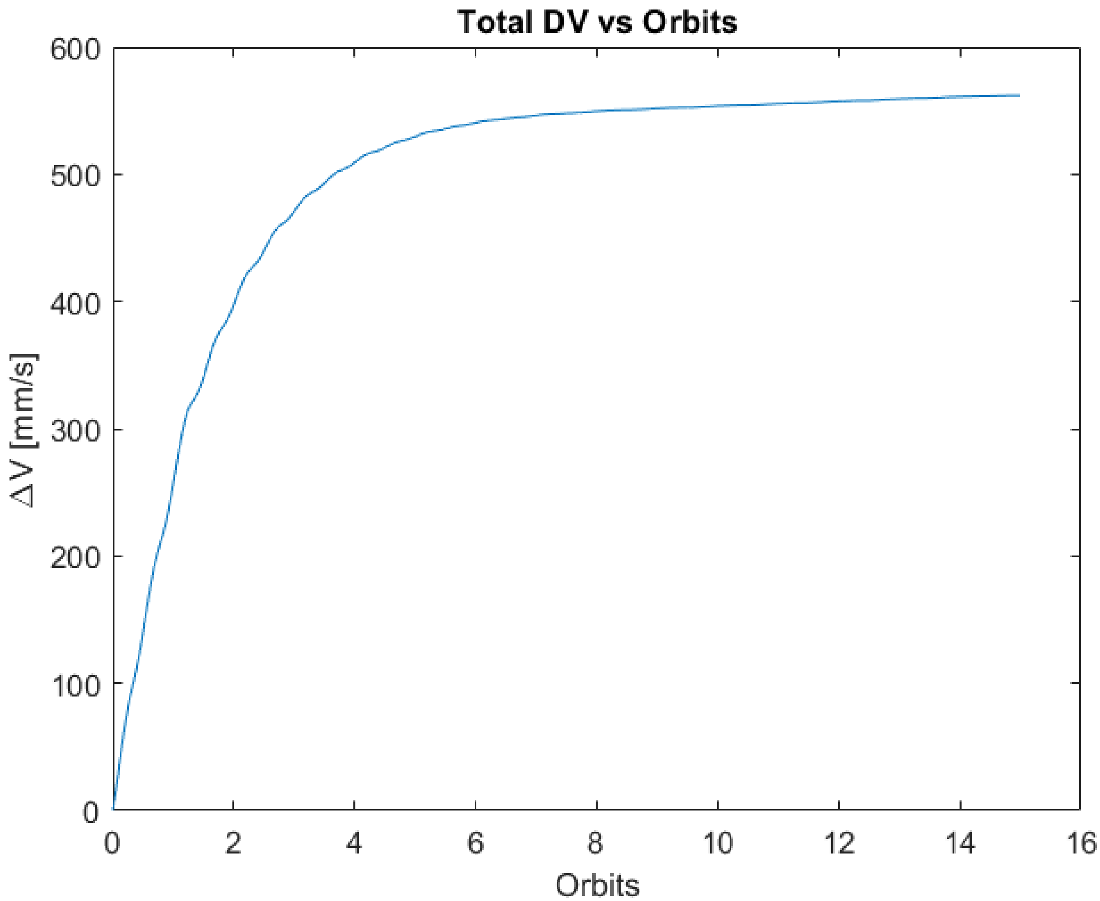

Figure 3.8: ΔV over time (in orbits).

Chapter 4

Collision Avoidance using Artificial Potential functions

4.1 Mathematical Overview

4.1.1 Introduction

Satellites in a formation might need to maneuver to avoid potential collisions that may occur when a satellite within the formation drifts into the path of another. In order to guide and control satellites toward their desired final states while assuring collision avoidance at the same time, we need to find a way to guide the state vector along collision-free reference trajectories. To do so, the following strategy is presented in this work:

- Definition of a *Reference Governor* strategy in order to guide the satellite state vector along a reference trajectory, the controller will track the instant *applied reference* instead of the desired reference itself;
- Calculation of the minimum distance between satellites using Eccentricity/Inclination vectors separation [25];
- Definition of an Artificial Potential Field in order to update the applied reference at each timestep.

4.1.2 Reference Governor

Instead of applying a control of the type $\overline{u}\,(t) = -\boldsymbol{K}\delta\overline{Y} + \boldsymbol{K}_d\delta\overline{X}_d$ that will guide the state vector linearly towards the desired reference, we can think about introducing an *applied reference* $\delta\overline{X}_a$ that can be used to guide the state $\delta\overline{X}$ along a reference trajectory. In order to do so, we need to apply a control in the form:

$$\overline{u}\,(t) = -\boldsymbol{K}\delta\overline{Y} + \boldsymbol{K}_d\delta\overline{X}_a \tag{4.1}$$

and we need to update $\delta\overline{X}_a$ at each iteration according to some particular law that allows us to compute $\delta\dot{\overline{X}}_a$.

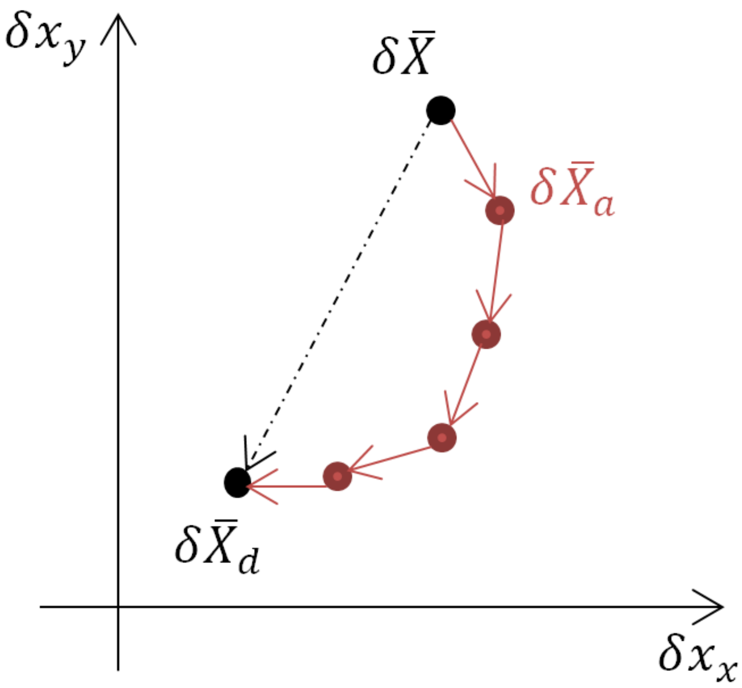

Figure 4.1: Applied reference concept.

In order to guarantee that $\delta\overline{X}_a$ would converge to $\delta\overline{X}_d$, we need to define a *global attractive potential field* centered in $\delta\overline{X}_d$ that allows us to compute the required $\delta\dot{\overline{X}}_a$ [29]. This potential field can be defined as:

$$\varphi_{global} = \begin{cases} \left|\delta\overline{X}_a - \delta\overline{X}_d\right| & if \left|\delta\overline{X}_a - \delta\overline{X}_d\right| \geq \eta \\ \frac{1}{2}\frac{\left|\delta\overline{X}_a - \delta\overline{X}_d\right|^2}{\eta} + \frac{1}{2}\eta & otherwise \end{cases} \tag{4.2}$$

where $\eta \in \mathbb{R}$ and $\eta \geq 1$.
The *gradient* of this potential field is given by:

$$\nabla\overline{\varphi}_{global} = \frac{\delta\overline{X}_a - \delta\overline{X}_d}{max\left(\left|\delta\overline{X}_a - \delta\overline{X}_d\right|, \eta\right)} \tag{4.3}$$

Which is unitary if $\left|\delta\overline{X}_a - \delta\overline{X}_d\right| \geq \eta$ and tends to zero if $\left|\delta\overline{X}_a - \delta\overline{X}_d\right| < \eta$. The parameter η is defined such that the gradient tends to zero for very small tracking errors with respect to the desired reference $\delta\overline{X}_d$.
At this point we can compute the applied reference gradient as follows:

$$\overline{\rho}_{global} = -\varepsilon\nabla\overline{\varphi}_{global} \tag{4.4}$$

$$\delta\dot{\overline{X}}_a = \overline{\rho}_{global} \tag{4.5}$$

where $\varepsilon \in \mathbb{R}^+$ is an arbitrary small scaling factor, $\varepsilon = \frac{1}{\tau}$ will be assumed.
Now we can update the applied reference:

$$\delta\overline{X}_a\left(t+\tau\right) = \delta\overline{X}_a\left(t\right) + \delta\dot{\overline{X}}_a\tau \tag{4.6}$$

4.1.3 Reference Governor model testing and results

Let's test this Finite-Horizon Reference Governor-based model using the same scenario of the previous chapter.

Input Data

- $\overline{X}_c$ as in (3.35);
- t_0 and T as in (3.37) and (3.38);
- Initial and Desired states as in table 3.1.

The chosen $\boldsymbol{Q}$ and $\boldsymbol{R}$ matrices are:

$$\boldsymbol{Q} = \begin{bmatrix} 2 & 0 & 0 & 0 & 0 & 0 \\ 0 & 2 & 0 & 0 & 0 & 0 \\ 0 & 0 & 2 & 0 & 0 & 0 \\ 0 & 0 & 0 & 2 & 0 & 0 \\ 0 & 0 & 0 & 0 & 2 & 0 \\ 0 & 0 & 0 & 0 & 0 & 2 \end{bmatrix} \tag{4.7}$$

$$\boldsymbol{R} = \begin{bmatrix} 1 & 0 & 0 \\ 0 & 1 & 0 \\ 0 & 0 & 1 \end{bmatrix} \tag{4.8}$$

State

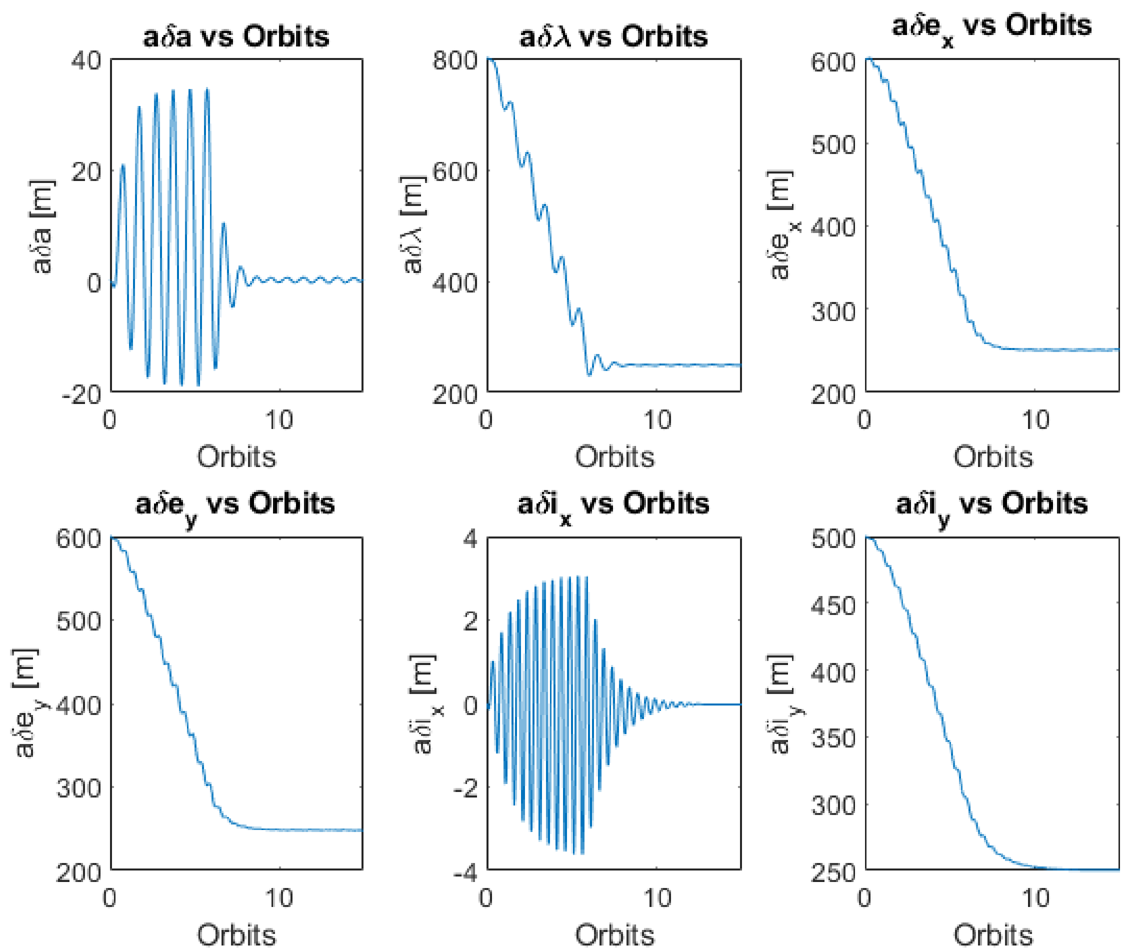

Figure 4.2: Finite-Horizon Reference Governor model relative state evolution.

ROE Variable	Desired	Final
$a_c \cdot 1000 \cdot \delta a$	$0m$	$0.2139m$
$a_c \cdot 1000 \cdot \delta \lambda$	$250m$	$248.5m$
$a_c \cdot 1000 \cdot \delta e_x$	$250m$	$251.5m$
$a_c \cdot 1000 \cdot \delta e_y$	$250m$	$248.0m$
$a_c \cdot 1000 \cdot \delta i_x$	$0m$	$-0.02274m$
$a_c \cdot 1000 \cdot \delta i_y$	$250m$	$250.4m$

Table 4.1: Finite-Horizon RG: Desired and final relative states.

Control

A thrust range constraint of $0.1\mu N - 2mN$ has been imposed also in this case; if the thrust level is below the minimum limit, the thruster will be turned off as in (3.41).

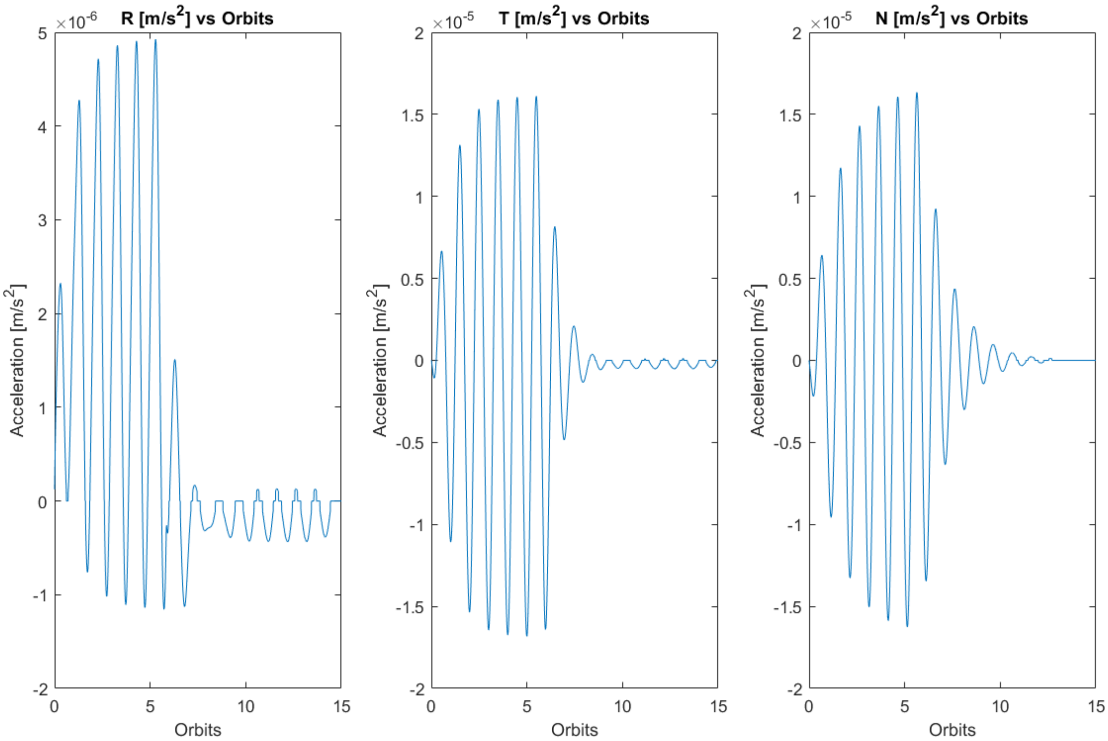

Figure 4.3: Finite-Horizon RG: Control Accelerations in the RTN Directions.

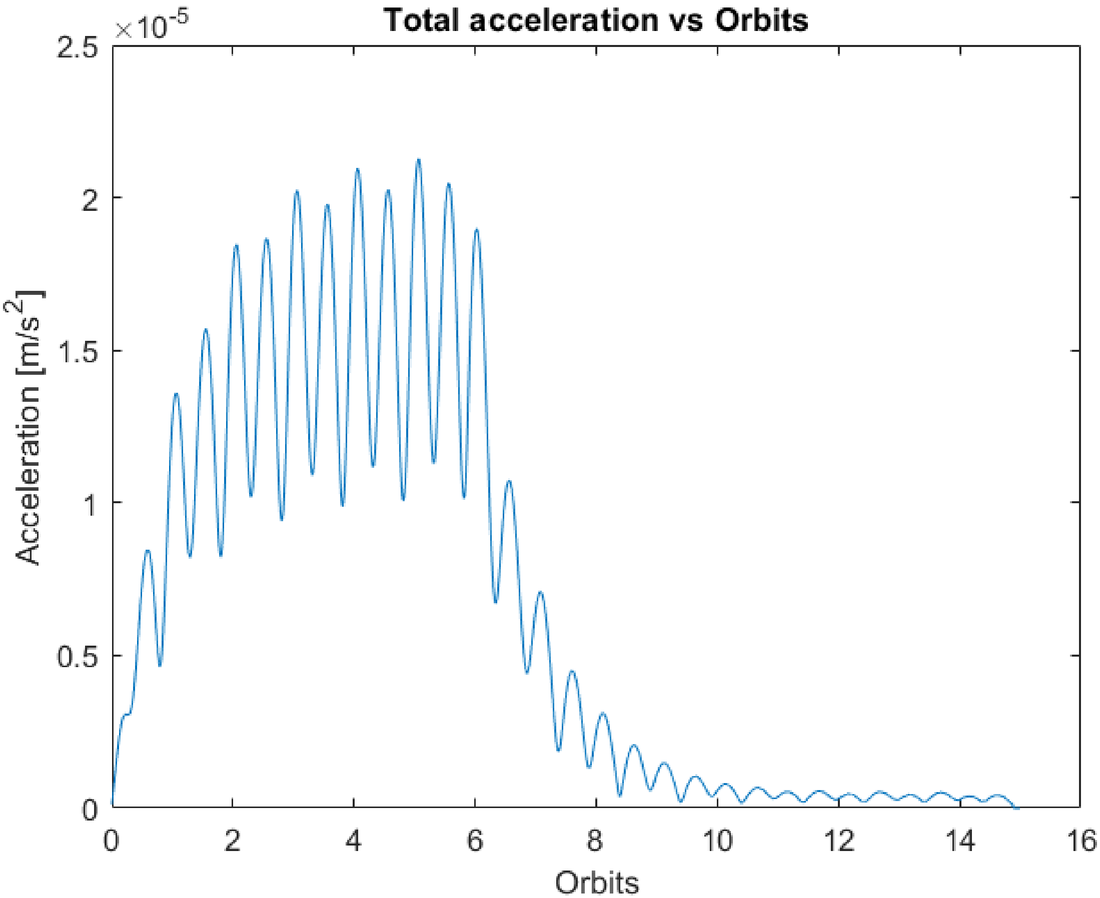

Figure 4.4: Finite-Horizon RG: Total acceleration magnitude over time (in orbits).

ΔV

The ΔV lower bound for the maneuver can be computed in the same way as (3.43).
The numerical integration of the acceleration magnitude profile (fig. 4.4) is shown in fig. 4.5.
A comparison between the value of the real ΔV required by the maneuver, the real ΔV of the previous scenario and the lower bound can be found in 4.2.

	Lower Bound	Finite-Horizon	Reference Governor
ΔV	$0.5504\frac{m}{s}$	$0.5619\frac{m}{s}$	$0.5563\frac{m}{s}$
% more than LB	0	2.1	1.1

Table 4.2: Comparison between the RG ΔV, the FH ΔV and the lower bound.

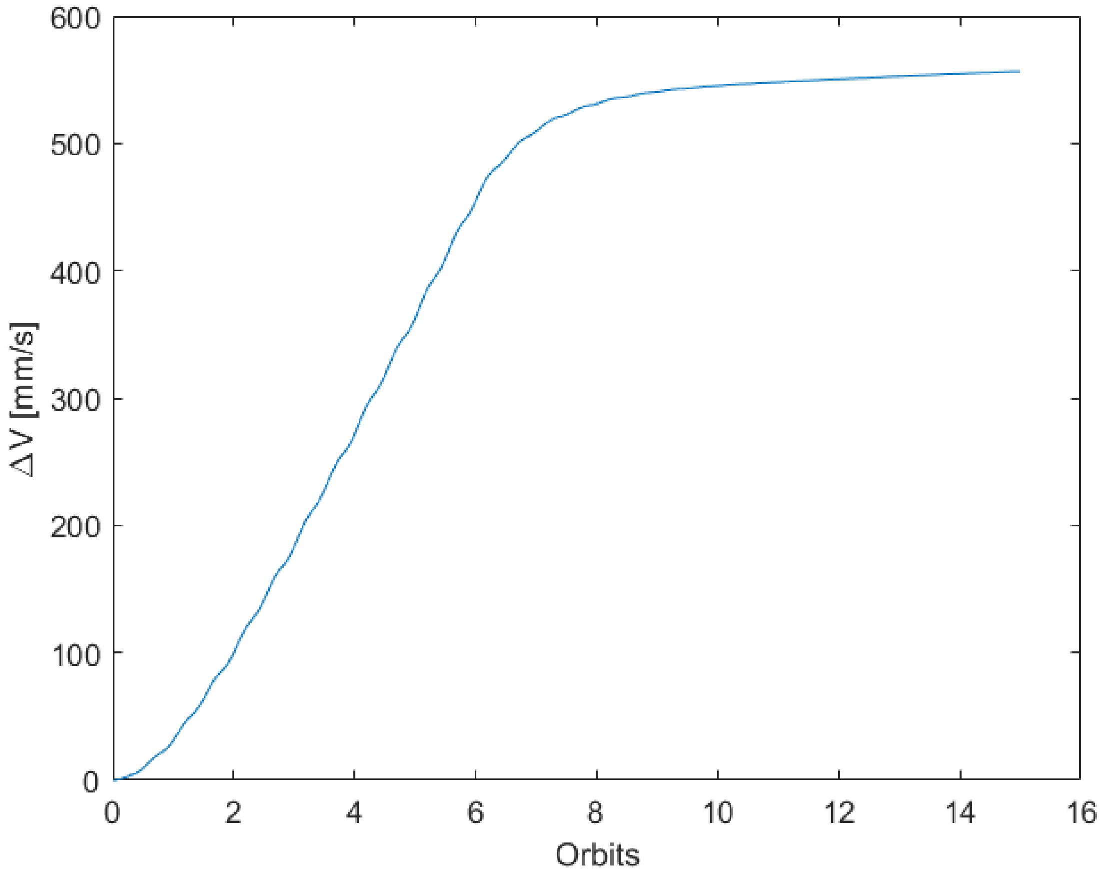

Figure 4.5: Finite-Horizon RG: ΔV over time (in orbits).

As we can see, the Reference Governor-based model performs better both in terms of state convergence and fuel optimality.

4.1.4 Minimum distance using Eccentricity/Inclination vector separation

The concept of e/i-vector separation has originally been developed for the safe collocation of geostationary satellites [24], but can likewise be applied for proximity operations in LEO formations [25], as showed in section *2.1.3*. It is based on the consideration that the uncertainty in predicting the along-track separation of two spacecraft is generally much higher than for the radial and cross-track component. Because of the coupling between semi-major axis and orbital period, small uncertainties in the initial position and velocity result in a corresponding drift error and thus a secularly growing along-track error. Predictions of the relative motion over extended periods of time are therefore particularly sensitive to both orbit determination errors and maneuver execution errors [10].
To avoid a collision hazard in the presence of along-track position uncertainties, care must be taken to properly separate the two spacecraft in radial and cross-track direction. As shown for GEO satellites, this can be achieved by a parallel (or anti-parallel) alignment of the relative eccentricity and inclination vectors. It is utterly important to avoid at all costs that eccentricity and inclination vectors become perpendicular, because in that case the distance in radial and cross-track direction vanishes and collision avoidance cannot be guaranteed (fig. 2.4). The relative distance between deputy and chief spacecraft, projected onto the cross-track/radial

plane, is:

$$\delta r_{nr} = \sqrt{\delta r_n^2 + \delta r_r^2} \tag{4.9}$$

Using relative orbital elements, and assuming bounded relative motion $\delta a = 0$, the minimum distance in the radial and cross-track plane can be expressed in meters as:

$$\delta r_{nr}^{min} = a_c \cdot 1000 \cdot \frac{\sqrt{2}\left|\delta\overline{e} \cdot \delta\overline{i}\right|}{\left(\left|\delta\overline{e}\right|^2 + \left|\delta\overline{i}\right|^2 + \left|\delta\overline{e} + \delta\overline{i}\right| \cdot \left|\delta\overline{e} - \delta\overline{i}\right|\right)^{\frac{1}{2}}} \tag{4.10}$$

It can be seen that this distance is maximum when eccentricity and inclination vectors are parallel (or anti-parallel) and is null when they are perpendicular. Furthermore, considering parallel eccentricity and inclination vectors, this distance increases as $\delta\overline{e}$ and $\delta\overline{i}$ increase.

4.1.5 Artificial Potential Field for Collision Avoidance

Let's consider two satellites with state vectors $\delta\overline{X}_1$ and $\delta\overline{X}_2$, we can compute the relative state between these two satellites as:

$$\Delta\delta\overline{X} = \delta\overline{X}_1 - \delta\overline{X}_2 = \begin{pmatrix} \Delta\delta a \\ \Delta\delta\lambda \\ \Delta\delta e_x \\ \Delta\delta e_y \\ \Delta\delta i_x \\ \Delta\delta i_y \end{pmatrix} \tag{4.11}$$

The relative applied reference state can be computed as well:

$$\Delta\delta\overline{X}_a = \delta\overline{X}_{a_1} - \delta\overline{X}_{a_2} = \begin{pmatrix} \Delta\delta a_a \\ \Delta\delta\lambda \\ \Delta\delta e_{x_a} \\ \Delta\delta e_{y_a} \\ \Delta\delta i_{x_a} \\ \Delta\delta i_{y_a} \end{pmatrix} \tag{4.12}$$

Since the Artificial Potential field will affect the applied references, it makes sense to consider the minimum radial and cross-track relative distance between the two applied references:

$$\delta r_{a_{nr}}^{min} = a_c \cdot 1000 \cdot \frac{\sqrt{2}\left|\Delta\delta\overline{e}_a \cdot \Delta\delta\overline{i}_a\right|}{\left(\left|\Delta\delta\overline{e}_a\right|^2 + \left|\Delta\delta\overline{i}_a\right|^2 + \left|\Delta\delta\overline{e}_a + \Delta\delta\overline{i}_a\right| \cdot \left|\Delta\delta\overline{e}_a - \Delta\delta\overline{i}_a\right|\right)^{\frac{1}{2}}} \tag{4.13}$$

Assumption:

- $\Delta\delta\overline{e}_a$ and $\Delta\delta\overline{i}_a$ are never perpendicular throughout the mission.

In order to define the potential field for collision avoidance, few parameters should be introduced first:

- ζ is the *influence distance*, i.e. the distance from where the repulsive potential field starts to act;
- γ is the *safety margin*, i.e. the distance where the repulsive potential field reaches its maximum;

Since the distance depends on $\Delta\delta\bar{e}_a$ and $\Delta\delta\bar{i}_a$, we can think about defining a 4D repulsive potential field; we need then a matrix that enables those variables of the state vector:

$$\boldsymbol{G} = \begin{bmatrix} 0 & 0 & 1 & 0 & 0 & 0 \\ 0 & 0 & 0 & 1 & 0 & 0 \\ 0 & 0 & 0 & 0 & 1 & 0 \\ 0 & 0 & 0 & 0 & 0 & 1 \end{bmatrix}^T \tag{4.14}$$

The *repulsive potential field* is defined as [29]:

$$\varphi_{collision} = \begin{cases} \frac{1}{2}\frac{\gamma^2(\delta r_{a_{nr}} - \zeta)^2}{\delta r_{a_{nr}}(\gamma^2 - \zeta^2)} & if\ \delta r_{a_{nr}} \leq \zeta \\ 0 & otherwise \end{cases} \tag{4.15}$$

The gradient of this potential field is given by:

$$\nabla\overline{\varphi}_{collision} = max\left(min\left(\frac{\gamma^2\left(\delta r^2_{a_{nr}} - \zeta^2\right)}{\delta r^2_{a_{nr}}\left(\gamma^2 - \zeta^2\right)}, 1\right), 0\right) \cdot \boldsymbol{G} \cdot \frac{\boldsymbol{G}^T \Delta\delta\overline{X}_a}{\left|\boldsymbol{G}^T \Delta\delta\overline{X}_a\right|} \tag{4.16}$$

It can be seen that $\nabla\overline{\varphi}_{collision} = \overline{0}$ if $\delta r^{min}_{a_{nr}} \geq \zeta$, $\nabla\overline{\varphi}_{collision} = \boldsymbol{G} \cdot \frac{\boldsymbol{G}^T \Delta\delta\overline{X}_a}{\left|\boldsymbol{G}^T \Delta\delta\overline{X}_a\right|}$ if $\delta r^{min}_{a_{nr}} \leq \gamma$, $0 < \nabla\overline{\varphi}_{collision} < \boldsymbol{G} \cdot \frac{\boldsymbol{G}^T \Delta\delta\overline{X}_a}{\left|\boldsymbol{G}^T \Delta\delta\overline{X}_a\right|}$ if $\gamma < \delta r^{min}_{a_{nr}} < \zeta$.

$$\overline{\rho}_{1_{collision}} = \alpha\nabla\overline{\varphi}_{collision} \tag{4.17}$$

$$\overline{\rho}_{2_{collision}} = -\alpha\nabla\overline{\varphi}_{collision} \tag{4.18}$$

$$\delta\dot{\overline{X}}_{a_1} = \overline{\rho}_{1_{global}} + \overline{\rho}_{1_{collision}} \tag{4.19}$$

$$\delta\dot{\overline{X}}_{a_2} = \overline{\rho}_{2_{global}} + \overline{\rho}_{2_{collision}} \tag{4.20}$$

$$\delta\overline{X}_{a_1}(t+\tau) = \delta\overline{X}_{a_1}(t) + \delta\dot{\overline{X}}_{a_1}\tau \tag{4.21}$$

$$\delta\overline{X}_{a_2}(t+\tau) = \delta\overline{X}_{a_2}(t) + \delta\dot{\overline{X}}_{a_2}\tau \tag{4.22}$$

where $\alpha \in \mathbb{R}^+$ is an arbitrary small scaling factor.

4.2 Scenario for Collision Avoidance potential field testing

4.2.1 Input Data

Let's consider a scenario with two spacecraft whose relative state vector is expressed with respect to a virtual chief. Let the virtual chief orbit be the same as the previous scenarios, see (3.34) and (3.35).
Let's set the initial and final mission times:

- $t_0 = 0$;
- $T = 25T_{orbit} \simeq 141920s$

The initial and final states (expressed in meters) of the two spacecraft are:

ROE Variable	Initial	Final
$a_c \cdot 1000 \cdot \delta a$	$0m$	$0m$
$a_c \cdot 1000 \cdot \delta \lambda$	$0m$	$0m$
$a_c \cdot 1000 \cdot \delta e_x$	$150m$	$550m$
$a_c \cdot 1000 \cdot \delta e_y$	$150m$	$550m$
$a_c \cdot 1000 \cdot \delta i_x$	$100m$	$250m$
$a_c \cdot 1000 \cdot \delta i_y$	$100m$	$250m$

Table 4.3: Collision Avoidance: Initial and final relative states of Spacecraft 1.

ROE Variable	Initial	Final
$a_c \cdot 1000 \cdot \delta a$	$0m$	$0m$
$a_c \cdot 1000 \cdot \delta \lambda$	$0m$	$0m$
$a_c \cdot 1000 \cdot \delta e_x$	$190m$	$348m$
$a_c \cdot 1000 \cdot \delta e_y$	$95m$	$696m$
$a_c \cdot 1000 \cdot \delta i_x$	$126m$	$195m$
$a_c \cdot 1000 \cdot \delta i_y$	$63m$	$290m$

Table 4.4: Collision Avoidance: Initial and final relative states of Spacecraft 2.

The chosen $\boldsymbol{Q}$ and $\boldsymbol{R}$ matrices are:

$$\boldsymbol{Q}_1 = \boldsymbol{Q}_2 = \begin{bmatrix} 2 & 0 & 0 & 0 & 0 & 0 \\ 0 & 2 & 0 & 0 & 0 & 0 \\ 0 & 0 & 2 & 0 & 0 & 0 \\ 0 & 0 & 0 & 2 & 0 & 0 \\ 0 & 0 & 0 & 0 & 2 & 0 \\ 0 & 0 & 0 & 0 & 0 & 2 \end{bmatrix} \tag{4.23}$$

$$\boldsymbol{R}_1 = \boldsymbol{R}_2 = \begin{bmatrix} 1 & 0 & 0 \\ 0 & 1 & 0 \\ 0 & 0 & 1 \end{bmatrix} \tag{4.24}$$

A $\alpha = 0.015$ will be chosen.
Three different cases will be simulated:

- *Case 1*: $\gamma = 0m$, $\zeta = 0m$, i.e. no collision avoidance;
- *Case 2*: $\gamma = 20m$, $\zeta = 25m$;
- *Case 3*: $\gamma = 35m$, $\zeta = 40m$;

4.2.2 Results

State

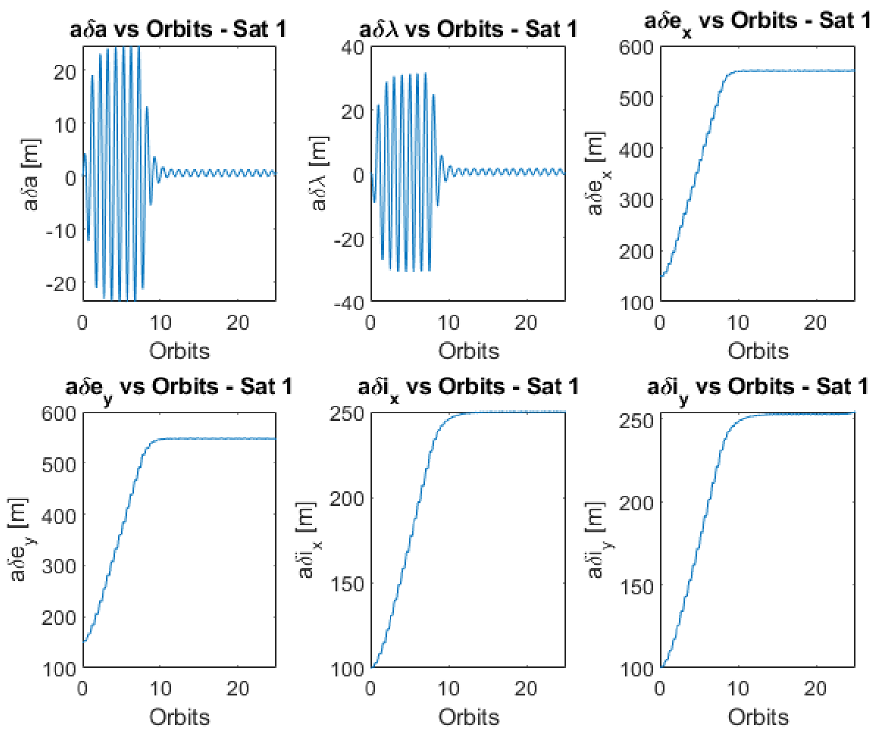

(a) Case 1: Spacecraft 1 state evolution.

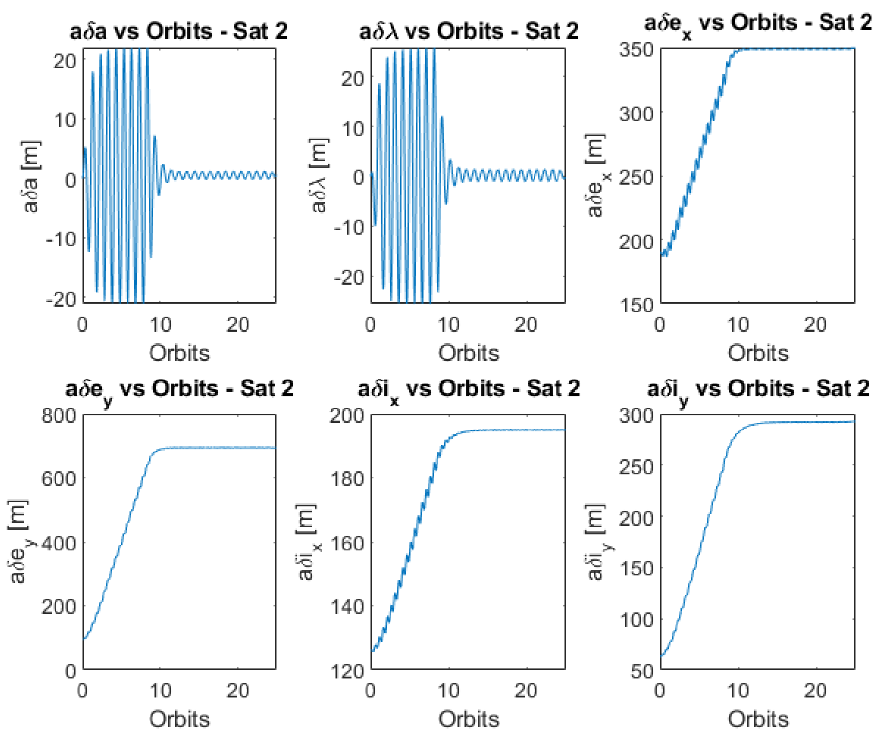

(b) Case 1: Spacecraft 2 state evolution.

Figure 4.6: Case 1: Spacecraft 1 and 2 relative state evolutions.

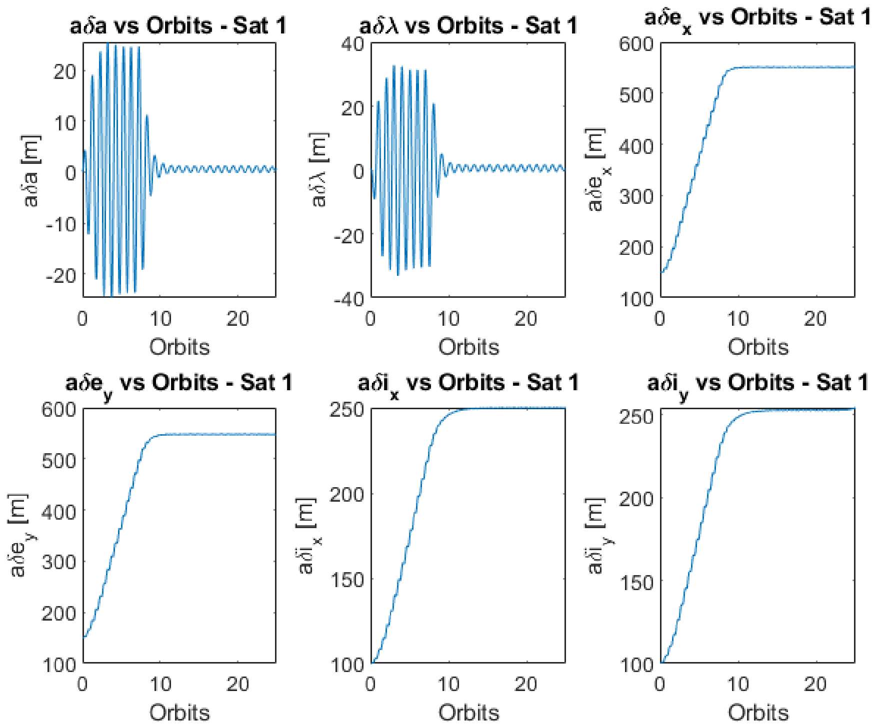

(a) Case 2: Spacecraft 1 state evolution.

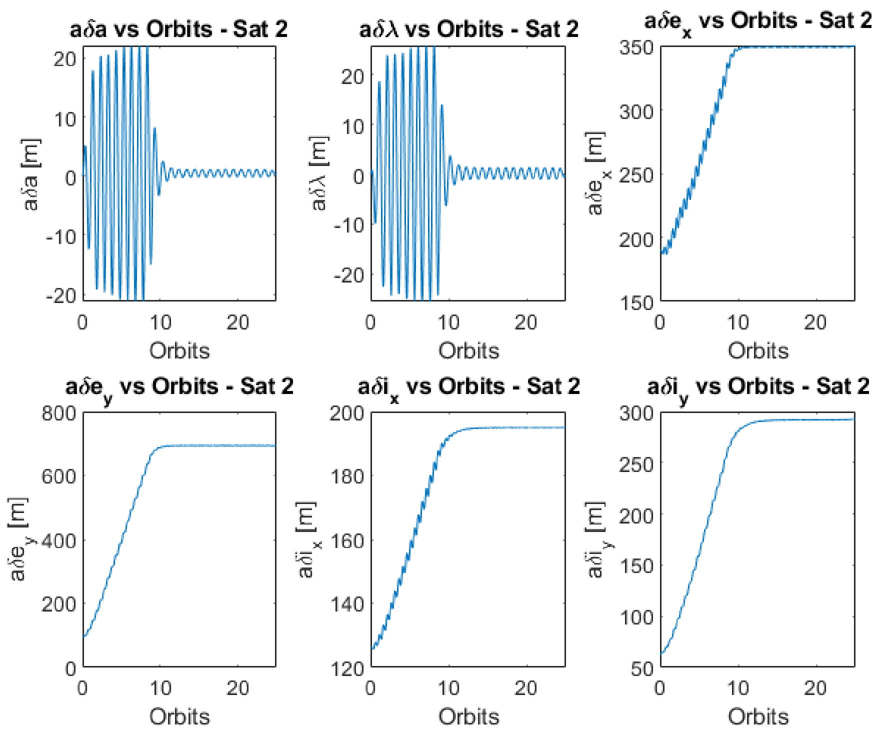

(b) Case 2: Spacecraft 2 state evolution.

Figure 4.7: Case 2: Spacecraft 1 and 2 relative state evolutions.

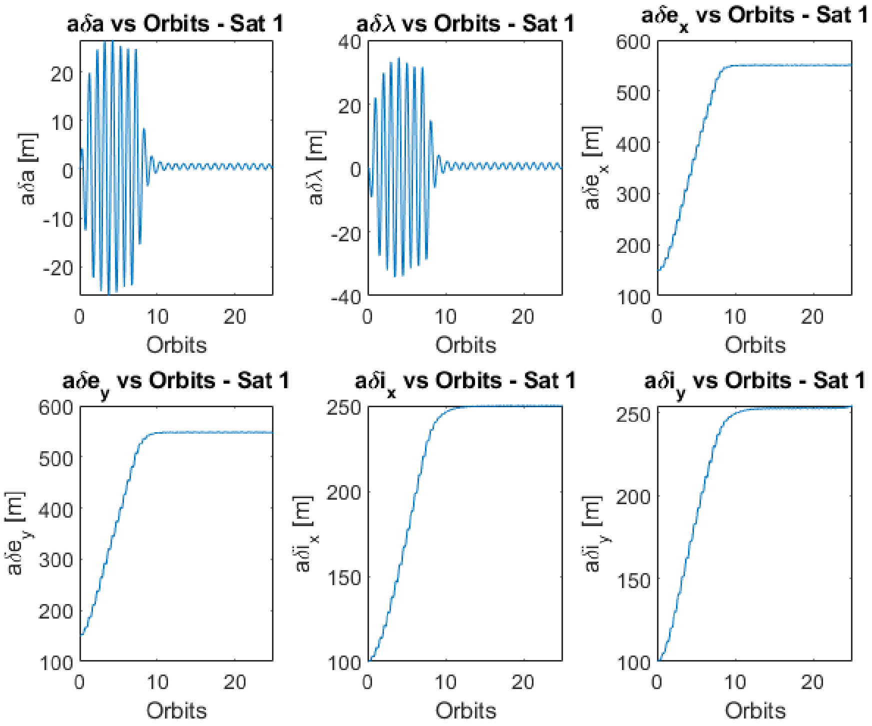

(a) Case 3: Spacecraft 1 state evolution.

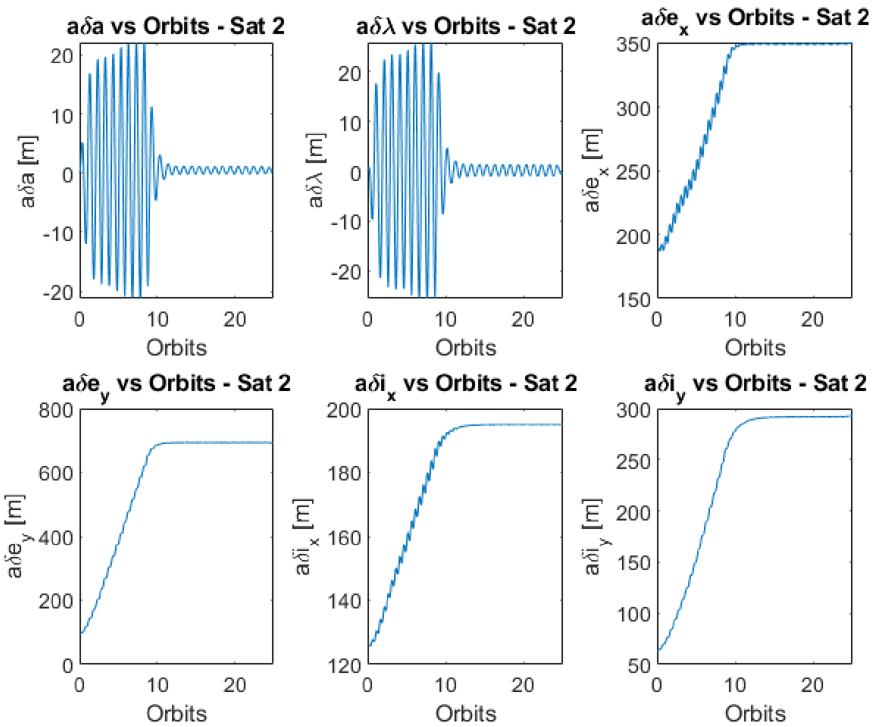

(b) Case 3: Spacecraft 2 state evolution.

Figure 4.8: Case 3: Spacecraft 1 and 2 relative state evolutions.

It can be seen that the difference in the relative state vector's evolution is slightly different for the three cases.

Minimum separation in RN plane and angle between $\Delta\delta\bar{e}_a$ and $\Delta\delta\bar{i}_a$

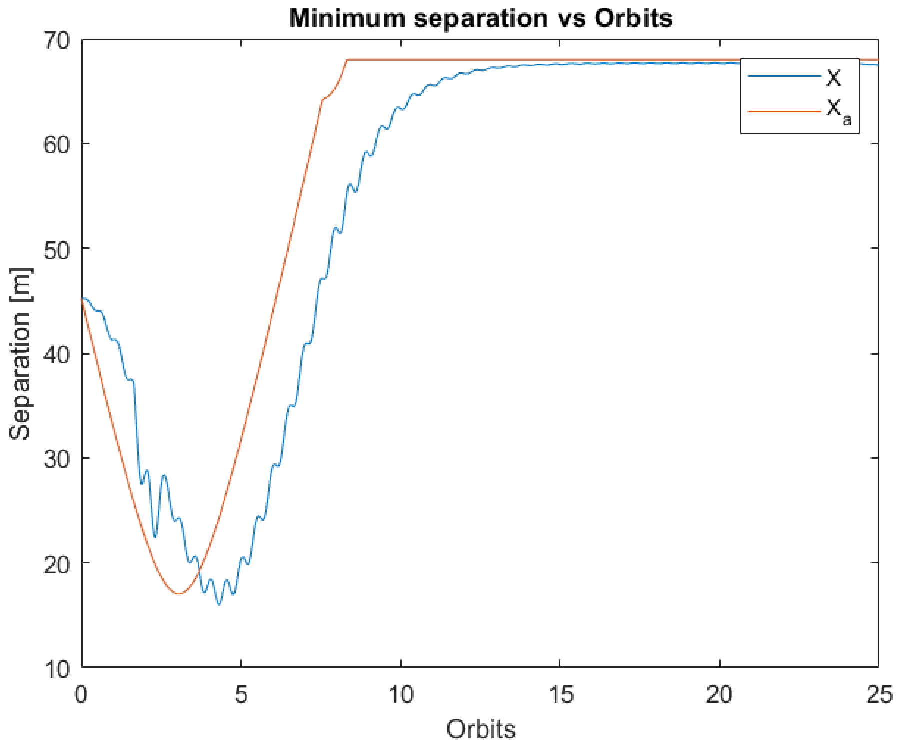

(a) Case 1: $\gamma = 0$, $\zeta = 0$.

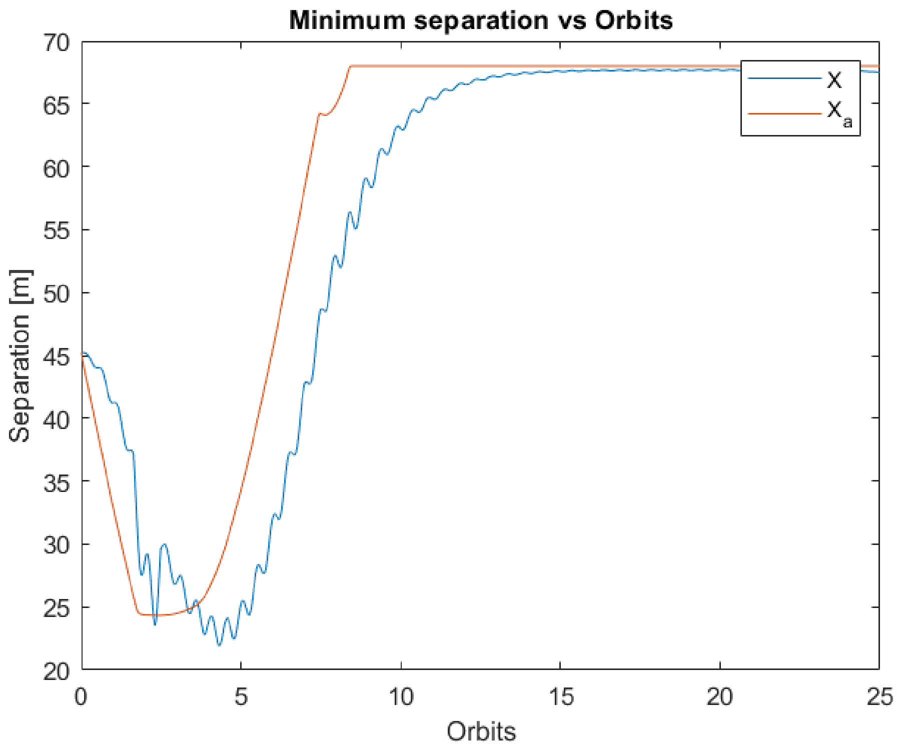

(b) Case 2: $\gamma = 20$, $\zeta = 25$.

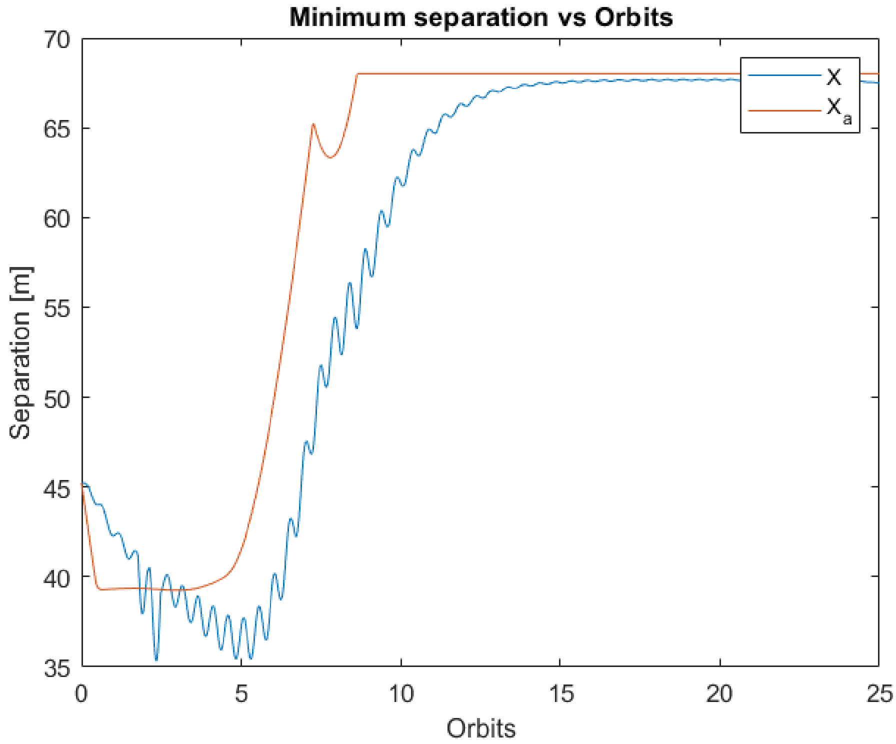

(c) Case 3: $\gamma = 35$, $\zeta = 40$.

Figure 4.9: Minimum separation between the applied references and the state vectors for the three cases.

The collision avoidance algorithm has been proven to work since the constraints given by ζ and γ are satisfied for each of the three cases.
As regards the angle between $\Delta\delta\bar{e}_a$ and $\Delta\delta\bar{i}_a$, since the repulsive potential field is proportional to the difference $\left|\delta\overline{X}_{a_1} - \delta\overline{X}_{a_2}\right|$, it can be deduced how the algorithm itself tends to parallelize the two vectors, decreasing the angle between them. This can be seen in fig. 4.10a, 4.10b, 4.10c.
This is a good property since the assumption of non-orthogonality between the two vectors is satisfied as long as the maneuver without collision avoidance is planned properly.

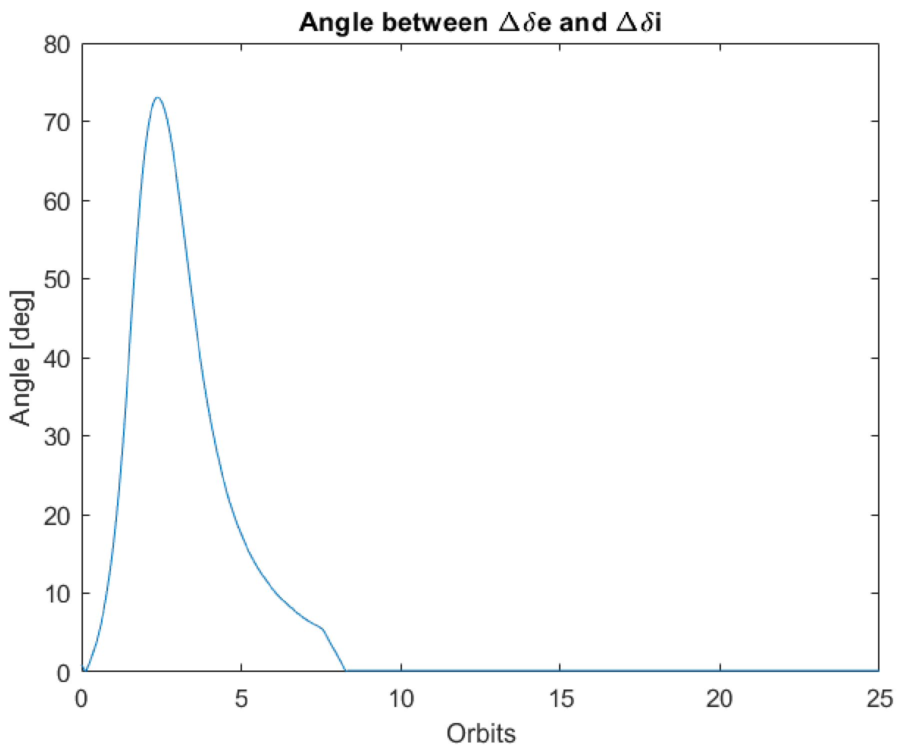

(a) Case 1: Angle between $\Delta\delta\bar{e}_a$ and $\Delta\delta\bar{i}_a$.

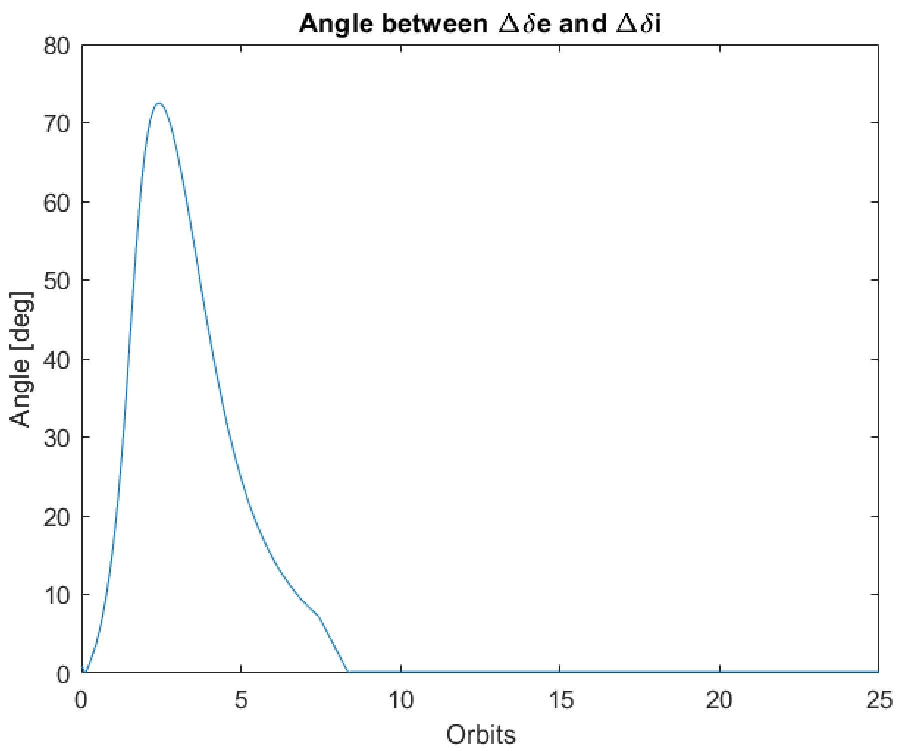

(b) Case 2: Angle between $\Delta\delta\bar{e}_a$ and $\Delta\delta\bar{i}_a$.

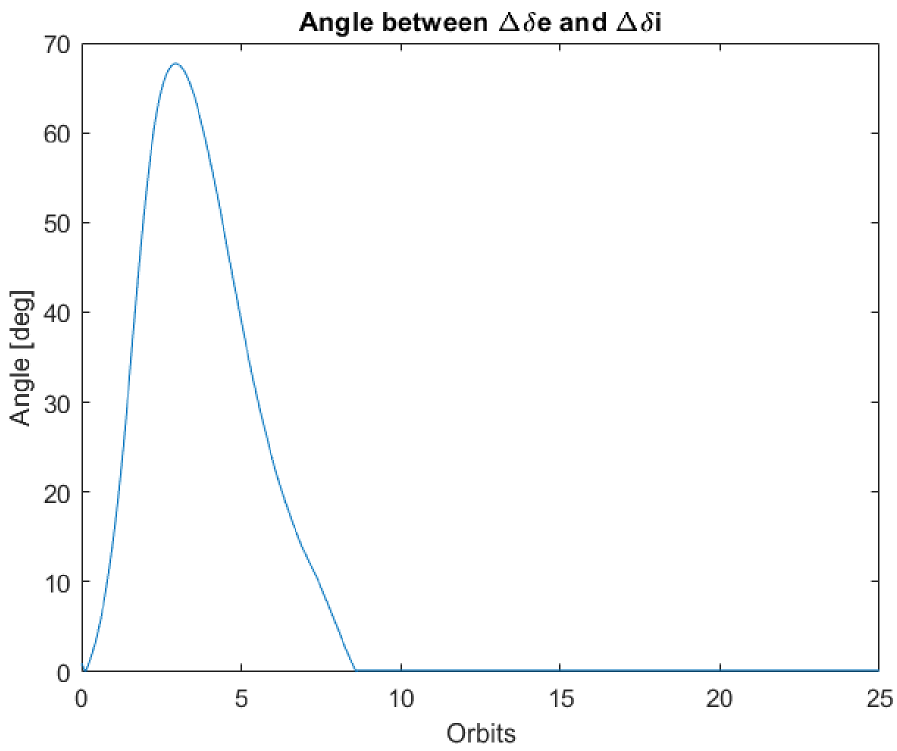

(c) Case 3: Angle between $\Delta\delta\overline{e}_a$ and $\Delta\delta\overline{i}_a$.

Figure 4.10: Angle between $\Delta\delta\overline{e}_a$ and $\Delta\delta\overline{i}_a$ for the three cases.

ΔV

	Lower Bound	Case 1	Case 2	Case3
ΔV	$0.5476\frac{m}{s}$	$0.5650\frac{m}{s}$	$0.5655\frac{m}{s}$	$0.5683\frac{m}{s}$
% more than LB	0	3.2	3.3	3.8

Table 4.5: Sat 1: Comparison between the ΔVs of the three cases with the lower bound.

	Lower Bound	Case 1	Case 2	Case3
ΔV	$0.6063\frac{m}{s}$	$0.6096\frac{m}{s}$	$0.6093\frac{m}{s}$	$0.6095\frac{m}{s}$
% more than LB	0	0.54	0.49	0.53

Table 4.6: Sat 2: Comparison between the ΔVs of the three cases with the lower bound.

Chapter 5

Fuel Balance between satellites

Fuel Balance between all the spacecraft in a formation is a very important issue that must be addressed in order to avoid that a satellite would run out of fuel before the other ones. If this happens, the controllability of the whole formation is irremediably lost.
In this chapter, two different strategies to prevent this issue will be presented:

- Exploitation of the $\boldsymbol{R}$ *matrix* in the LQR theory, increasing the fuel consumption of the less-consuming spacecraft;
- Smart mission and maneuver planning to let the LQR controller achieve Fuel Balance automatically.

5.1 Fuel Balance exploiting the $\boldsymbol{R}$ matrix

5.1.1 Basic Idea

As already discussed in the LQR chapter, the cost function minimized by the *Linear Quadratic Regulator* is given by (3.33).
In particular, the $\boldsymbol{R}$ matrix modulates the effect of the control vector in the cost function. This means that if we increase the elements in $\boldsymbol{R}$, we force the control parameters to be smaller, viceversa if we decrease the values in $\boldsymbol{R}$ the control parameters will be larger. So, considering a scenario with only two satellites, we can think about implementing an iterative algorithm that decreases the values in the $\boldsymbol{R}$ matrix of the satellite with the smaller real ΔV, until the difference between the ΔVs of the two spacecraft is below a certain tolerance value.

5.1.2 Algorithm Implementation

Let's suppose that satellite 2 consumes more than satellite 1. If we express the $\boldsymbol{R}$ matrices of the two satellites as follows:

$$\boldsymbol{R}_2 = a \cdot \begin{bmatrix} 1 & 0 & 0 \\ 0 & 1 & 0 \\ 0 & 0 & 1 \end{bmatrix} \tag{5.1}$$

$$\boldsymbol{R}_1 = b \cdot \begin{bmatrix} 1 & 0 & 0 \\ 0 & 1 & 0 \\ 0 & 0 & 1 \end{bmatrix} \tag{5.2}$$

The algorithm itself is a basic search of the right value for b such that $\frac{|\Delta V_2 - \Delta V_1|}{\Delta V_2} < tol$. Let's impose a constraint on b in order to avoid singularities in the problem:

$$b > 10^{-2.5} \tag{5.3}$$

The pseudocode of the algorithm is presented in *Algorithm* 1.

Algorithm 1: Algorithm Pseudocode.

$flag = 0$;
% This flag is used to check if $\frac{|\Delta V_2 - \Delta V_1|}{\Delta V_2} < tol$;

$incr = 0$;
$ss = 0.2$;
% ss is a step value used for the calculation of b;

$$\boldsymbol{R}_2 = a \cdot \begin{bmatrix} 1 & 0 & 0 \\ 0 & 1 & 0 \\ 0 & 0 & 1 \end{bmatrix};$$

while $flag == 0$ **do**

$$\boldsymbol{R}_1 = 10^{incr \cdot ss} \cdot \begin{bmatrix} 1 & 0 & 0 \\ 0 & 1 & 0 \\ 0 & 0 & 1 \end{bmatrix};$$

  Configure controller and perform analysis;
  Compute ΔV_1 and ΔV_2;
  if $\frac{|\Delta V_2 - \Delta V_1|}{\Delta V_2} > tol$ **then**
    if $\Delta V_1 > \Delta V_2$ **then**
      $incr = incr + floor\left(\frac{\frac{|\Delta V_2 - \Delta V_1|}{\Delta V_2}}{tol}\right)$;
    else
      $incr = incr - floor\left(\frac{\frac{|\Delta V_2 - \Delta V_1|}{\Delta V_2}}{tol}\right)$;
    end
  else
    $flag = 1$;
  end
end

5.1.3 Algorithm testing and results

Introduction to Scenario

This scenario consists in the deployment of two 3U Cubesats (4 kg each) from a chief spacecraft in LEO; the LQR control system will then actively guide to and maintain the satellites on two elliptical trajectories around the chief spacecraft in order to perform proximity operations. This scenario is based on some existing Cubesats mission:

- The *AAReST mission* [30] (expected to launch in 2019-2020), led by California Institute of Technology and Surrey Space Centre and funded by Keck Institute for Space Studies, aims to demonstrate autonomous assembly and reconfiguration of a space telescope by having two 3U CubeSats autonomously un-dock and re-dock with a central 9U nanosatellite core. The central nanosatellite houses two fixed mirrors and a boom-deployed focal plane assembly, while the two 3U CubeSats each carry an electrically actuated adaptive mirror.
- The *QUEST mission* [4], which is a joint project between Arizona State University, Santa

Clara University, and Kyushu University, Japan; aims to first deploy a 2 km long tether in space and then maintain a formation by cooperatively controlling the main satellite and sub-satellite.

Input Data

- $\overline{X}_c$ as in (3.35);
- $t_0 = 0$;
- $T = 25T_{orbit} = 141920s$;
- $tol = 0.05$.

The initial and final states (expressed in meters) of the two spacecraft are:

ROE Variable	Initial	Final
$a_c \cdot 1000 \cdot \delta a$	$0m$	$0m$
$a_c \cdot 1000 \cdot \delta\lambda$	$0m$	$0m$
$a_c \cdot 1000 \cdot \delta e_x$	$1m$	$350m$
$a_c \cdot 1000 \cdot \delta e_y$	$1m$	$350m$
$a_c \cdot 1000 \cdot \delta i_x$	$1m$	$250m$
$a_c \cdot 1000 \cdot \delta i_y$	$1m$	$250m$

Table 5.1: R Exploitation: Initial and final relative states of Spacecraft 1.

ROE Variable	Initial	Final
$a_c \cdot 1000 \cdot \delta a$	$0m$	$0m$
$a_c \cdot 1000 \cdot \delta\lambda$	$0m$	$0m$
$a_c \cdot 1000 \cdot \delta e_x$	$-1m$	$-450m$
$a_c \cdot 1000 \cdot \delta e_y$	$-1m$	$-450m$
$a_c \cdot 1000 \cdot \delta i_x$	$-1m$	$-450m$
$a_c \cdot 1000 \cdot \delta i_y$	$-1m$	$-450m$

Table 5.2: R Exploitation: Initial and final relative states of Spacecraft 2.

Initial and final states were chosen in order to assure that $\Delta\delta\overline{e}$ and $\Delta\delta\overline{i}$ remain parallel while φ_1, θ_1 and φ_2, θ_2 are out of phase by 180 deg. Because of this, collision avoidance is assured and the relative motion of the two spacecraft with respect to the virtual chief is defined by (2.14), (2.15) and (2.16).
Two different cases will be simulated, one without fuel balancing and another with the aforementioned algorithm:

- *Case 1*: $a = b = 3$;
- *Case 2*: $a = 3$, b according to the aforementioned iterative procedure.

State

As regards *Case 2*, the algorithm converges after 2 iterations with the following results:

$$incr = -3 \tag{5.4}$$

$$b = 10^{-0.6} \tag{5.5}$$

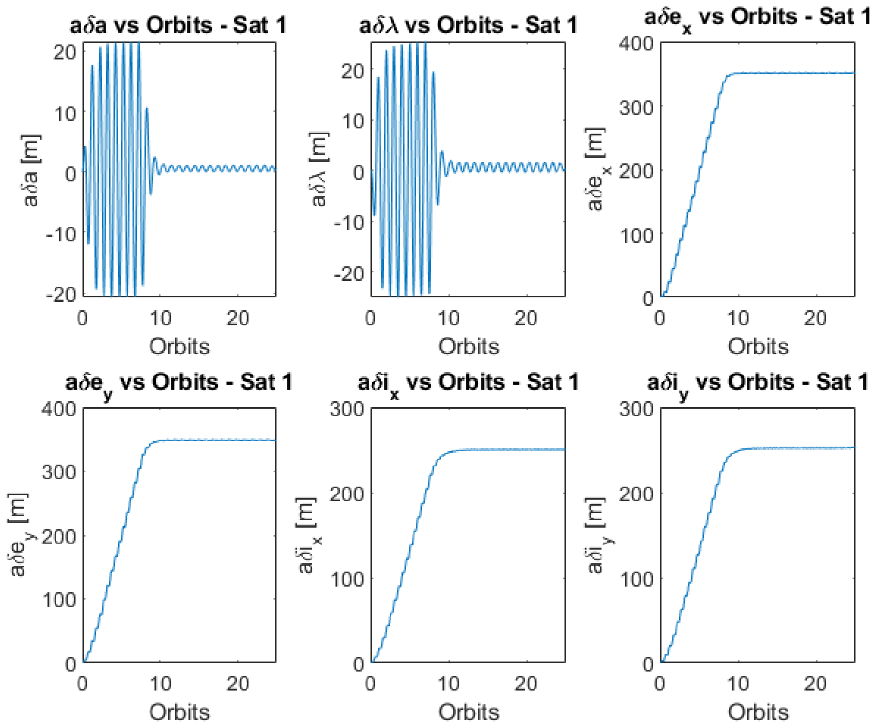

(a) Case 1: Spacecraft 1 state evolution.

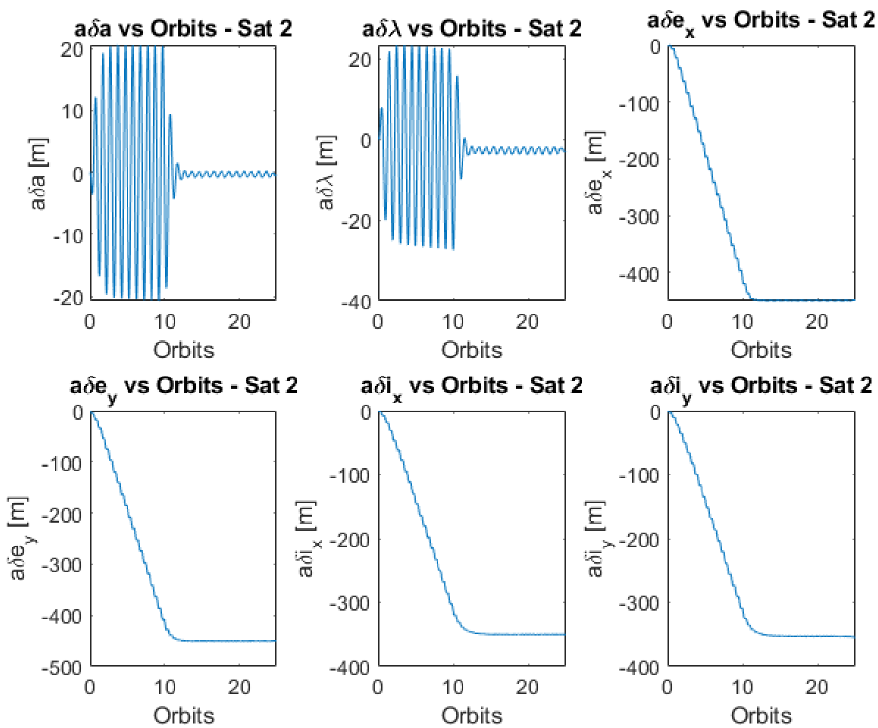

(b) Case 1: Spacecraft 2 state evolution.

Figure 5.1: Case 1: spacecraft state evolution.

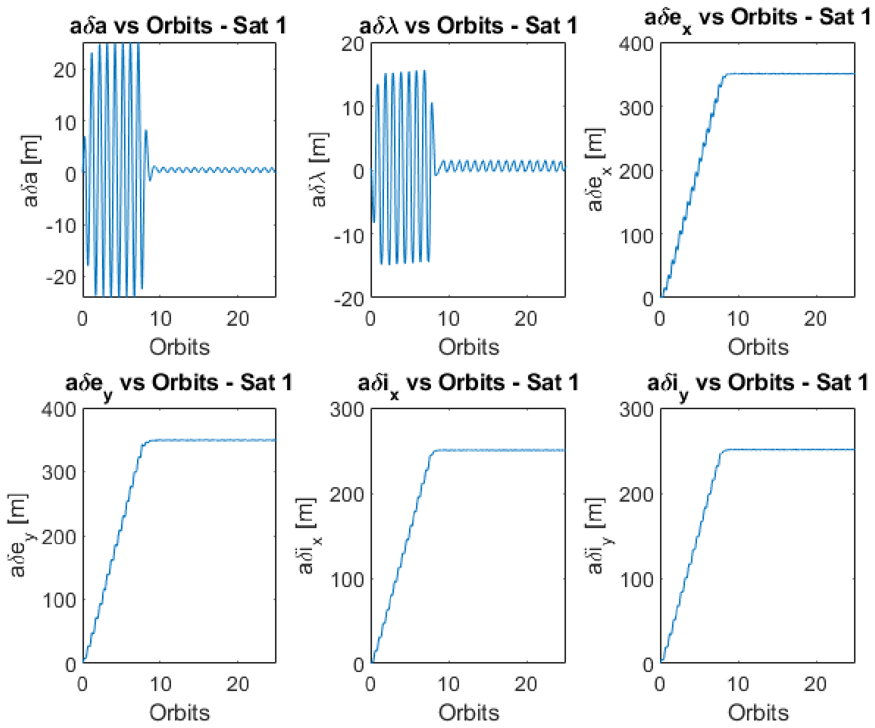

(a) Case 2: Spacecraft 1 state evolution.

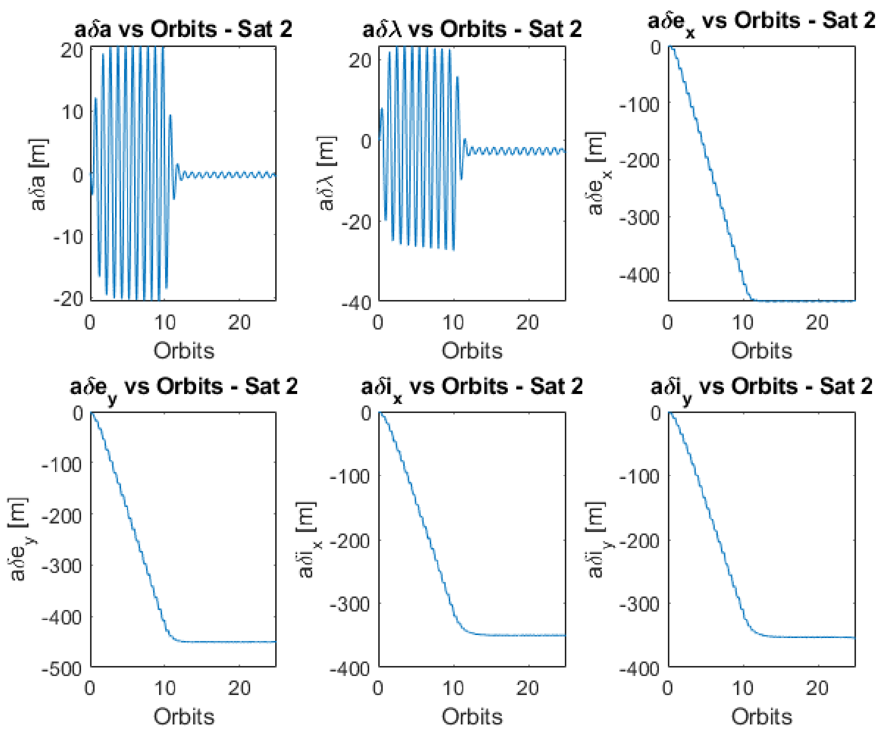

(b) Case 2: Spacecraft 2 state evolution.

Figure 5.2: Case 2: spacecraft state evolution.

Minimum separation in RN plane and angle between $\Delta\delta\bar{e}_a$ and $\Delta\delta\bar{i}_a$

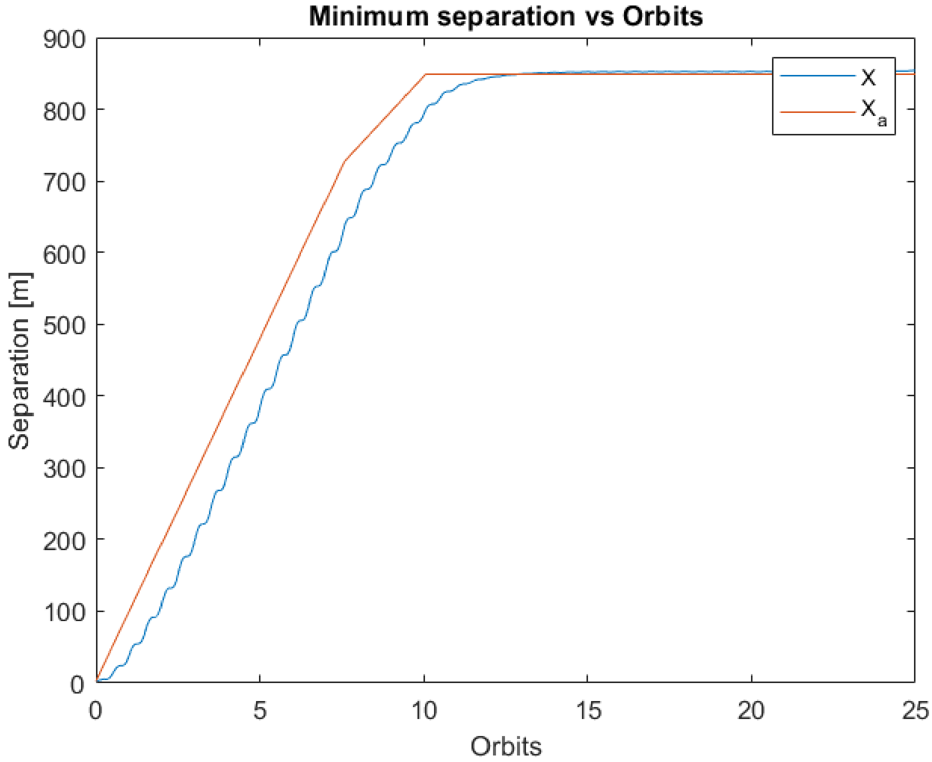

Figure 5.3: Case 1-2: Minimum separation between the applied references and the state vectors.

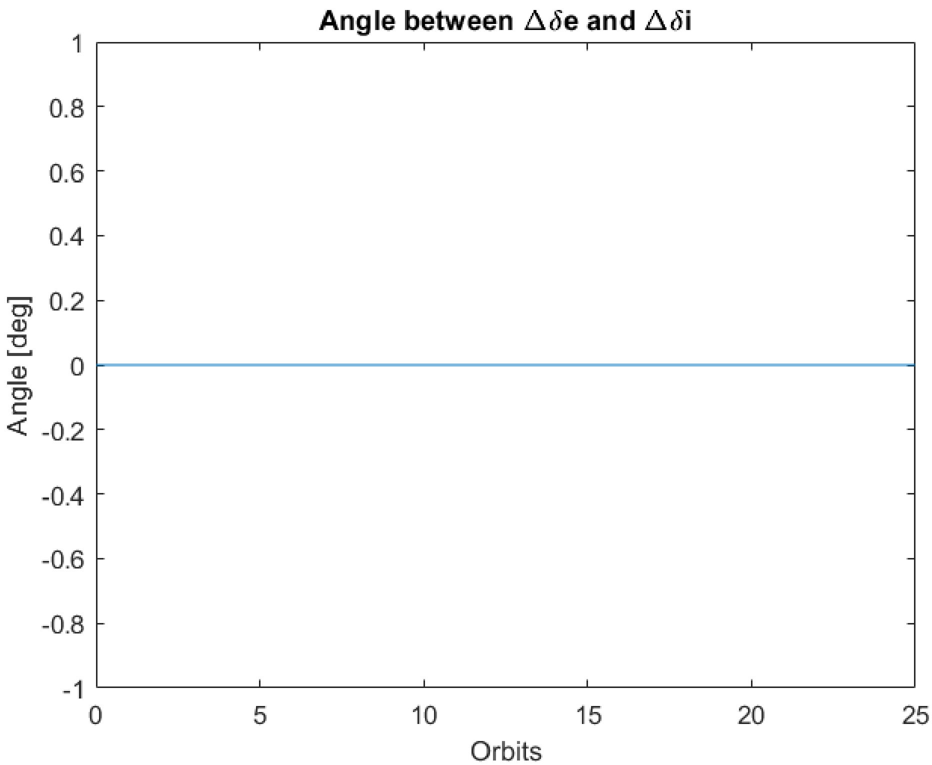

Figure 5.4: Case 1-2: Angle between $\Delta\delta\bar{e}_a$ and $\Delta\delta\bar{i}_a$.

ΔV

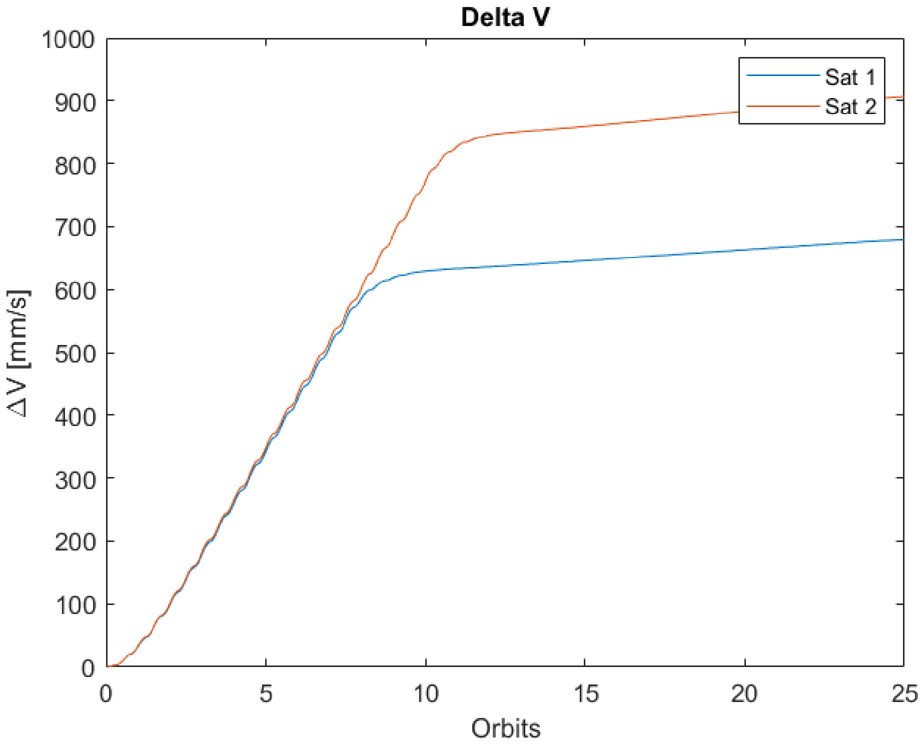

(a) Case 1: ΔV over time.

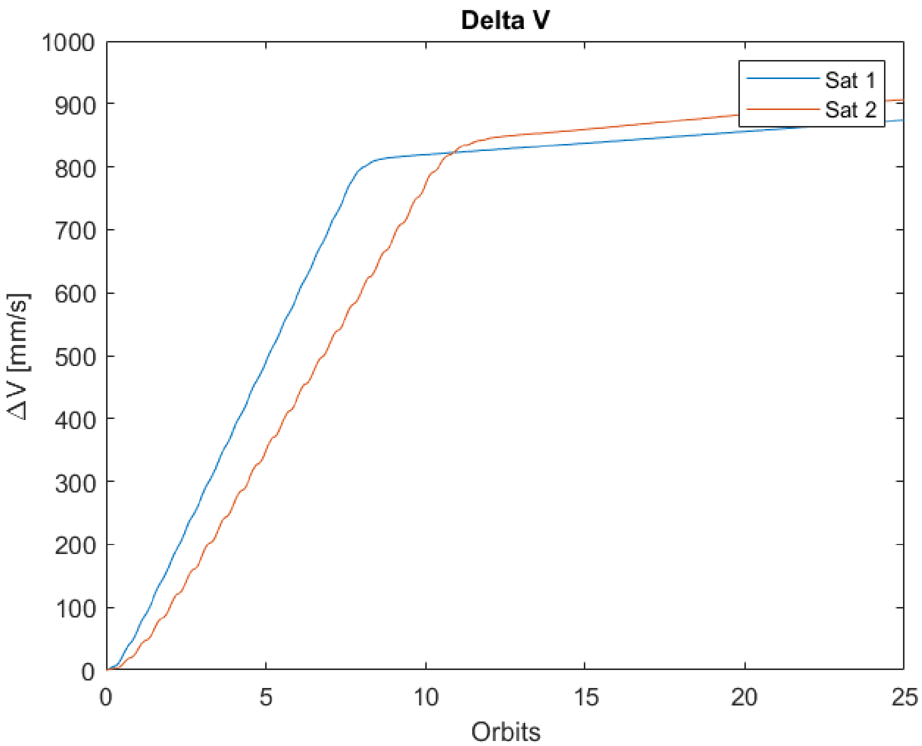

(b) Case 2: ΔV over time.

Figure 5.5: ΔV over time for cases 1-2.

	Lower Bound	Case 1	Case 2
ΔV	$0.6625\frac{m}{s}$	$0.6786\frac{m}{s}$	$0.874\frac{m}{s}$
% more than LB	0	2.4	32

Table 5.3: Sat 1: Comparison between the ΔVs of the two cases with the lower bound.

	Lower Bound	Case 1	Case 2
ΔV	$0.8972\frac{m}{s}$	$0.906\frac{m}{s}$	$0.906\frac{m}{s}$
% more than LB	0	0.98	0.98

Table 5.4: Sat 2: Comparison between the ΔVs of the two cases with the lower bound.

Case	$\frac{\lvert\Delta V_2 - \Delta V_1\rvert}{\Delta V_2}$
Case 1	25%
Case 2	3.5%

Table 5.5: Percentual relative difference in ΔV between the two satellites in the two cases.

Relative motion in the RT and RN planes

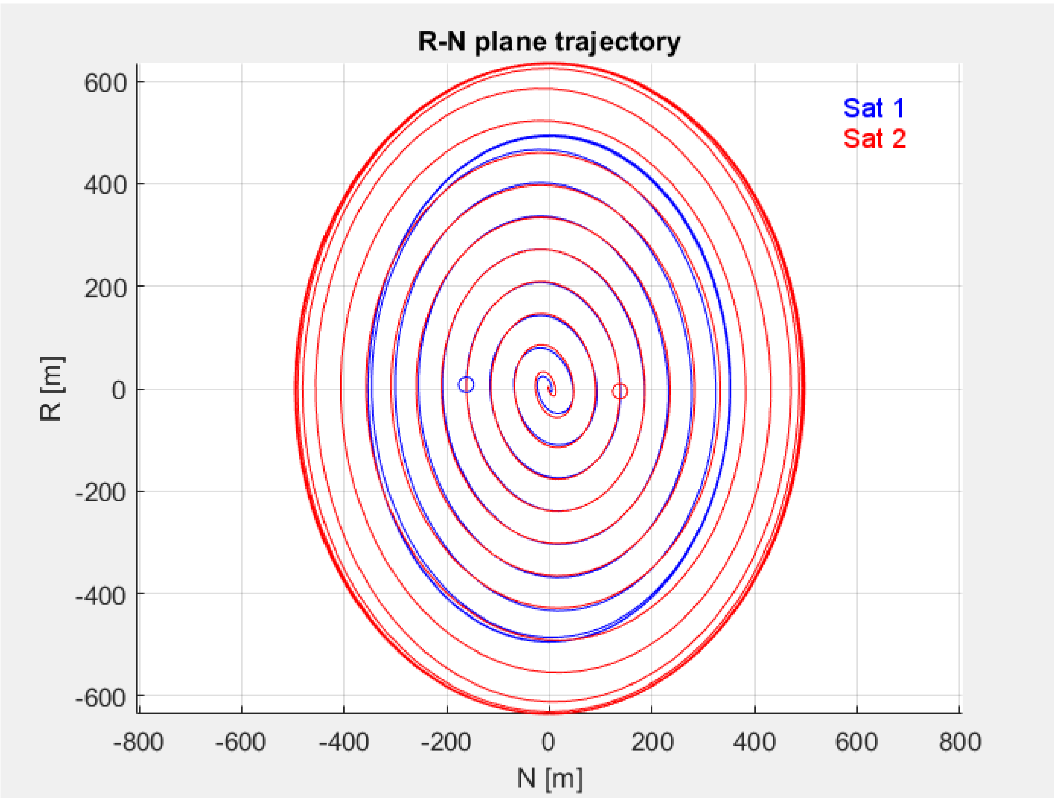

Figure 5.6: Relative motion in the RN plane.

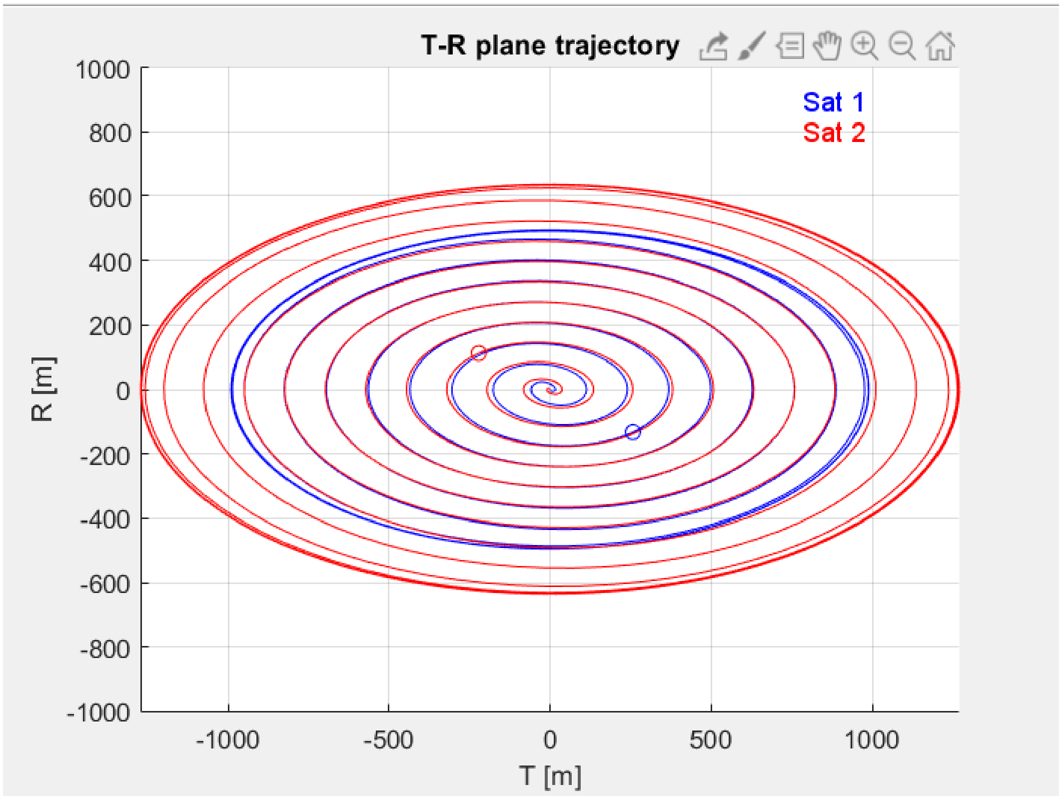

Figure 5.7: Relative motion in the RT plane.

Conclusion

An observation should be done regarding the maximum ΔV_1 achievable using the $b = 10^{-2.5}$ lower bound; running multiple simulations showed that we can achieve in most cases $\Delta V_{1_{max}} = 1.5 \cdot \Delta V_{1_{min}}$, but in order to be sure that this strategy works we should assure that at least:

$$\frac{|\Delta V_{2_{LB}} - \Delta V_{1_{LB}}|}{\Delta V_{2_{LB}}} < 35\% - 40\% \tag{5.6}$$

It is clear how this kind of strategy is quite inefficient, since we force one satellite to consume more than necessary.

5.2 Fuel Balance through smart mission and maneuver planning

A better approach to this problem, from the fuel efficiency perspective, would be to wisely design the final states in order to match the mission constraints and achieve automatically fuel balance with the LQR controller at the same time. In order to show this kind of approach, some scenarios will be presented in the next sections.

5.2.1 Scenario 1: TanDEM-X like mission

The TanDEM-X mission is an extension of the TerraSAR-X mission, coflying a second satellite of nearly identical capability in a close formation [3]. TanDEM-X was Germanys first national remote sensing formation that has been realized in a public private partnership between DLR and industry. This formation had been supplying high quality radar images for scientific and

commercial applications. The TanDEM-X operational scenario requires the coordinated operation of two satellites flying in close formation in order to operate a Synthetic Aperture Radar configuration.
Several possible configuration have been investigated, and the Helix satellite formation shown in fig. 5.8 has finally been selected for operational DEM generation. This formation combines an out-of-plane (horizontal) orbital displacement by different ascending nodes with a radial (vertical) separation by different eccentricity vectors, resulting in a helix-like relative movement of the satellites along the orbit. Since there exists no crossing of the satellite orbits, arbitrary shifts of the satellites along their orbits are allowed. This enables a safe spacecraft operation without the necessity for autonomous control.

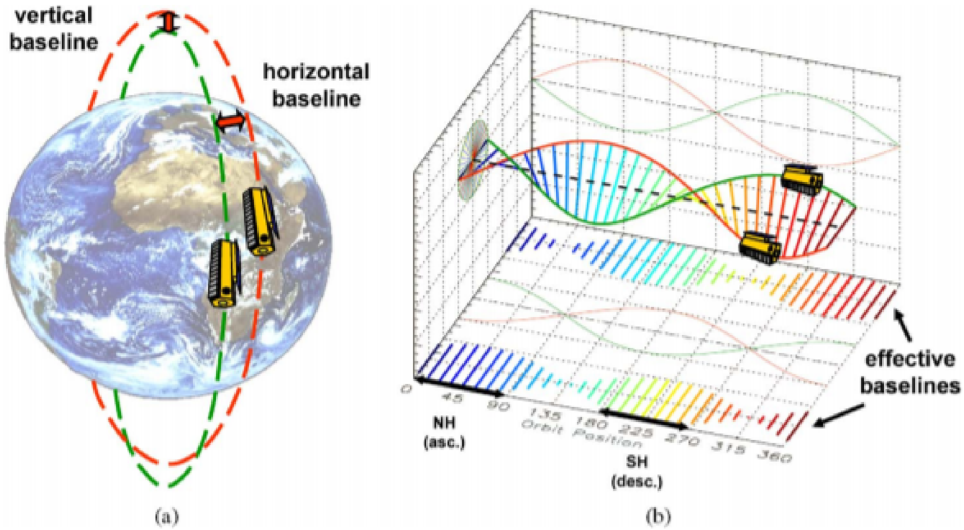

Figure 5.8: TanDEM-X Helix configuration [3].

Referring to fig. 2.3 and 2.4, it can be seen that as long as $\delta\overline{e}$ and $\delta\overline{i}$ are parallel for each of the two satellites while φ_1, θ_1 and φ_2, θ_2 are out of phase by 180 deg, the maximum horizontal and vertical baselines are given by:

$$B_H = a_c \cdot 1000 \cdot \left|\Delta\delta\overline{i}\right| \tag{5.7}$$

$$B_V = a_c \cdot 1000 \cdot \left|\Delta\delta\overline{e}\right| \tag{5.8}$$

where $\Delta\delta\overline{e} = \delta\overline{e}_1 - \delta\overline{e}_2$ and $\Delta\delta\overline{i} = \delta\overline{i}_1 - \delta\overline{i}_2$.
This Scenario will involve a TanDEM-X like configuration, from the deployment of the two satellites to the achievement of the target configuration.
Mission constraint:

- horizontal and vertical maximum baselines in the range $700 - 750m$.

Input Data

The chief reference orbit expressed in absolute relative elements will be:

$$\overline{X}_c = \begin{pmatrix} a_c \\ e_c \\ i_c \\ \Omega_c \\ \omega_c \\ f_c \end{pmatrix} = \begin{pmatrix} 6878km \\ 0.0002 \\ 97.4\,\text{deg} \\ 260\,\text{deg} \\ 90\,\text{deg} \\ 315\,\text{deg} \end{pmatrix} \tag{5.9}$$

The mean relative elements are computed using GMAT and the Brouwer-Lyddane method. i_c has been chosen in order to realize a *Sun-Synchronous* orbit.
Time data:

- $t_0 = 0$;
- $T = 25T_{orbit} = 141920s$.

Initial and final states:

ROE Variable	Initial	Final
$a_c \cdot 1000 \cdot \delta a$	$0m$	$0m$
$a_c \cdot 1000 \cdot \delta \lambda$	$0m$	$0m$
$a_c \cdot 1000 \cdot \delta e_x$	$1m$	$250m$
$a_c \cdot 1000 \cdot \delta e_y$	$1m$	$250m$
$a_c \cdot 1000 \cdot \delta i_x$	$1m$	$250m$
$a_c \cdot 1000 \cdot \delta i_y$	$1m$	$250m$

Table 5.6: TanDEM-X 1: Initial and final relative states of Spacecraft 1.

ROE Variable	Initial	Final
$a_c \cdot 1000 \cdot \delta a$	$0m$	$0m$
$a_c \cdot 1000 \cdot \delta \lambda$	$0m$	$0m$
$a_c \cdot 1000 \cdot \delta e_x$	$-1m$	$-250m$
$a_c \cdot 1000 \cdot \delta e_y$	$-1m$	$-250m$
$a_c \cdot 1000 \cdot \delta i_x$	$-1m$	$-250m$
$a_c \cdot 1000 \cdot \delta i_y$	$-1m$	$-250m$

Table 5.7: TanDEM-X 1: Initial and final relative states of Spacecraft 2.

Final states are chosen in order to keep $\delta\bar{e}$ and $\delta\bar{i}$ parallel for each of the two satellites while φ_1, θ_1 and φ_2, θ_2 are out of phase by 180 deg. Using the final states, the final baselines can be computed:

$$B_H = B_V \simeq 707m \tag{5.10}$$

$$\boldsymbol{Q}_1 = \boldsymbol{Q}_2 = 10 \cdot \begin{bmatrix} 1 & 0 & 0 & 0 & 0 & 0 \\ 0 & 1 & 0 & 0 & 0 & 0 \\ 0 & 0 & 1 & 0 & 0 & 0 \\ 0 & 0 & 0 & 1 & 0 & 0 \\ 0 & 0 & 0 & 0 & 1 & 0 \\ 0 & 0 & 0 & 0 & 0 & 1 \end{bmatrix} \tag{5.11}$$

$$\boldsymbol{R}_1 = \boldsymbol{R}_2 = 10 \cdot \begin{bmatrix} 1 & 0 & 0 \\ 0 & 1 & 0 \\ 0 & 0 & 1 \end{bmatrix} \tag{5.12}$$

State

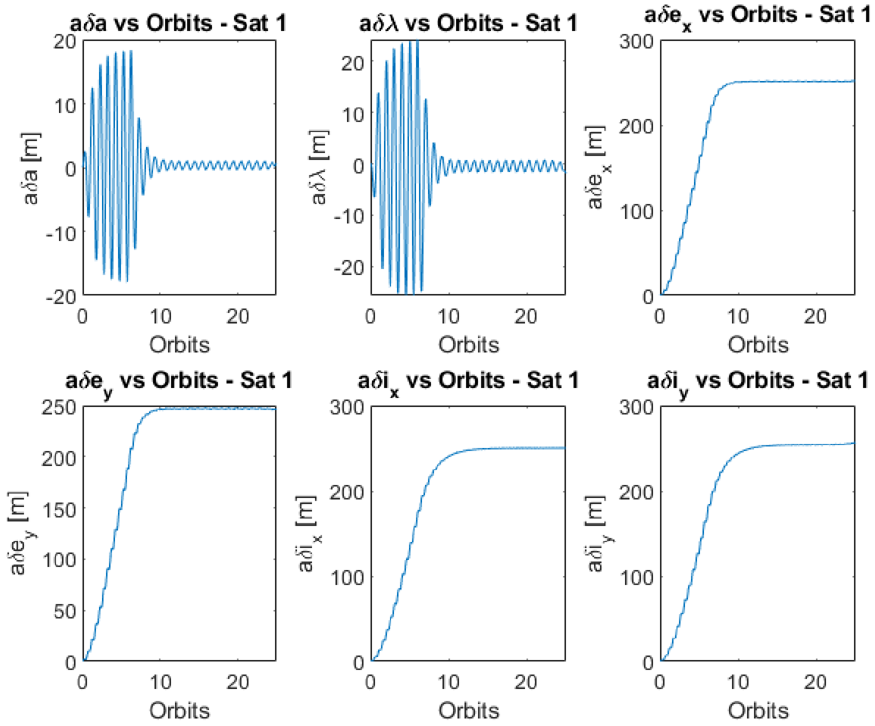

(a) TanDEM 1: Spacecraft 1 state evolution.

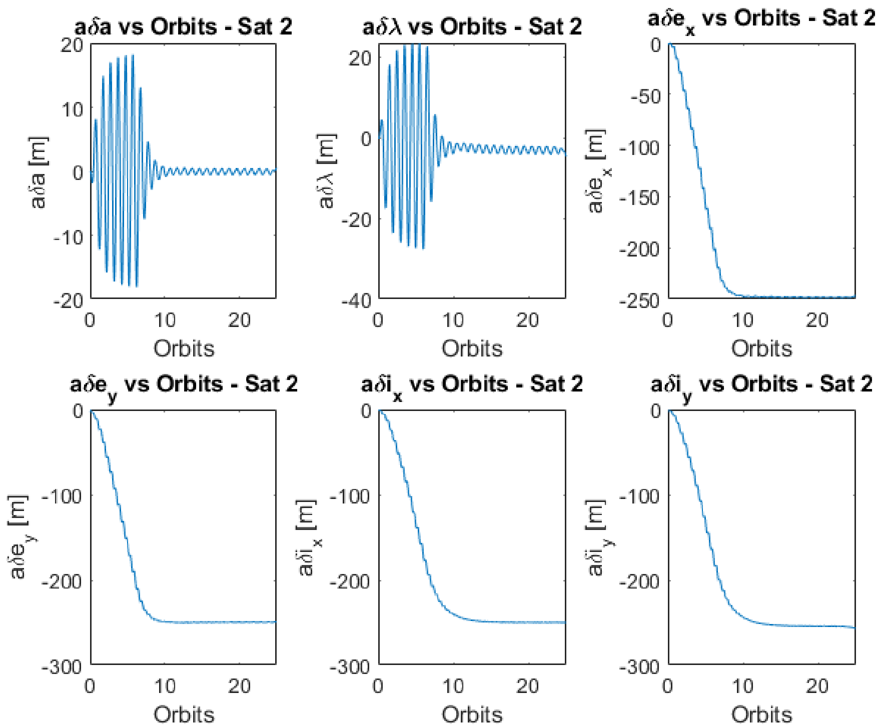

(b) TanDEM 1: Spacecraft 2 state evolution.

Figure 5.9: TanDEM 1: spacecraft state evolution.

ΔV

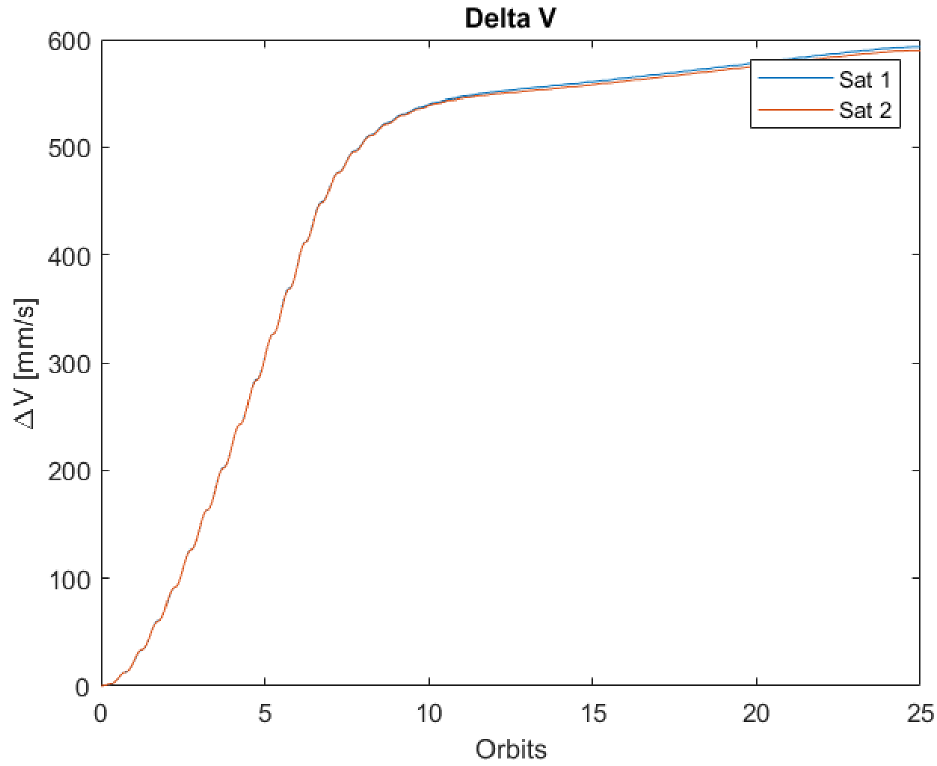

Figure 5.10: ΔV over time.

	Lower Bound	Scenario
ΔV	$0.5840\frac{m}{s}$	$0.5932\frac{m}{s}$
% more than LB	0	1.6

Table 5.8: Sat 1: Comparison between the scenario ΔV with the lower bound.

	Lower Bound	Scenario
ΔV	$0.5840\frac{m}{s}$	$0.5897\frac{m}{s}$
% more than LB	0	1

Table 5.9: Sat 2: Comparison between the scenario ΔV with the lower bound.

Let's suppose $tol = 5\%$, the fuel balance is achieved since:

$$\frac{|\Delta V_2 - \Delta V_1|}{\Delta V_2} = 0.6\% \tag{5.13}$$

Relative motion in the RT and RN planes

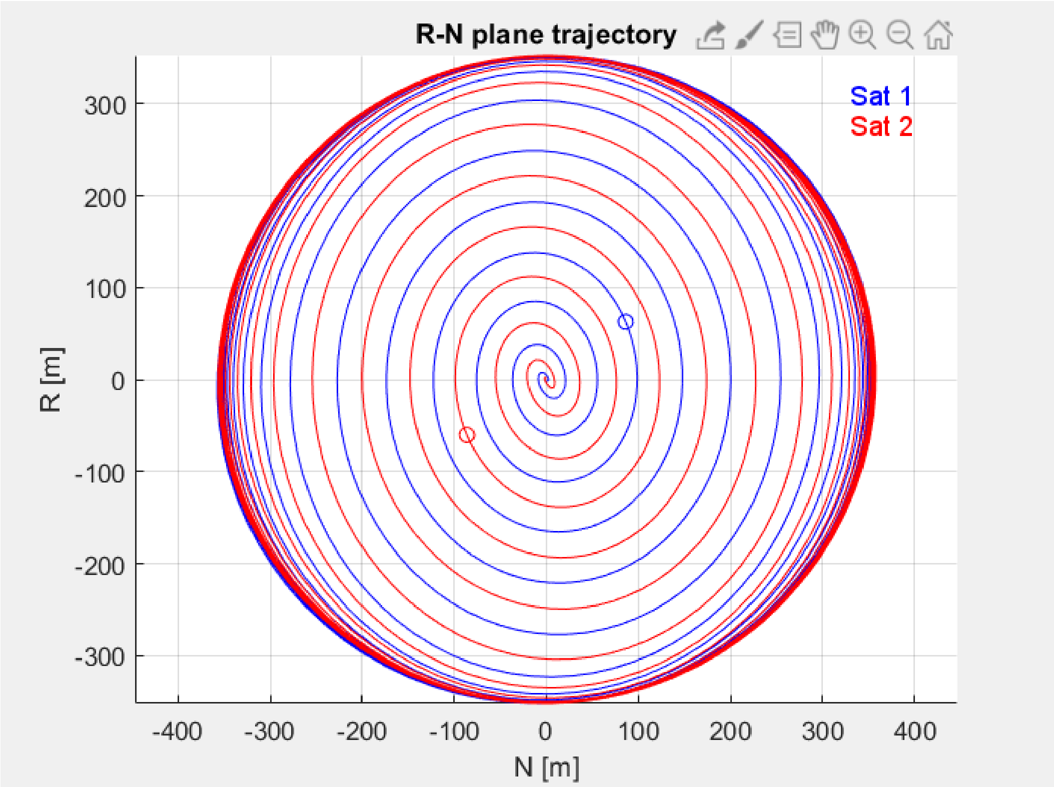

Figure 5.11: Relative motion in the RN plane.

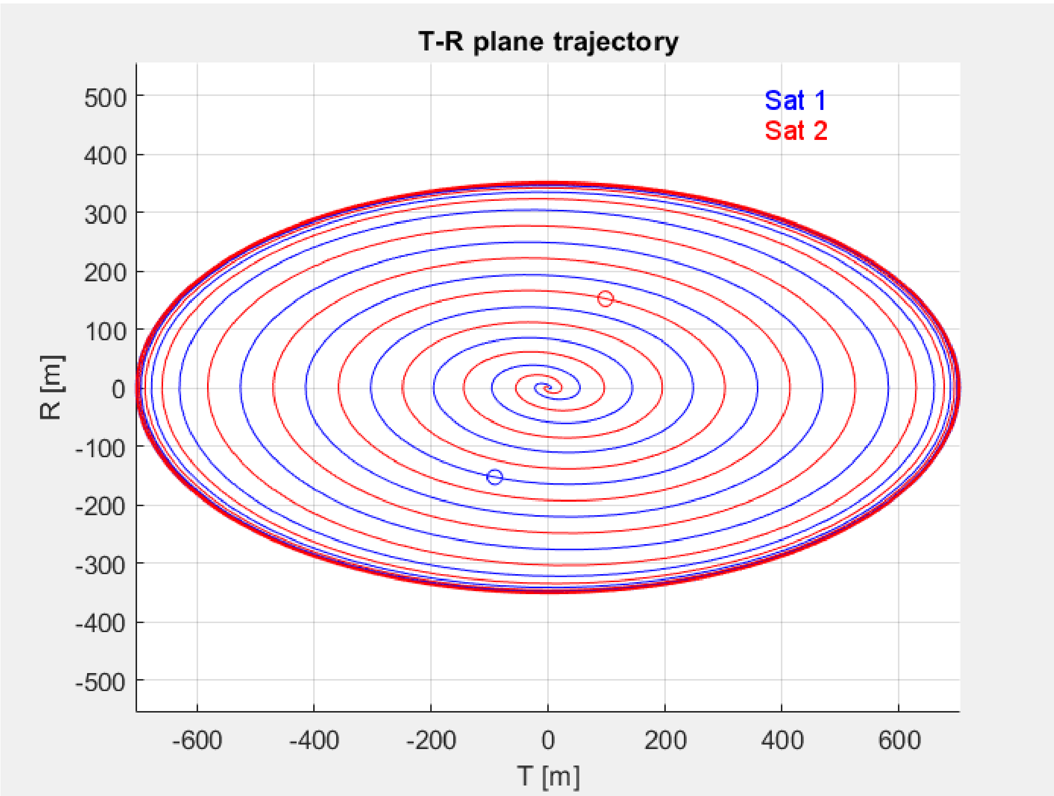

Figure 5.12: Relative motion in the RT plane.

Helix formation

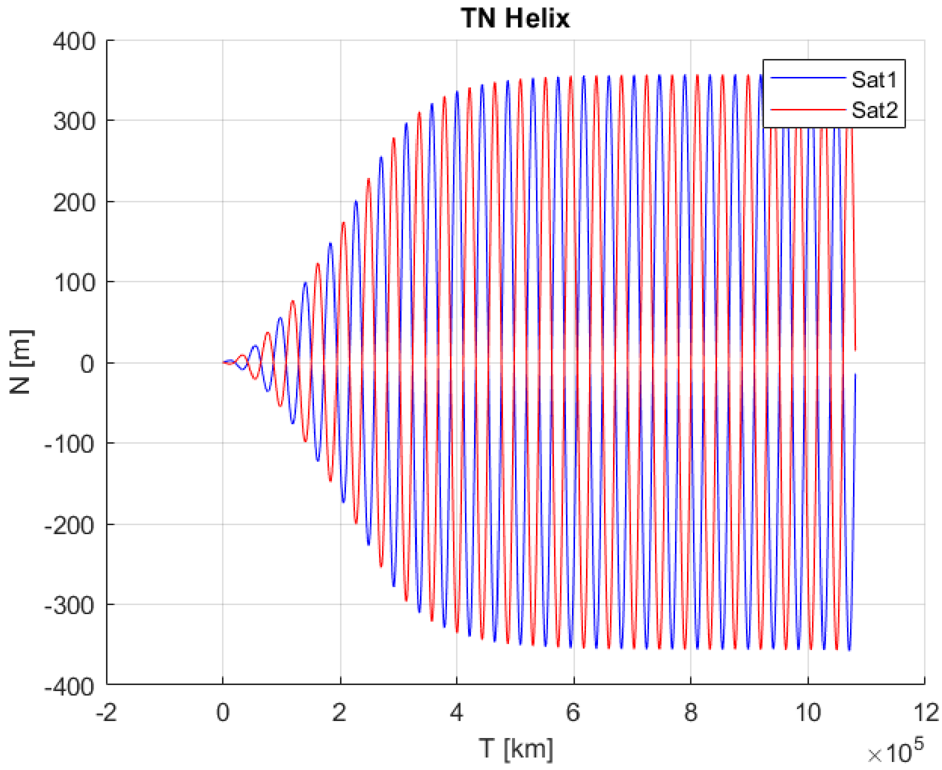

Figure 5.13: Helix projection in TN plane.

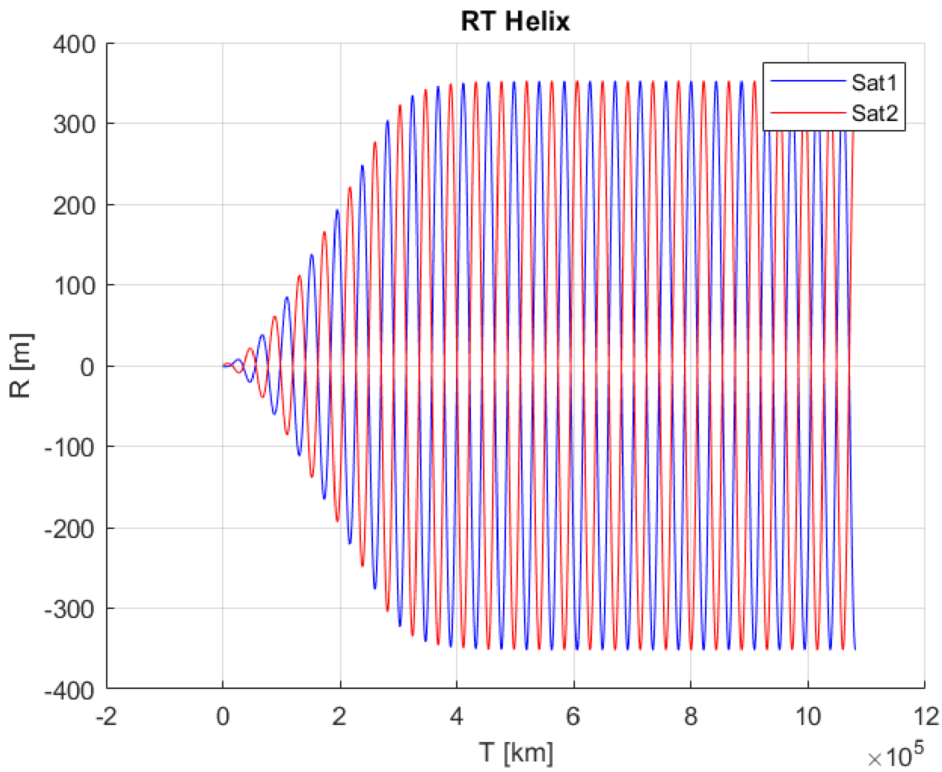

Figure 5.14: Helix projection in RT plane.

We can see the final Horizontal Baseline in fig. 5.13 and the Vertical Baseline in fig. 5.14. In this case the two are equal $B_H = B_V \simeq 707m$. Both the mission constraint and the fuel balance are satisfied.

5.2.2 Scenario 2: Deployment of a 4-sats formation with along-track separation

Another viable configuration for an Interferometric SAR mission would be to allocate the satellites on the same orbit assuring a fixed along-track separation, i.e. a relative mean longitude $\Delta\delta\lambda$.
As already said regarding (2.36), as the mission time increases, ΔM increases as well and a mean longitude separation $\Delta\delta\lambda$ could be achieved with a lower ΔV_{LB}. In particular, if the ΔV_{LB} requested to change the eccentricity/inclination vectors is greater than the one requested for the mean longitude change, then we can achieve this kind of separation 'for free'.
This Scenario will simulate the deployment of four satellites from a chief spacecraft, the LQR will compute the control necessary to reach a target along-track separation.
Mission Goal:

- Achieve an along-track separation of $720m$ between consecutive satellites.

Input Data

The chief reference orbit expressed in absolute relative elements will be:

$$\overline{X}_c = \begin{pmatrix} a_c \\ e_c \\ i_c \\ \Omega_c \\ \omega_c \\ f_c \end{pmatrix} = \begin{pmatrix} 6878km \\ 0.0002 \\ 97.4\,\text{deg} \\ 260\,\text{deg} \\ 90\,\text{deg} \\ 315\,\text{deg} \end{pmatrix} \tag{5.14}$$

The mean relative elements are computed using GMAT and the Brouwer-Lyddane method.
i_c has been chosen in order to realize a *Sun-Synchronous* orbit.
Time data:

- $t_0 = 0$;
- $T = 25T_{orbit} = 141920s$.

Initial and final states:

ROE Variable	Initial	Final
$a_c \cdot 1000 \cdot \delta a$	$0m$	$0m$
$a_c \cdot 1000 \cdot \delta\lambda$	$1m$	$360m$
$a_c \cdot 1000 \cdot \delta e_x$	$1m$	$250m$
$a_c \cdot 1000 \cdot \delta e_y$	$1m$	$250m$
$a_c \cdot 1000 \cdot \delta i_x$	$1m$	$150m$
$a_c \cdot 1000 \cdot \delta i_y$	$1m$	$150m$

Table 5.10: 4 Sats: Initial and final relative states of Spacecraft 1.

ROE Variable	Initial	Final
$a_c \cdot 1000 \cdot \delta a$	$0m$	$0m$
$a_c \cdot 1000 \cdot \delta\lambda$	$1m$	$1080m$
$a_c \cdot 1000 \cdot \delta e_x$	$1m$	$250m$
$a_c \cdot 1000 \cdot \delta e_y$	$1m$	$250m$
$a_c \cdot 1000 \cdot \delta i_x$	$1m$	$150m$
$a_c \cdot 1000 \cdot \delta i_y$	$1m$	$150m$

Table 5.11: 4 Sats: Initial and final relative states of Spacecraft 2.

ROE Variable	Initial	Final
$a_c \cdot 1000 \cdot \delta a$	$0m$	$0m$
$a_c \cdot 1000 \cdot \delta\lambda$	$-1m$	$-360m$
$a_c \cdot 1000 \cdot \delta e_x$	$1m$	$250m$
$a_c \cdot 1000 \cdot \delta e_y$	$1m$	$250m$
$a_c \cdot 1000 \cdot \delta i_x$	$1m$	$150m$
$a_c \cdot 1000 \cdot \delta i_y$	$1m$	$150m$

Table 5.12: 4 Sats: Initial and final relative states of Spacecraft 3.

ROE Variable	Initial	Final
$a_c \cdot 1000 \cdot \delta a$	$0m$	$0m$
$a_c \cdot 1000 \cdot \delta\lambda$	$-1m$	$-1080m$
$a_c \cdot 1000 \cdot \delta e_x$	$1m$	$250m$
$a_c \cdot 1000 \cdot \delta e_y$	$1m$	$250m$
$a_c \cdot 1000 \cdot \delta i_x$	$1m$	$150m$
$a_c \cdot 1000 \cdot \delta i_y$	$1m$	$150m$

Table 5.13: 4 Sats: Initial and final relative states of Spacecraft 4.

It can be seen how final states have been chosen in order to keep $\delta\overline{e}$ and $\delta\overline{i}$ parallel while φ_1, φ_2, φ_3, φ_4 and θ_1, θ_2, θ_3, θ_4 are in phase.

$$\boldsymbol{Q}_1 = \boldsymbol{Q}_2 = \boldsymbol{Q}_3 = \boldsymbol{Q}_4 = \frac{13}{2} \cdot \begin{bmatrix} 1 & 0 & 0 & 0 & 0 & 0 \\ 0 & 1 & 0 & 0 & 0 & 0 \\ 0 & 0 & 1 & 0 & 0 & 0 \\ 0 & 0 & 0 & 1 & 0 & 0 \\ 0 & 0 & 0 & 0 & 1 & 0 \\ 0 & 0 & 0 & 0 & 0 & 1 \end{bmatrix} \tag{5.15}$$

$$\boldsymbol{R}_1 = \boldsymbol{R}_2 = \boldsymbol{R}_3 = \boldsymbol{R}_4 = 5 \cdot \begin{bmatrix} 1 & 0 & 0 \\ 0 & 1 & 0 \\ 0 & 0 & 1 \end{bmatrix} \tag{5.16}$$

ΔV

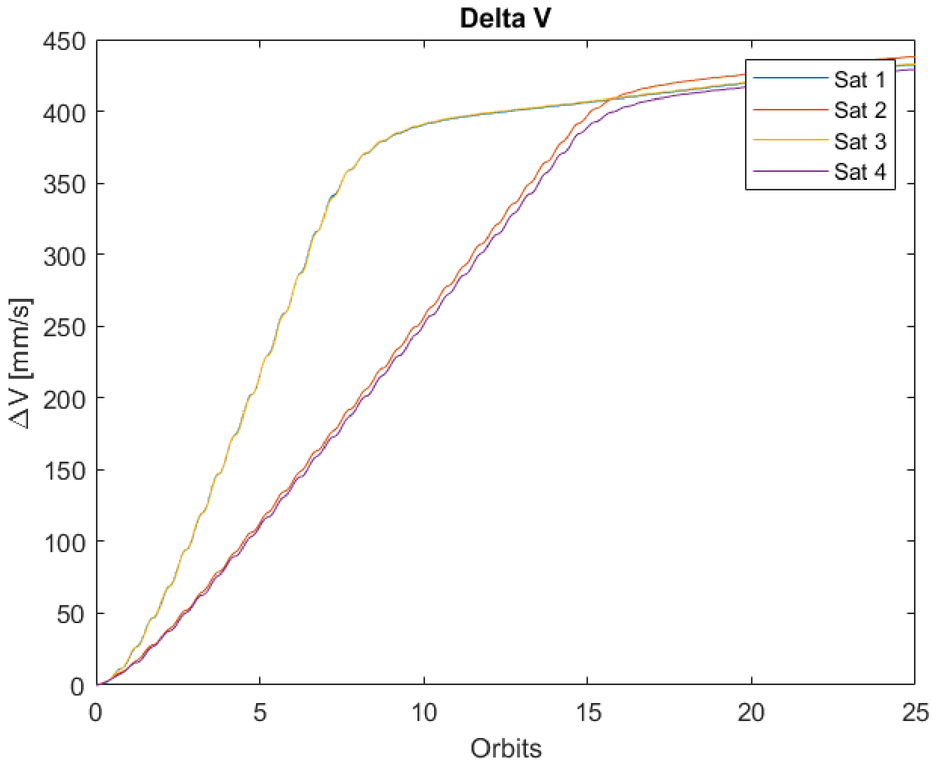

Figure 5.15: ΔV over time.

Sat	Lower Bound	Scenario	% more than LB
1	$0.4277\frac{m}{s}$	$0.4322\frac{m}{s}$	1.1
2	$0.4277\frac{m}{s}$	$0.4378\frac{m}{s}$	2.4
3	$0.4277\frac{m}{s}$	$0.4327\frac{m}{s}$	1.2
4	$0.4277\frac{m}{s}$	$0.4288\frac{m}{s}$	0.26

Table 5.14: 4 Sats: Comparison between the scenario ΔV with the lower bound.

Let's suppose $tol = 5\%$, the fuel balance is achieved since the maximum fuel difference is:

$$\frac{|\Delta V_2 - \Delta V_4|}{\Delta V_2} = 2.1\% \tag{5.17}$$

RT plane relative motion

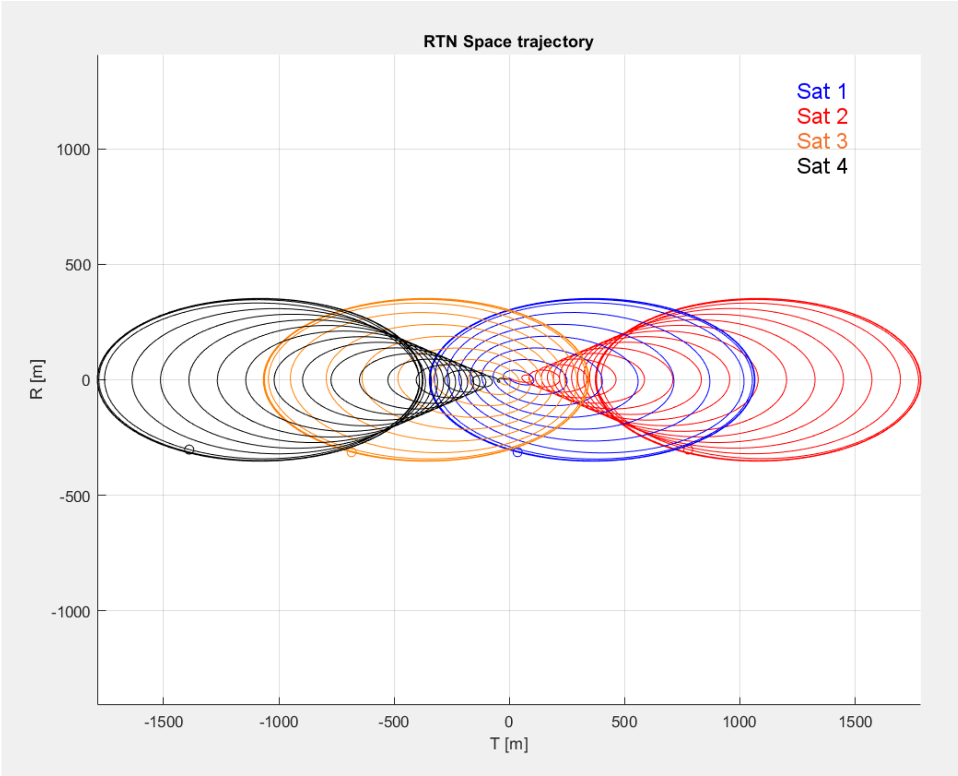

Figure 5.16: RT plane motion relative to the virtual chief.

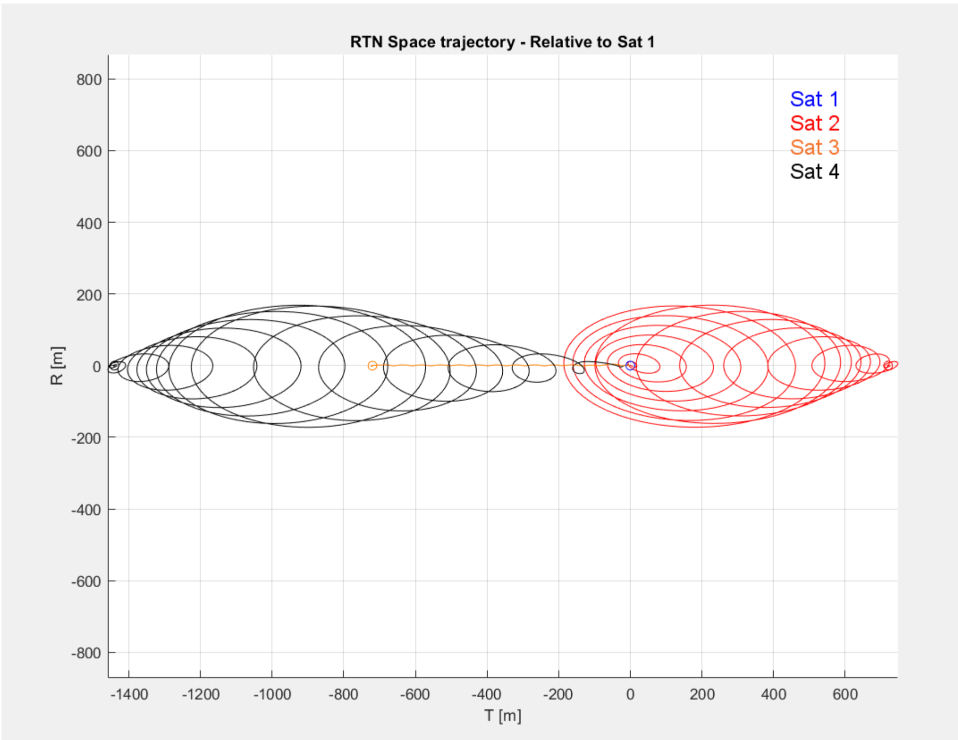

Figure 5.17: RT plane motion relative to Sat 1.

Sat	Desired $\delta\lambda$	Real $\delta\lambda$
1	$360m$	$358m$
2	$1080m$	$1078m$
3	$-360m$	$-361m$
4	$-1080m$	$-1081m$

Table 5.15: 4 Sats: Comparison between desired and real $\delta\lambda$.

It can be seen from 5.15 that the along-track separation between adjacent satellites is $\simeq 720m$.

Minimum and real separations between satellites

Assuming that in this case we can eliminate the along-track uncertainties, the minimum separation between satellites is given by:

$$\delta r_{min} = \sqrt{\delta r_t^2 + \delta r_{nr}^2} \tag{5.18}$$

δr_{nr} is given by (4.10) and

$$\delta r_t = \begin{cases} 0 \quad\quad if \;\; |\Delta\delta\lambda| - 2\,|\Delta\delta\bar{e}| < 0 \\ a_c \cdot 1000 \cdot (|\Delta\delta\lambda| - 2\,|\Delta\delta\bar{e}|) \quad\quad if \;\; |\Delta\delta\lambda| - 2\,|\Delta\delta\bar{e}| > 0 \end{cases} \tag{5.19}$$

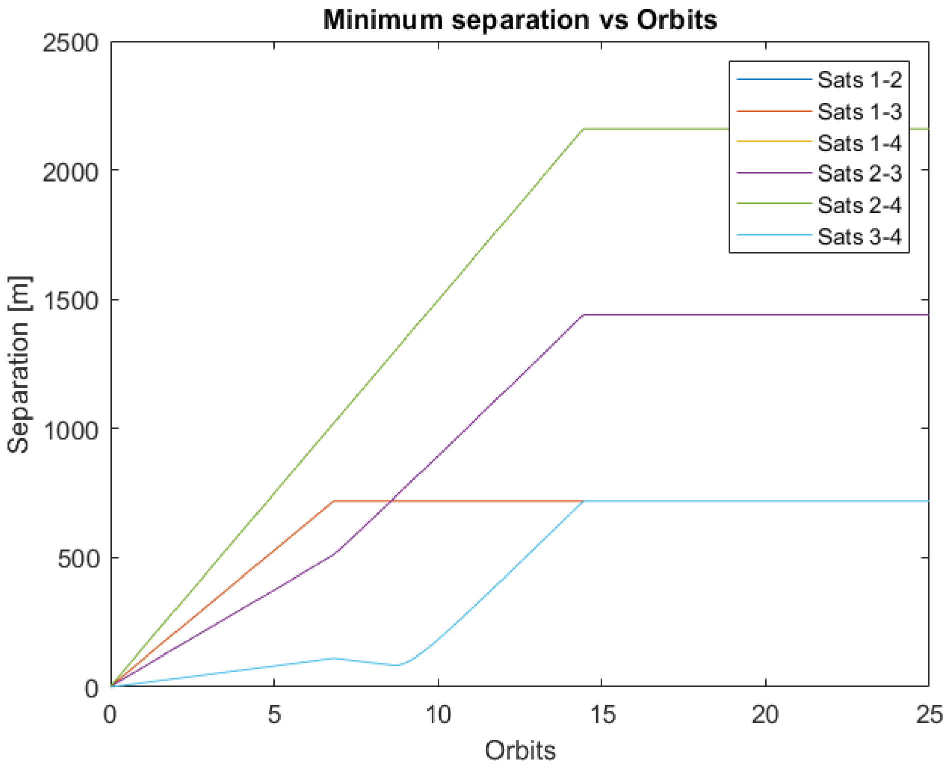

Figure 5.18: 4 Sats: Minimum separation over time.

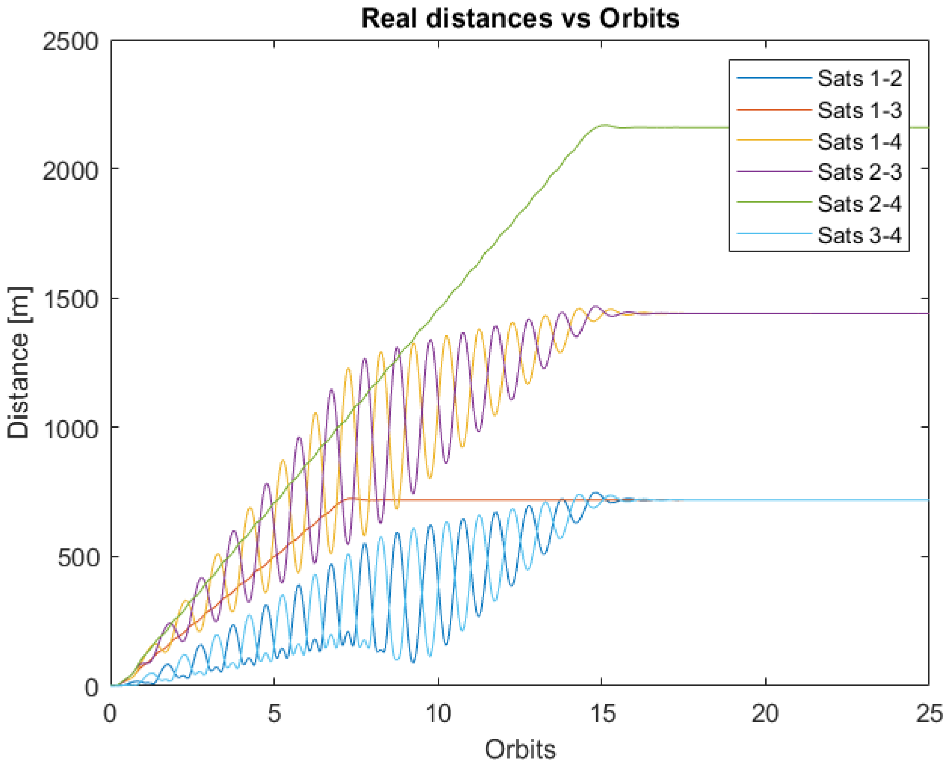

Figure 5.19: 4 Sats: Real separation over time.

5.2.3 Scenario 3: TanDEM-X like mission with initial fuel unbalance

This Scenario is very similar to Scenario 1, the main difference is that we will suppose an initial fuel unbalance between the two spacecraft due to previous maneuvering errors or collision avoidance burns.
Let's suppose that for some reason Satellite 2 consumed $0.15\frac{m}{s}$ more than Satellite 1; then we should design our maneuver such that:

$$\Delta V_1 - \Delta V_2 = 0.15\frac{m}{s} \tag{5.20}$$

In this scenario, a reconfiguration maneuver will be simulated, from a configuration where the two baselines are in the range $1450 - 1550m$ to the final configuration according to mission constraints.
Mission constraint:

- Horizontal and Vertical baselines in the range $500 - 550m$.

Input Data

The chief reference orbit expressed in absolute relative elements will be:

$$\overline{X}_c = \begin{pmatrix} a_c \\ e_c \\ i_c \\ \Omega_c \\ \omega_c \\ f_c \end{pmatrix} = \begin{pmatrix} 6878km \\ 0.0002 \\ 97.4\,\text{deg} \\ 260\,\text{deg} \\ 90\,\text{deg} \\ 315\,\text{deg} \end{pmatrix} \tag{5.21}$$

The mean relative elements are computed using GMAT and the Brouwer-Lyddane method.
i_c has been chosen in order to realize a *Sun-Synchronous* orbit.
Time data:

- $t_0 = 0$;
- $T = 25T_{orbit} = 141920s$.

Initial and final states:

ROE Variable	Initial	Final
$a_c \cdot 1000 \cdot \delta a$	$0m$	$0m$
$a_c \cdot 1000 \cdot \delta\lambda$	$0m$	$0m$
$a_c \cdot 1000 \cdot \delta e_x$	$530m$	$(190 - x)\,m$
$a_c \cdot 1000 \cdot \delta e_y$	$530m$	$(190 - x)\,m$
$a_c \cdot 1000 \cdot \delta i_x$	$530m$	$(190 - x)\,m$
$a_c \cdot 1000 \cdot \delta i_y$	$530m$	$(190 - x)\,m$

Table 5.16: TanDEM-X 2: Initial and final relative states of Spacecraft 1.

ROE Variable	Initial	Final
$a_c \cdot 1000 \cdot \delta a$	$0m$	$0m$
$a_c \cdot 1000 \cdot \delta\lambda$	$0m$	$0m$
$a_c \cdot 1000 \cdot \delta e_x$	$-530m$	$(-190 - x)\,m$
$a_c \cdot 1000 \cdot \delta e_y$	$-530m$	$(-190 - x)\,m$
$a_c \cdot 1000 \cdot \delta i_x$	$-530m$	$(-190 - x)\,m$
$a_c \cdot 1000 \cdot \delta i_y$	$-530m$	$(-190 - x)\,m$

Table 5.17: TanDEM-X 2: Initial and final relative states of Spacecraft 2.

Final states have been chosen in order to keep $\delta\bar{e}$ and $\delta\bar{i}$ parallel for each of the two satellites while φ_1, θ_1 and φ_2, θ_2 are out of phase by 180 deg. The initial baselines are:

$$B_{H_0} = a_c \cdot 1000 \cdot \left|\Delta\delta\bar{i}_0\right| = \left|\begin{pmatrix}1060m\\1060m\end{pmatrix}\right| = 1499m \tag{5.22}$$

$$B_{V_0} = a_c \cdot 1000 \cdot \left|\Delta\delta\bar{e}_0\right| = \left|\begin{pmatrix}1060m\\1060m\end{pmatrix}\right| = 1499m \tag{5.23}$$

Using the final states, the final baselines can be computed:

$$B_{H_f} = a_c \cdot 1000 \cdot \left|\Delta\delta\bar{i}_f\right| = \left|\begin{pmatrix}380m\\380m\end{pmatrix}\right| \simeq 537m \tag{5.24}$$

$$B_{V_f} = a_c \cdot 1000 \cdot \left|\Delta\delta\bar{e}_f\right| = \left|\begin{pmatrix}380m\\380m\end{pmatrix}\right| \simeq 537m \tag{5.25}$$

Since our controller can achieve a near-optimal ΔV, we can rewrite (5.20) as:

$$\Delta V_{min_1} - \Delta V_{min_2} = 0.15\frac{m}{s} = \Delta V_{unb} \tag{5.26}$$

Then, we should find the value of x such that (5.26) is satisfied.
Using (2.36), we can write:

$$\Delta V_{min_1} = 1000\left(a_c\frac{n_c}{\eta_c}\right)\left(\frac{\left|\delta\bar{e}_{0_1} - \delta\bar{e}_{d_1}\right|}{2} + (1 - e_c)\left|\delta\bar{i}_{0_1} - \delta\bar{i}_{d_1}\right|\right) \tag{5.27}$$

$$\Delta V_{min_2} = 1000 \left(a_c \frac{n_c}{\eta_c} \right) \left(\frac{|\delta \bar{e}_{0_2} - \delta \bar{e}_{d_2}|}{2} + (1 - e_c) \left| \delta \bar{i}_{0_2} - \delta \bar{i}_{d_2} \right| \right) \tag{5.28}$$

Substituting in (5.26) we find:

$$1000 \left(a_c \frac{n_c}{\eta_c} \right) \left(\frac{|\delta \bar{e}_{0_1} - \delta \bar{e}_{d_1}| - |\delta \bar{e}_{0_2} - \delta \bar{e}_{d_2}|}{2} + (1 - e_c) \left(\left| \delta \bar{i}_{0_1} - \delta \bar{i}_{d_1} \right| - \left| \delta \bar{i}_{0_2} - \delta \bar{i}_{d_2} \right| \right) \right) = \Delta V_{unb} \tag{5.29}$$

$$\sqrt{2}\,(340m + x) - \sqrt{2}\,(340m - x) = \frac{\eta_c}{n_c \left(\frac{1}{2} + 1 - e_c \right)} \Delta V_{unb} \tag{5.30}$$

$$x = \frac{1}{2\sqrt{2}} \frac{\eta_c}{n_c \left(\frac{3}{2} - e_c \right)} \Delta V_{unb} \simeq 32m \tag{5.31}$$

Other input data:

$$\boldsymbol{Q}_1 = \boldsymbol{Q}_2 = 10 \cdot \begin{bmatrix} 1 & 0 & 0 & 0 & 0 & 0 \\ 0 & 1 & 0 & 0 & 0 & 0 \\ 0 & 0 & 1 & 0 & 0 & 0 \\ 0 & 0 & 0 & 1 & 0 & 0 \\ 0 & 0 & 0 & 0 & 1 & 0 \\ 0 & 0 & 0 & 0 & 0 & 1 \end{bmatrix} \tag{5.32}$$

$$\boldsymbol{R}_1 = 4 \cdot \begin{bmatrix} 1 & 0 & 0 \\ 0 & 1 & 0 \\ 0 & 0 & 1 \end{bmatrix} \tag{5.33}$$

$$\boldsymbol{R}_2 = 15 \cdot \begin{bmatrix} 1 & 0 & 0 \\ 0 & 1 & 0 \\ 0 & 0 & 1 \end{bmatrix} \tag{5.34}$$

$\boldsymbol{\Delta V}$

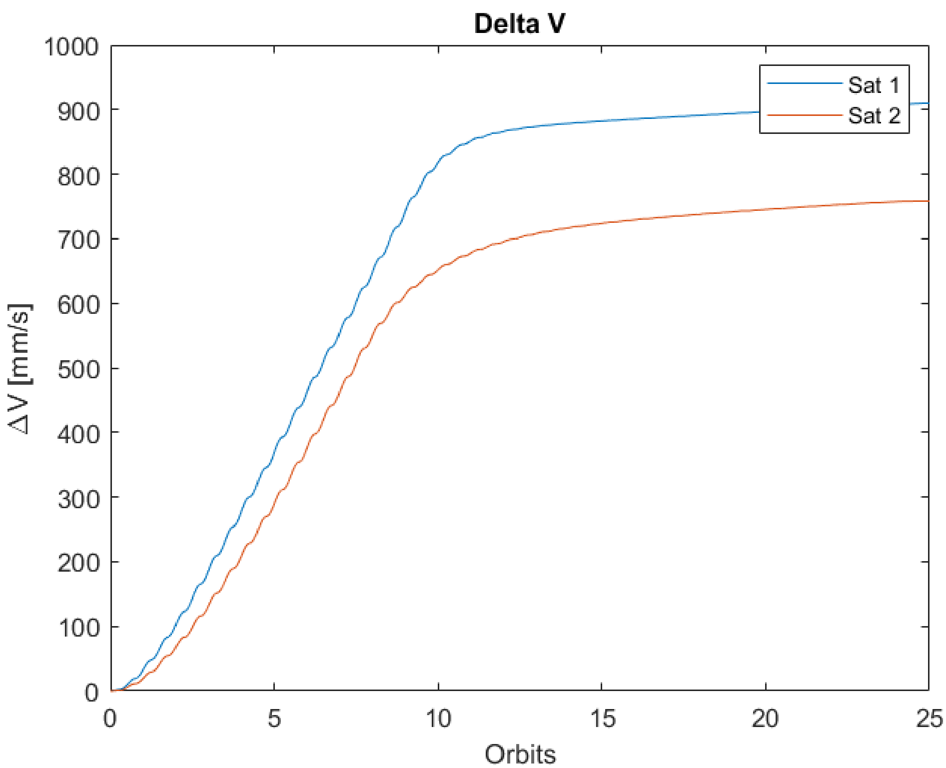

Figure 5.20: ΔV over time.

Sat	Lower Bound	Scenario	% more than LB
Sat1	$0.8725\frac{m}{s}$	$0.91\frac{m}{s}$	4.3
Sat2	$0.7225\frac{m}{s}$	$0.758\frac{m}{s}$	4.9

Table 5.18: TanDEM 2: Comparison between the scenario ΔV with the lower bound.

$$\Delta V_1 - \Delta V_2 = 0.152\frac{m}{s} \tag{5.35}$$

Relative motion in the RT and RN planes

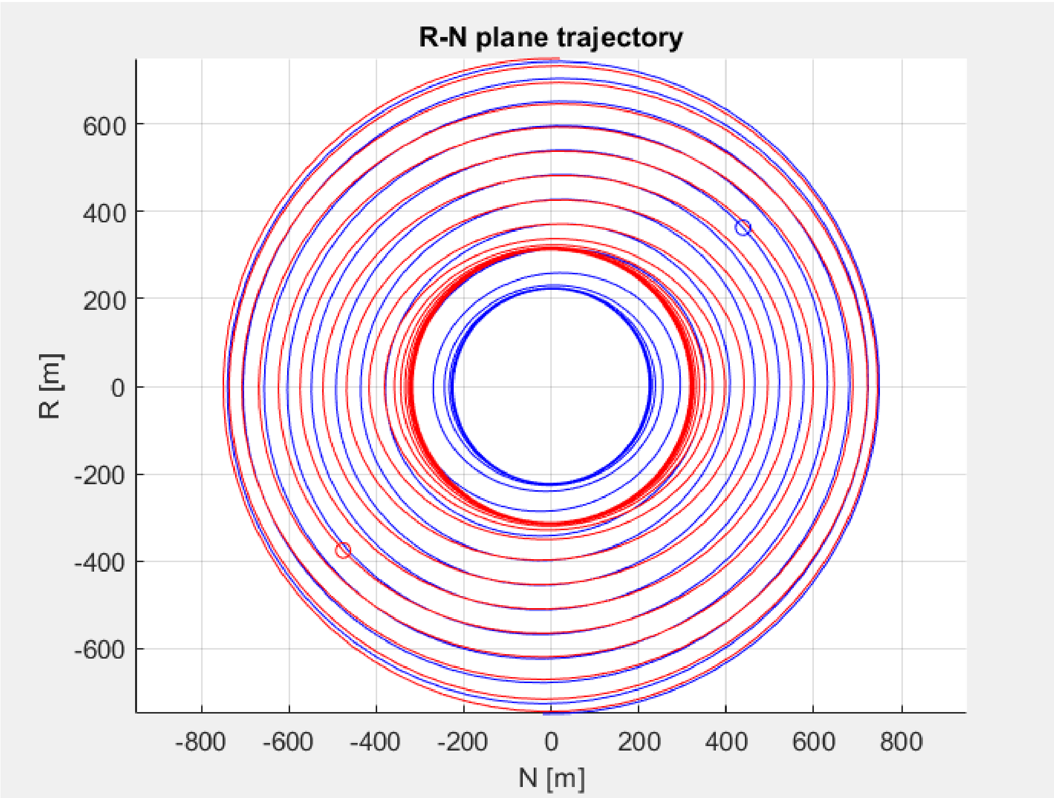

Figure 5.21: Relative motion in the RN plane.

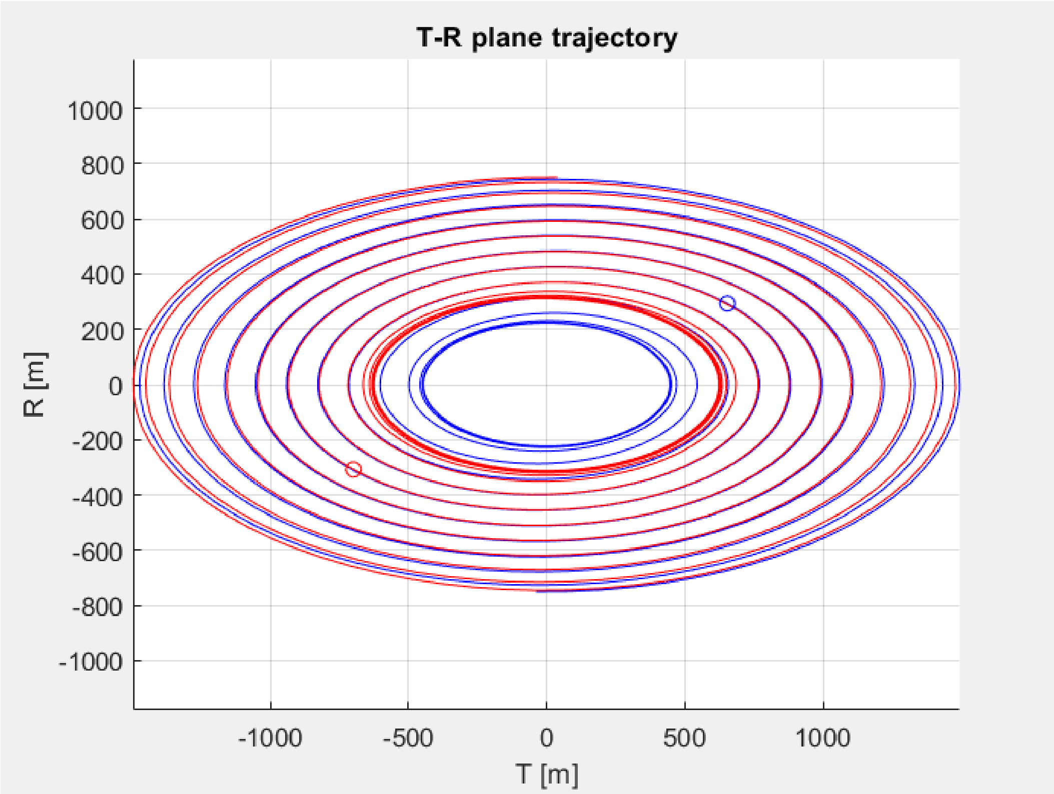

Figure 5.22: Relative motion in the RT plane.

Helix formation

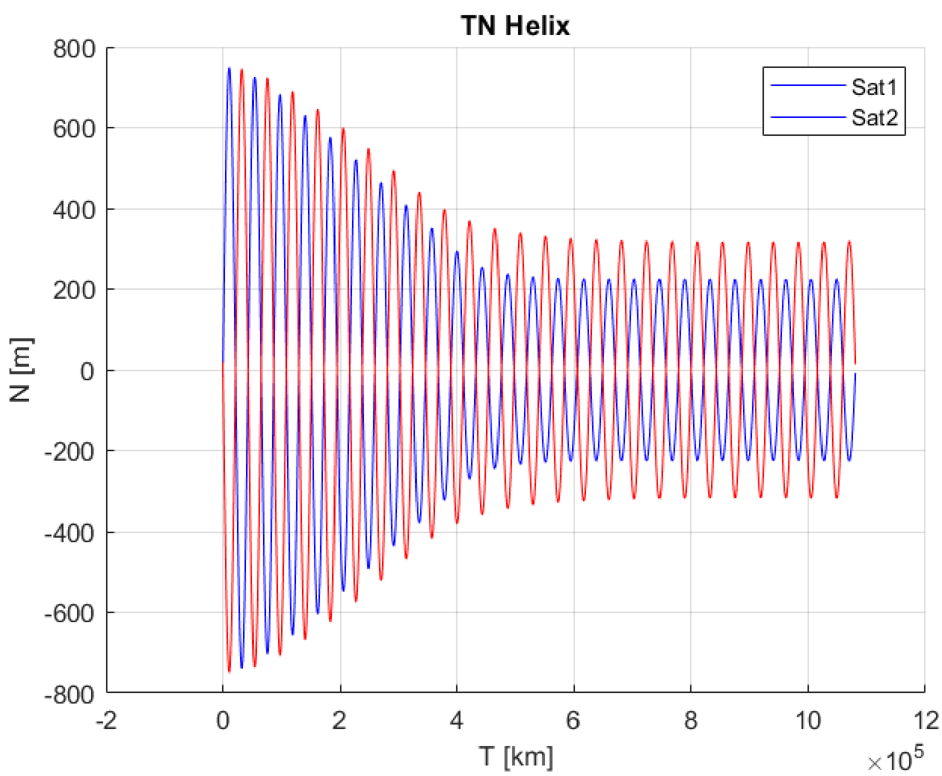

Figure 5.23: Helix projection in TN plane.

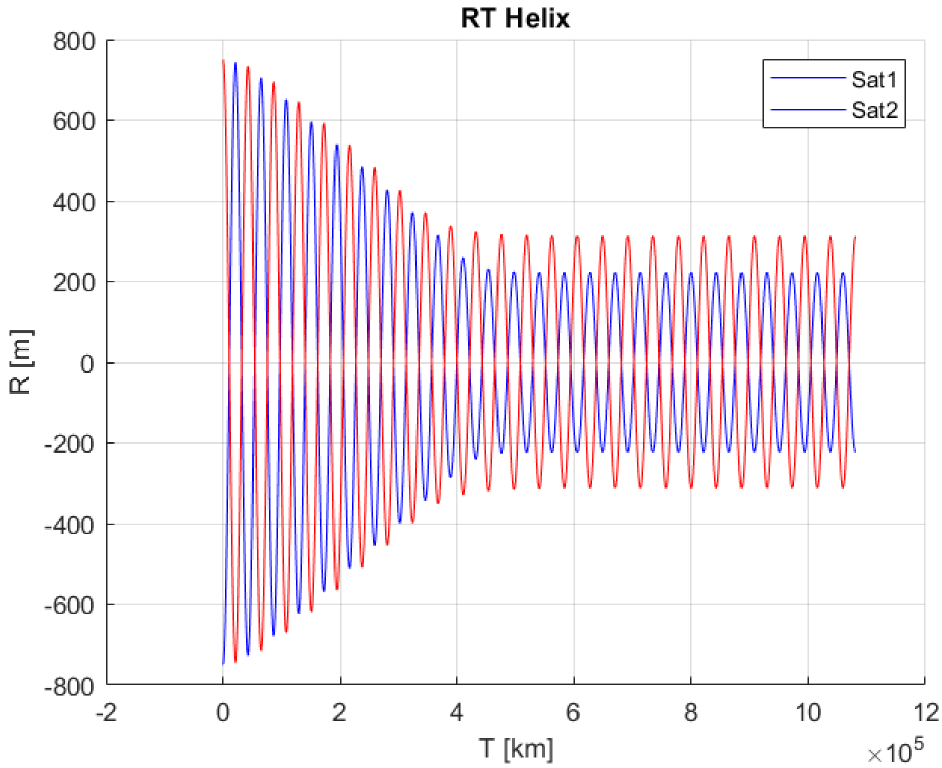

Figure 5.24: Helix projection in RT plane.

We can see the final Horizontal Baseline in fig. 5.23 and the Vertical Baseline in fig. 5.24. In this case the two are equal $B_H = B_V \simeq 537m$. Both the mission constraint and the fuel balance are satisfied.

Chapter 6

Model Validation using GMAT

6.1 Chapter Overview

6.1.1 Introduction

The purpose of this chapter is to validate the proposed framework using the high-precision orbit propagator implemented on *GMAT* (logo in fig. 3.4).
General Mission Analysis Tool (GMAT) is an open source software system for space mission design, optimization, and navigation developed by *NASA* in collaboration with Universities and Research Institutes around the world.
At this scope, a Scenario will be first simulated using the proposed framework and then validated using GMAT, in order to show the equality of the results.

6.1.2 Validation Procedure

This kind of analysis will follow the following steps:

- Definition of a Scenario;
- Simulation of that Scenario using the proposed LQR framework;
- Exportation of control accelerations to GMAT environment;
- Orbit propagation using GMAT.

At the end, the state results from the *MATLAB* and *GMAT* simulations will be compared.

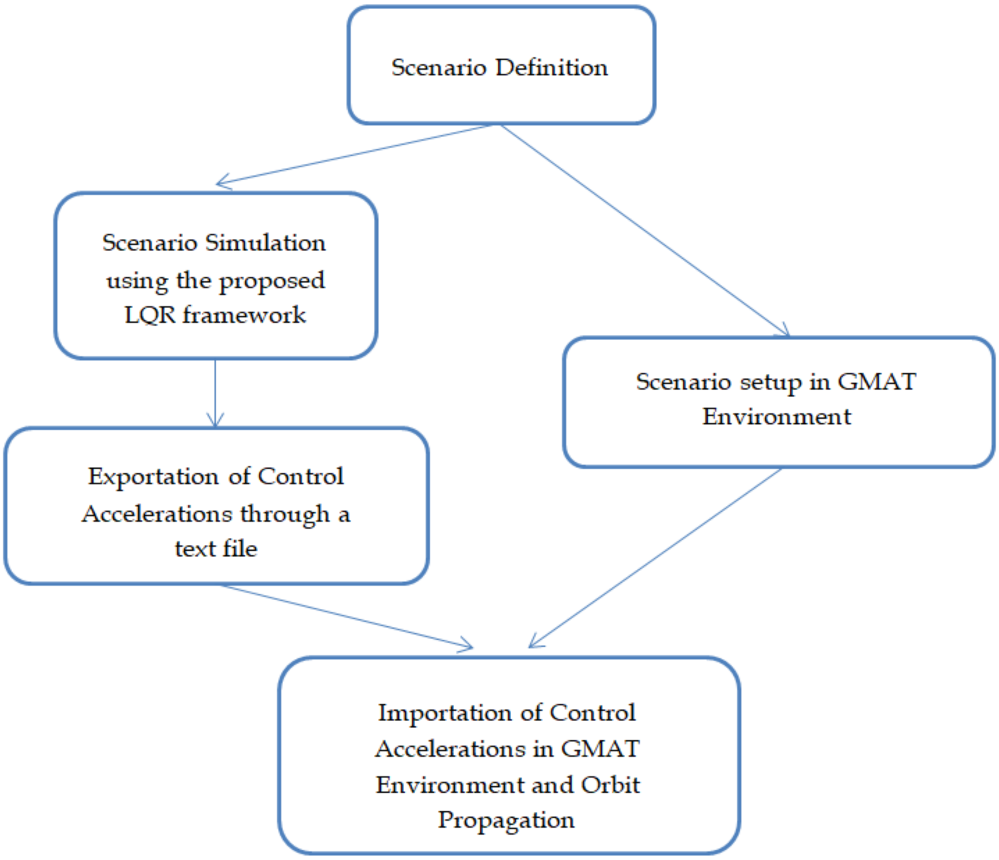

Figure 6.1: Validation procedure scheme.

6.2 Scenario for Model Validation

6.2.1 Scenario Introduction

This scenario consists in the deployment of two 3U cubesats (4 kg) from a chief spacecraft in order to perform proximity operations, the goal is to make them orbit around the chief at a fixed minimum distance in the RT plane (different for each satellite).
Mission constraints:

- Fixed minimum distance between Sat 1 and virtual chief in the RT plane $r_{min_1} = 495m$;
- Fixed minimum distance between Sat 2 and virtual chief in the RT plane $r_{min_2} = 565m$;
- Fuel Balance;
- Collision Free deployment.

Input Data

- $\overline{X}_c$ as in (3.35);
- $t_0 = 0$;
- $T = 25T_{orbit} = 141920s$;
- $tol = 0.05$.

The initial and final states (expressed in meters) of the two spacecraft are:

ROE Variable	Initial	Final
$a_c \cdot 1000 \cdot \delta a$	$0m$	$0m$
$a_c \cdot 1000 \cdot \delta\lambda$	$0m$	$0m$
$a_c \cdot 1000 \cdot \delta e_x$	$1m$	$350m$
$a_c \cdot 1000 \cdot \delta e_y$	$1m$	$350m$
$a_c \cdot 1000 \cdot \delta i_x$	$1m$	$250m$
$a_c \cdot 1000 \cdot \delta i_y$	$1m$	$250m$

Table 6.1: GMAT Scenario: Initial and final relative states of Spacecraft 1.

ROE Variable	Initial	Final
$a_c \cdot 1000 \cdot \delta a$	$0m$	$0m$
$a_c \cdot 1000 \cdot \delta\lambda$	$0m$	$0m$
$a_c \cdot 1000 \cdot \delta e_x$	$-1m$	$-400m$
$a_c \cdot 1000 \cdot \delta e_y$	$-1m$	$-400m$
$a_c \cdot 1000 \cdot \delta i_x$	$-1m$	$x\ m$
$a_c \cdot 1000 \cdot \delta i_y$	$-1m$	$x\ m$

Table 6.2: GMAT Scenario: Initial and final relative states of Spacecraft 2.

Initial and final states were chosen in order to assure that $\Delta\delta\bar{e}$ and $\Delta\delta\bar{i}$ remain parallel while φ_1, θ_1 and φ_2, θ_2 are out of phase by 180 deg. Because of this, collision avoidance is assured and the relative motion of the two spacecraft with respect to the virtual chief is defined by (2.14), (2.15) and (2.16).
Furthermore, the RT plane minimum distance constraints are satisfied:

$$r_{min_1} = a_c \cdot 1000 \cdot |\delta\bar{e}_{d_1}| = 495m \tag{6.1}$$

$$r_{min_2} = a_c \cdot 1000 \cdot |\delta\bar{e}_{d_2}| = 565m \tag{6.2}$$

We should compute x in order to achieve fuel balance. We know that:

$$\Delta V_{min_1} = 1000\left(a_c\frac{n_c}{\eta_c}\right)\left(\frac{|\delta\bar{e}_{0_1} - \delta\bar{e}_{d_1}|}{2} + (1-e_c)\left|\delta\bar{i}_{0_1} - \delta\bar{i}_{d_1}\right|\right) \tag{6.3}$$

$$\Delta V_{min_2} = 1000\left(a_c\frac{n_c}{\eta_c}\right)\left(\frac{|\delta\bar{e}_{0_2} - \delta\bar{e}_{d_2}|}{2} + (1-e_c)\left|\delta\bar{i}_{0_2} - \delta\bar{i}_{d_2}\right|\right) \tag{6.4}$$

The condition that must be imposed is:

$$\Delta V_{min_1} = \Delta V_{min_2} \tag{6.5}$$

By solving (6.5) for x we obtain:

$$x = -225m \tag{6.6}$$

Other input data:

$$\boldsymbol{Q}_1 = \boldsymbol{Q}_2 = 10 \cdot \begin{bmatrix} 1 & 0 & 0 & 0 & 0 & 0 \\ 0 & 1 & 0 & 0 & 0 & 0 \\ 0 & 0 & 1 & 0 & 0 & 0 \\ 0 & 0 & 0 & 1 & 0 & 0 \\ 0 & 0 & 0 & 0 & 1 & 0 \\ 0 & 0 & 0 & 0 & 0 & 1 \end{bmatrix} \tag{6.7}$$

$$\boldsymbol{R}_1 = \boldsymbol{R}_2 = 3 \cdot \begin{bmatrix} 1 & 0 & 0 \\ 0 & 1 & 0 \\ 0 & 0 & 1 \end{bmatrix} \tag{6.8}$$

6.2.2 Model Results

State

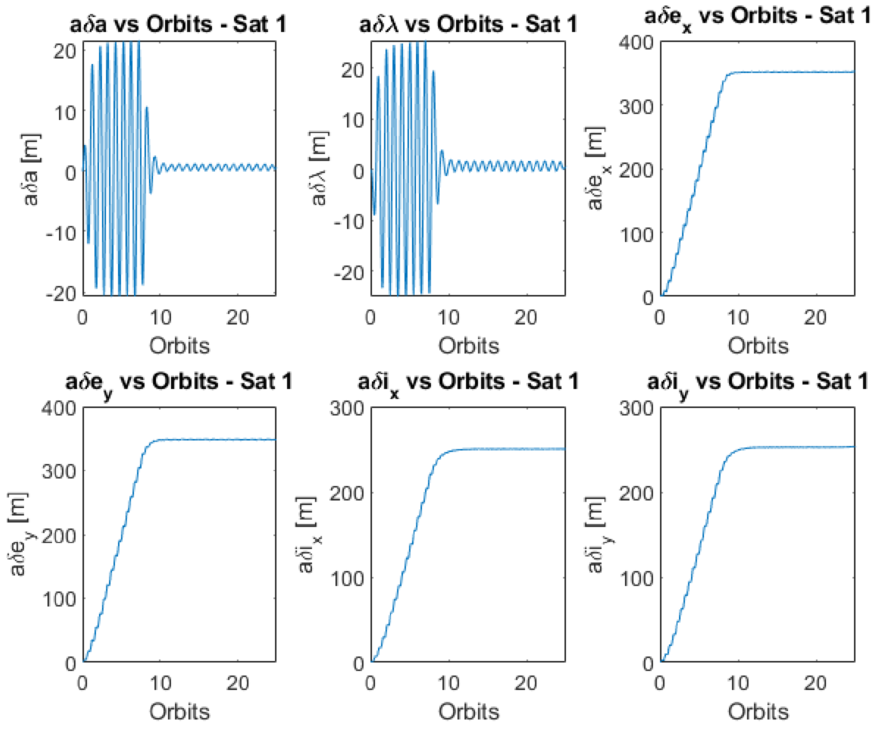

(a) GMAT Scenario: Spacecraft 1 state evolution.

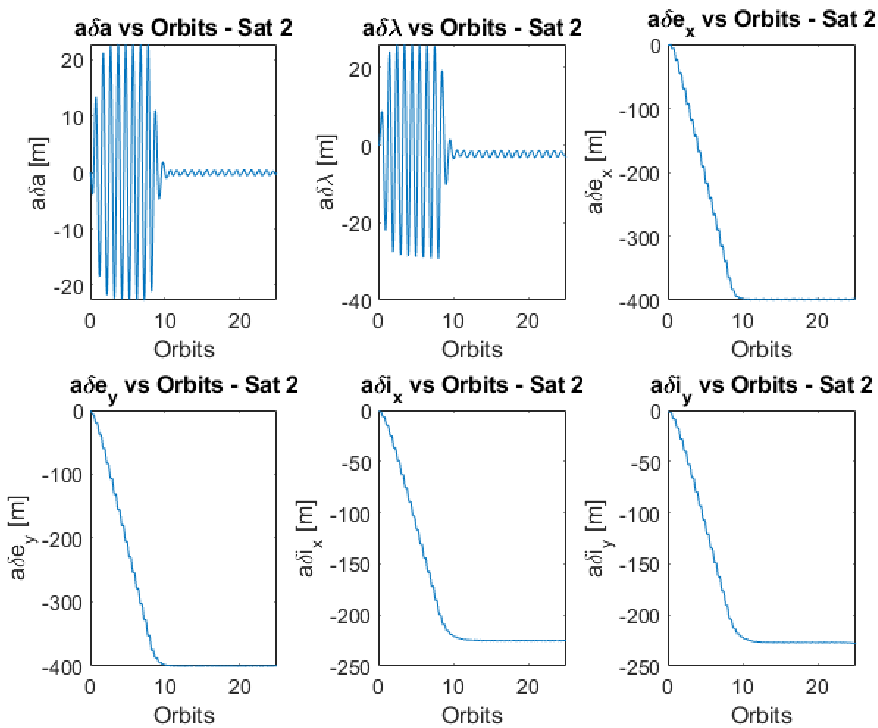

(b) GMAT Scenario: Spacecraft 2 state evolution.

Figure 6.2: GMAT Scenario: spacecraft state evolution.

Control

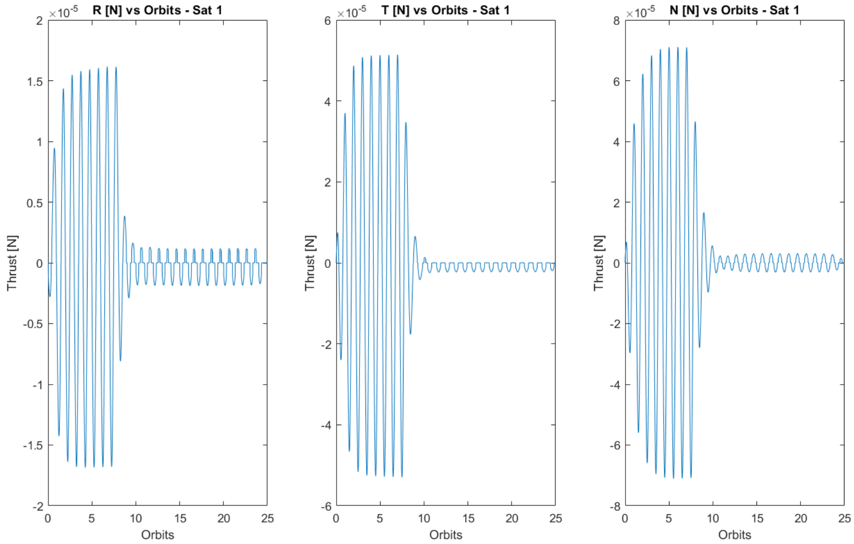

(a) GMAT Scenario: Spacecraft 1 control accelerations.

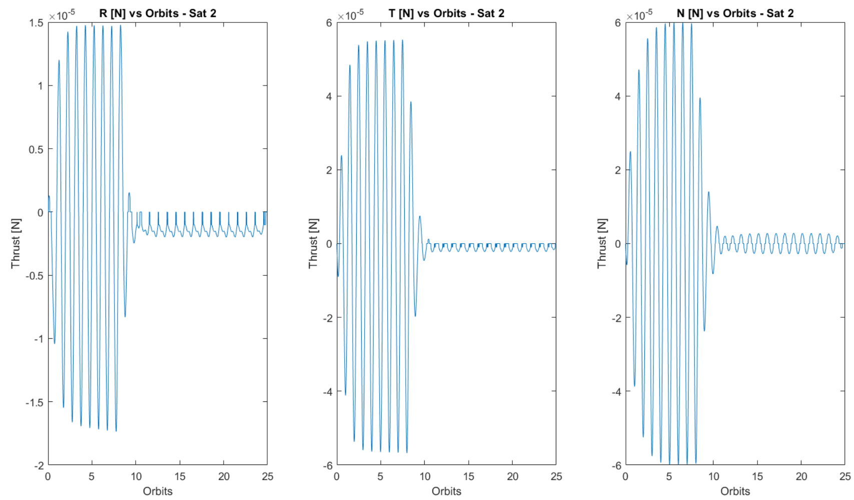

(b) GMAT Scenario: Spacecraft 2 control accelerations.

Figure 6.3: GMAT Scenario: spacecraft control accelerations.

The accelerations in fig. 6.3a and 6.3b will be exported as a text file and then imported in the GMAT environment.

Minimum separation and angle between $\Delta\delta\bar{e}$ and $\Delta\delta\bar{i}$

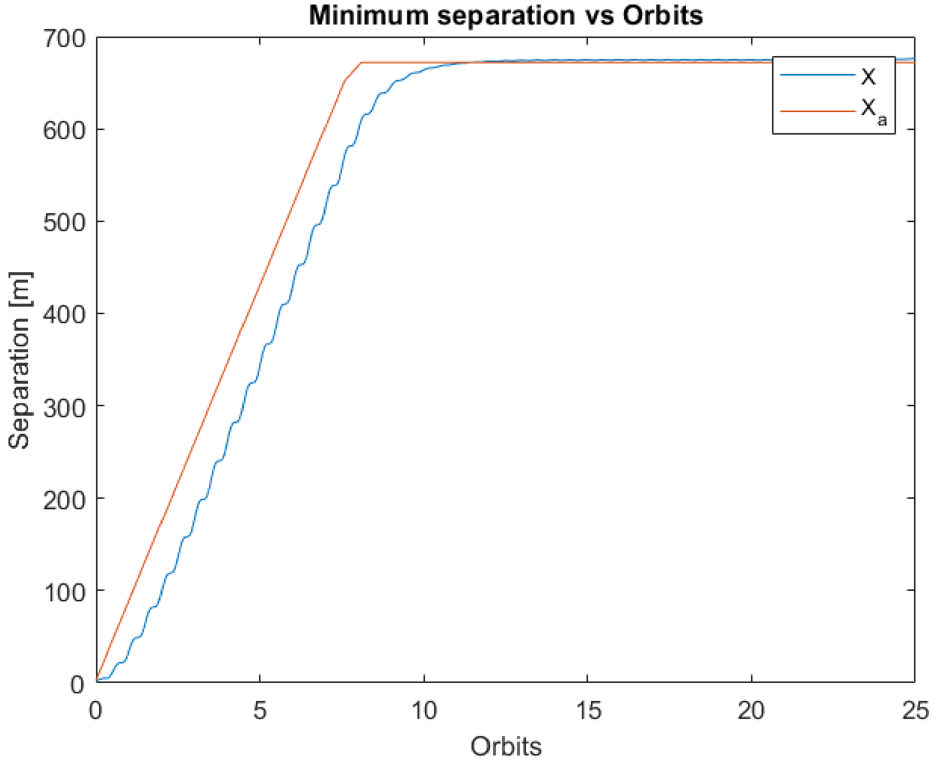

Figure 6.4: GMAT Scenario: Minimum separation between the applied references and state vectors of the two satellites.

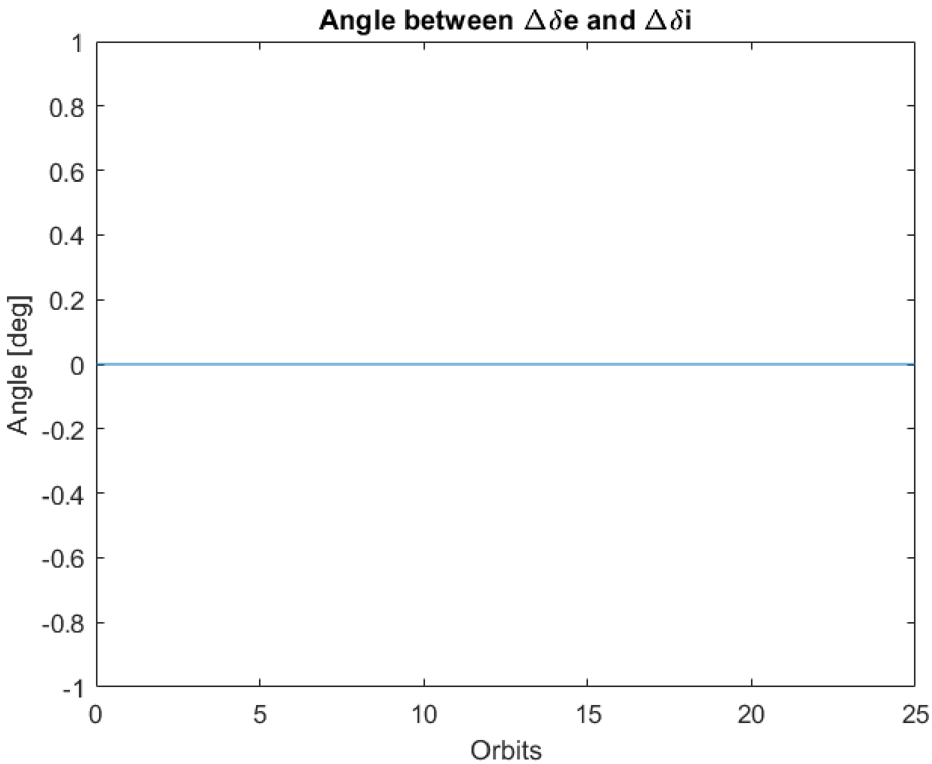

Figure 6.5: GMAT Scenario: Angle between $\Delta\delta\bar{e}$ and $\Delta\delta\bar{i}$.

It can be seen from fig. 6.4 and 6.5 how collision avoidance is assured.

Relative motion in the RT and RN planes

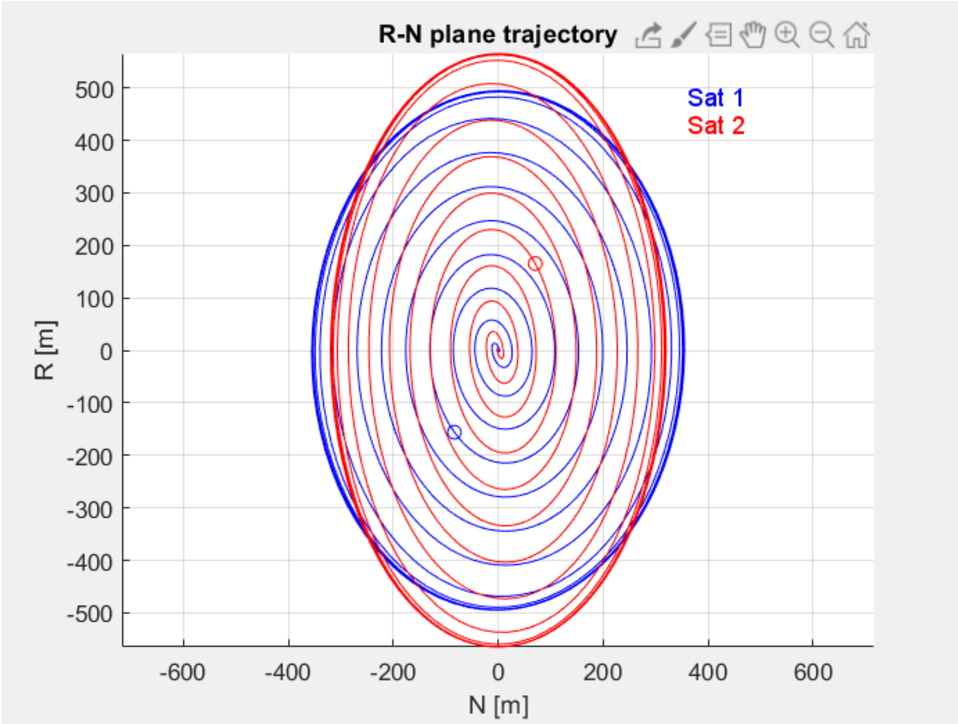

Figure 6.6: Relative motion in the RN plane.

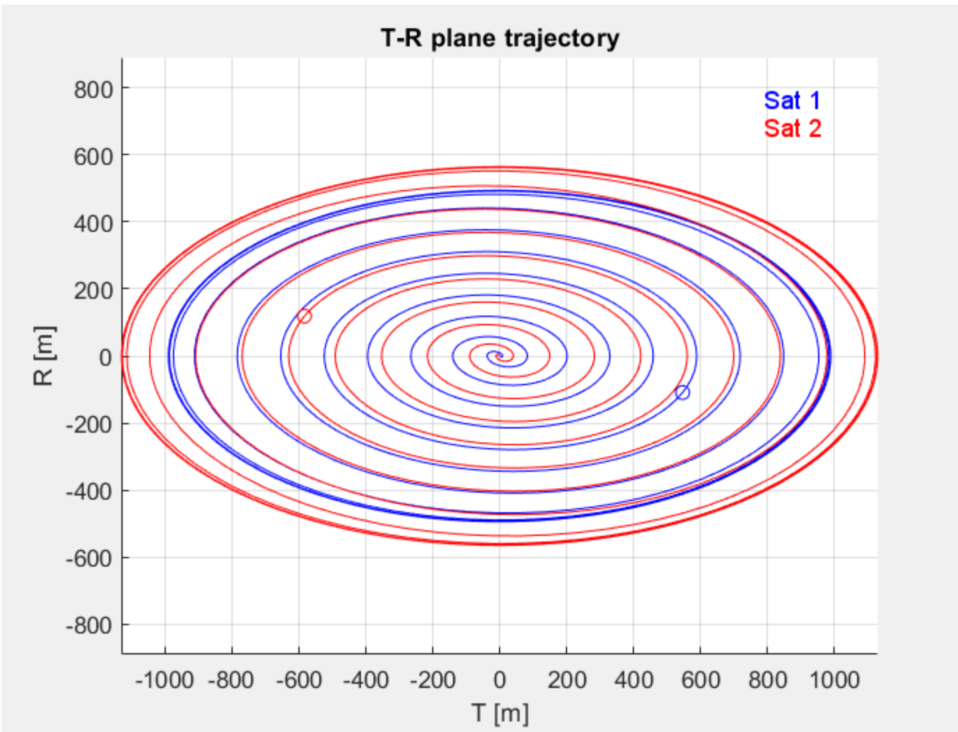

Figure 6.7: Relative motion in the RT plane.

ΔV

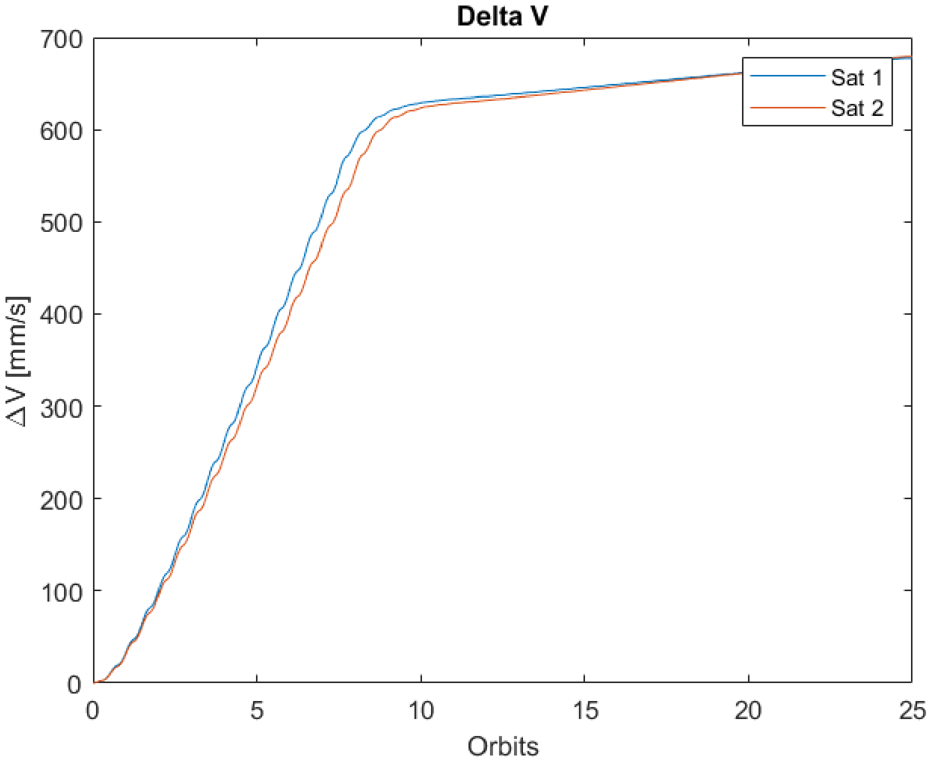

Figure 6.8: ΔV over time.

Sat	Lower Bound	Scenario	% more than LB
Sat1	$0.6625\frac{m}{s}$	$0.677\frac{m}{s}$	2.2
Sat2	$0.6625\frac{m}{s}$	$0.679\frac{m}{s}$	2.5

Table 6.3: GMAT Scenario: Comparison between the scenario ΔV with the lower bound.

Since $tol = 5\%$, fuel balance is achieved:

$$\frac{|\Delta V_2 - \Delta V_1|}{\Delta V_2} = 0.3\% \tag{6.9}$$

6.2.3 GMAT Simulation

The script implemented on GMAT is similar to the following pseudocode:

Algorithm 2: GMAT Script Pseudocode.

Chief orbit configuration;
Sat1 orbit configuration;
Sat2 orbit configuration;

Configuration of tanks and engines for Sat1 and Sat2;
Propagator configuration;
Continuous maneuvers definition;
Plots and Reports declaration;
Matlab function call in order to read the accelerations text file;

Begin Mission Sequence;
Control vector (u) and time vector (t) input from text file;
for *i in t* **do**
  Set engine accelerations u(i) from text file;
  Propagate;
  Compute state variables to display on plots;
end
End Mission Sequence;

Integrator	RungeKutta89
Central Body	Earth
Gravity Model	JGM-2 Degree: 2 Order: 2
Drag	MSISE-90

Table 6.4: GMAT Scenario: Propagator properties.

State variables results

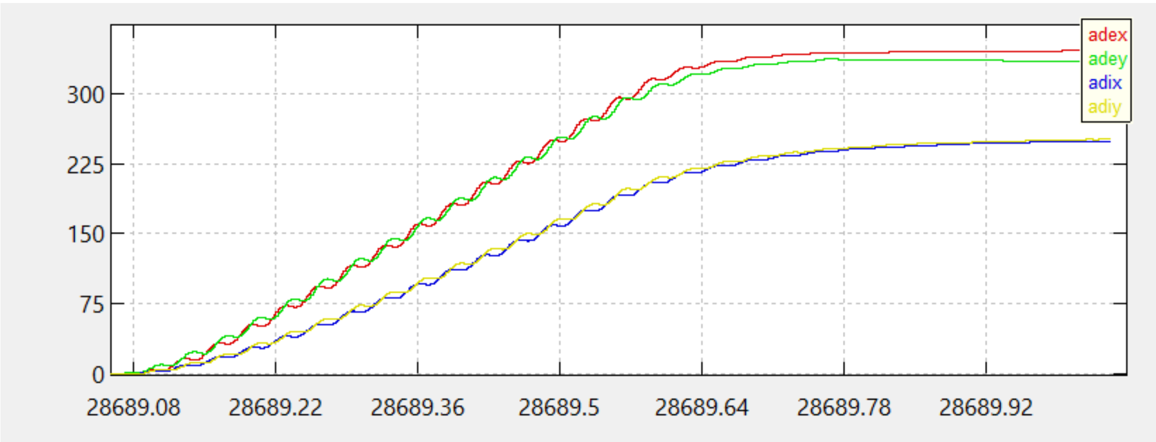

(a) GMAT Sim: Spacecraft 1 state evolution.

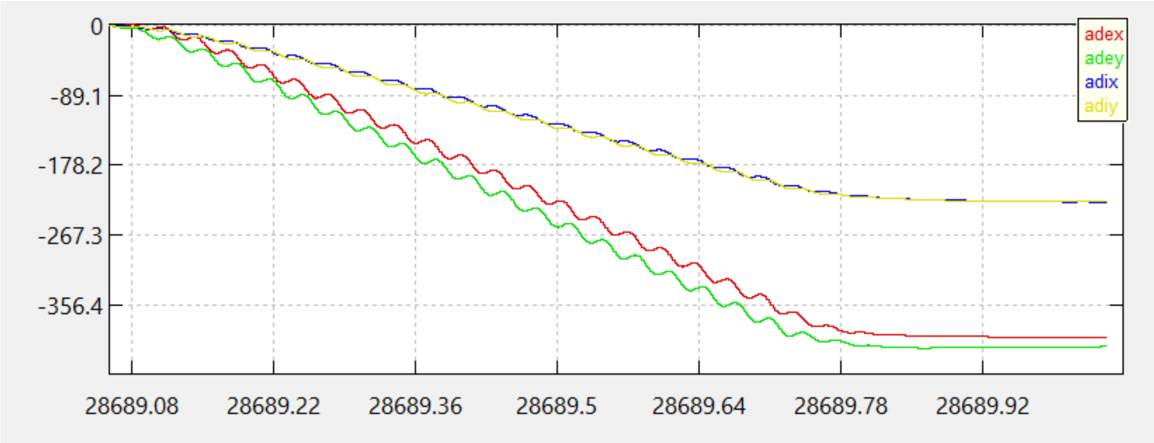

(b) GMAT Sim: Spacecraft 2 state evolution.

Figure 6.9: GMAT Sim: spacecraft state evolution.

6.2.4 Conclusion

Let's compare the results obtained with both the *MATLAB* and *GMAT* simulations:

ROE Variable	Desired	MATLAB	GMAT
$a_c \cdot 1000 \cdot \delta e_x$	$350m$	$351m$	$356m$
$a_c \cdot 1000 \cdot \delta e_y$	$350m$	$348m$	$344m$
$a_c \cdot 1000 \cdot \delta i_x$	$250m$	$250m$	$249m$
$a_c \cdot 1000 \cdot \delta i_y$	$250m$	$253m$	$252m$

Table 6.5: GMAT Scenario: Comparison between MATLAB and GMAT results for relative state variables of Spacecraft 1.

ROE Variable	Desired	MATLAB	GMAT
$a_c \cdot 1000 \cdot \delta e_x$	$-400m$	$-398m$	$-397m$
$a_c \cdot 1000 \cdot \delta e_y$	$-400m$	$-400m$	$-408m$
$a_c \cdot 1000 \cdot \delta i_x$	$-225m$	$-225m$	$-224m$
$a_c \cdot 1000 \cdot \delta i_y$	$-225m$	$-228m$	$-223m$

Table 6.6: GMAT Scenario: Comparison between MATLAB and GMAT results for relative state variables of Spacecraft 2.

The greatest error between the simulation results is scored by δi_y for Sat 2:

$$err_{max} = \frac{\delta i_{y_{MATLAB}} - \delta i_{y_{GMAT}}}{\delta i_{y_{GMAT}}} = 2.2\% \tag{6.10}$$

This error is still very small, then we can consider validated the MATLAB model.

Chapter 7

Conclusions and future work

7.1 Conclusions about the Model

In this thesis, the workflow presented in 1.4 has been discussed completely and in detail: firstly explaining all of its parts from a theoretical and mathematical point of view, secondly showing the implementation method and how it could be applied to real-world scenarios.
The *Mean Relative Orbital Elements* (ROE) dynamical system, developed by [11, 26] very recently, has been found to be very practical and insightful for Formation-Flying applications in LEO. The main feature of this model was the linearity, thanks to which a Linear Quadratic Regulator could be implemented in order to control the relative motion; another incredible advantage of this dynamic system was the easy visualization of the relative motion with respect to the Chief spacecraft, thanks to the *eccentricity/inclination vector separation* [25, 24].
The Controller based on the *Linear Quadratic Regulator* Theory has proven itself to be very solid and accurate, either in terms of fuel optimality and desired state tracking accuracy, still requesting a limited computational load (only one ODE must be solved). The Controller was then improved for reference trajectory tracking using an elegant Reference Governor method [29], which has proven to perform outstandingly well.
Collision Avoidance could be implemented easily in the model using a powerful mathematical tool as Artificial Potential Functions, in combination with the aforementioned Reference Governor approach. In order to employ this method, parallelism between relative eccentricity and inclination vectors must be assured. This assumption can be easily satisfied by proper mission and maneuver planning, in particular by choosing wisely the desired states.
Fuel Balance between spacecraft in a formation is an often disregarded issue in literature but yet very important; in fact, it is vital to avoid that one spacecraft would run out of fuel before the other ones, which is a situation that would cause a loss of controllability for the entire formation. In this work, this issue has been thoroughly addressed by proposing two different strategies:

- $\boldsymbol{R}$ matrix values have been exploited in order to increase the fuel consumption of the less-consuming satellite;
- Fuel Balance has been achieved by smart reconfiguration planning, by choosing wisely the desired states in order to satisfy the mission goals and constraints.

A discussion about the two strategies has been made, showing how the first one has proven itself to be quite inefficient from a fuel-optimality point of view compared to the second strategy, which is then the preferred one.
Finally, the whole model has been succesfully validated by importing its results in the *GMAT* environment in order to perform an high-precision Orbit Propagation simulation, and then by comparing the final results.

7.2 Future Work

A very interesting idea for future work could be to perform a computational load analysis of the model an then adapt it for the purpose of implementing it on a real satellite On-board Computer. The model should be modified in order to use real noisy GPS measurements, which should be filtered by a *Kalman Filter.* This could be done by implementing a Controller based on *Linear Quadratic Gaussian* theory, which is an optimal control problem where a quadratic cost function is minimized when the plant has random initial conditions, white noise disturbance input, and white measurement noise.
After this, the algorithm should be coded in a programming language suitable for On-board computers, as:

- C
- C++
- Python

After this, a propulsion subsystem testing could be performed, involving state-of-the-art μ-Newton thrusters such as *Field Emission Electric Propulsion* thrusters (FEEP), which nowadays are starting to be sold also for commercial applications.

List of Figures

1.1 Comparison between a Constellation and a Formation. 5
1.2 Architecture of Formation Flying coordination.[2] 5
1.3 Leader/Follower architecture.[2] 6
1.4 Work Flowchart 8

2.1 Spherical triangles for the relative inclination vector definition [25] 12
2.2 Relative eccentricity vector definition [25] 13
2.3 In-plane relative motion of two spacecraft with e/i vector separation [25] 14
2.4 Out-of-plane relative motion of two spacecraft with parallel e/i vectors (top) and orthogonal e/i vectors (bottom) [25] 15
2.5 Effect of Keplerian and J_2 STMs on relative motion. [11] 19
2.6 Effect of differential drag on relative motion. [11] 20
2.7 RTN Frame. [25] 21

3.1 LQR Feedback Controller block scheme. 27
3.2 MATLAB® logo. Credits: *Mathworks* 28
3.3 Flowchart of the algorithm. 29
3.4 GMAT® logo. Credits: *NASA* 30
3.5 Comparison between Infinite-Horizon and Finite-Horizon relative state evolutions. 32
3.6 Control Accelerations in the RTN Directions. 33
3.7 Total acceleration magnitude over time (in orbits). 34
3.8 ΔV over time (in orbits). 35

4.1 Applied reference concept. 37
4.2 Finite-Horizon Reference Governor model relative state evolution. 38
4.3 Finite-Horizon RG: Control Accelerations in the RTN Directions. 39
4.4 Finite-Horizon RG: Total acceleration magnitude over time (in orbits). 40
4.5 Finite-Horizon RG: ΔV over time (in orbits). 41
4.6 Case 1: Spacecraft 1 and 2 relative state evolutions. 45
4.7 Case 2: Spacecraft 1 and 2 relative state evolutions. 46
4.8 Case 3: Spacecraft 1 and 2 relative state evolutions. 47
4.9 Minimum separation between the applied references and the state vectors for the three cases. 49
4.10 Angle between $\Delta\delta\bar{e}_a$ and $\Delta\delta\bar{i}_a$ for the three cases. 51

5.1 Case 1: spacecraft state evolution. 55
5.2 Case 2: spacecraft state evolution. 56
5.3 Case 1-2: Minimum separation between the applied references and the state vectors. 57
5.4 Case 1-2: Angle between $\Delta\delta\bar{e}_a$ and $\Delta\delta\bar{i}_a$. 57
5.5 ΔV over time for cases 1-2. 58
5.6 Relative motion in the RN plane. 59

5.7 Relative motion in the RT plane. 60
5.8 TanDEM-X Helix configuration [3]. 61
5.9 TanDEM 1: spacecraft state evolution. 63
5.10 ΔV over time. 64
5.11 Relative motion in the RN plane. 65
5.12 Relative motion in the RT plane. 65
5.13 Helix projection in TN plane. 66
5.14 Helix projection in RT plane. 66
5.15 ΔV over time. 69
5.16 RT plane motion relative to the virtual chief. 70
5.17 RT plane motion relative to Sat 1. 70
5.18 4 Sats: Minimum separation over time. 71
5.19 4 Sats: Real separation over time. 72
5.20 ΔV over time. 74
5.21 Relative motion in the RN plane. 75
5.22 Relative motion in the RT plane. 76
5.23 Helix projection in TN plane. 76
5.24 Helix projection in RT plane. 77

6.1 Validation procedure scheme. 79
6.2 GMAT Scenario: spacecraft state evolution. 81
6.3 GMAT Scenario: spacecraft control accelerations. 82
6.4 GMAT Scenario: Minimum separation between the applied references and state vectors of the two satellites. 83
6.5 GMAT Scenario: Angle between $\Delta\delta\overline{e}$ and $\Delta\delta\overline{i}$. 83
6.6 Relative motion in the RN plane. 84
6.7 Relative motion in the RT plane. 84
6.8 ΔV over time. 85
6.9 GMAT Sim: spacecraft state evolution. 87

List of Tables

2.1 ΔV lower bound in RTN directions during control interval identified by a shift of mean anomaly $\Delta M = M_f - M_0$ [26] 22

3.1 Initial and final relative states. 31
3.2 Finite-Horizon: Desired and final relative states. 33
3.3 Comparison between the real ΔV and the lower bound. 34

4.1 Finite-Horizon RG: Desired and final relative states. 39
4.2 Comparison between the RG ΔV, the FH ΔV and the lower bound. 40
4.3 Collision Avoidance: Initial and final relative states of Spacecraft 1. 44
4.4 Collision Avoidance: Initial and final relative states of Spacecraft 2. 44
4.5 Sat 1: Comparison between the ΔVs of the three cases with the lower bound. . 51
4.6 Sat 2: Comparison between the ΔVs of the three cases with the lower bound. . 51

5.1 R Exploitation: Initial and final relative states of Spacecraft 1. 54
5.2 R Exploitation: Initial and final relative states of Spacecraft 2. 54
5.3 Sat 1: Comparison between the ΔVs of the two cases with the lower bound. . . 59
5.4 Sat 2: Comparison between the ΔVs of the two cases with the lower bound. . . 59
5.5 Percentual relative difference in ΔV between the two satellites in the two cases. 59
5.6 TanDEM-X 1: Initial and final relative states of Spacecraft 1. 62
5.7 TanDEM-X 1: Initial and final relative states of Spacecraft 2. 62
5.8 Sat 1: Comparison between the scenario ΔV with the lower bound. 64
5.9 Sat 2: Comparison between the scenario ΔV with the lower bound. 64
5.10 4 Sats: Initial and final relative states of Spacecraft 1. 67
5.11 4 Sats: Initial and final relative states of Spacecraft 2. 68
5.12 4 Sats: Initial and final relative states of Spacecraft 3. 68
5.13 4 Sats: Initial and final relative states of Spacecraft 4. 68
5.14 4 Sats: Comparison between the scenario ΔV with the lower bound. 69
5.15 4 Sats: Comparison between desired and real $\delta\lambda$. 71
5.16 TanDEM-X 2: Initial and final relative states of Spacecraft 1. 73
5.17 TanDEM-X 2: Initial and final relative states of Spacecraft 2. 73
5.18 TanDEM 2: Comparison between the scenario ΔV with the lower bound. 75

6.1 GMAT Scenario: Initial and final relative states of Spacecraft 1. 80
6.2 GMAT Scenario: Initial and final relative states of Spacecraft 2. 80
6.3 GMAT Scenario: Comparison between the scenario ΔV with the lower bound. . 85
6.4 GMAT Scenario: Propagator properties. 86
6.5 GMAT Scenario: Comparison between MATLAB and GMAT results for relative state variables of Spacecraft 1. 87
6.6 GMAT Scenario: Comparison between MATLAB and GMAT results for relative state variables of Spacecraft 2. 87

Bibliography

[1] United Nations Office for Outer Space Affairs. Online index of objects launched into outer space, 2019.

[2] Guo-Ping Liu and Shijie Zhang. A survey on formation control of small satellites. *Proceedings of the IEEE*, 106:1–18, 02 2018.

[3] Gerhard Krieger, I. Hajnsek, K.P. Papathanassiou, Marwan Younis, and Alberto Moreira. Interferometric synthetic aperture radar (sar) missions employing formation flying. *Proceedings of the IEEE*, 98:816 – 843, 06 2010.

[4] Saptarshi Bandyopadhyay, Rebecca Foust, Giri Subramanian, Soon-Jo Chung, and Fred Hadaegh. Review of formation flying and constellation missions using nanosatellites. *Journal of Spacecraft and Rockets*, 53:1–12, 03 2016.

[5] I. Nason, Prof Puig-suari, and R. Twiggs. Development of a family of picosatellite deployers based on the cubesat standard. volume 1, pages 1–457, 02 2002.

[6] Ryan Nugent, Riki Munakata, Alexander Chin, Roland Coelho, and Prof Puig-suari. Cubesat: The pico-satellite standard for research and education. 09 2008.

[7] Daniel Scharf, Fred Hadaegh, and Scott Ploen. A survey of spacecraft formation flying guidance and control. part ii: control. volume 2, pages 2976 – 2985 vol.4, 01 2004.

[8] W. H. Clohessy and R. S. Wiltshire. Terminal guidance system for satellite rendezvous. *Journal of the Aerospace Sciences*, 27(9):653–658, 1960.

[9] D. Brouwer. Solution of the problem of artificial satellite theory without drag. *The Astronomical Journal*, 64:378, 1959.

[10] Simone D'Amico. *Autonomous Formation Flying in Low Earth Orbit.* PhD thesis, 01 2010.

[11] Adam Koenig, Tommaso Guffanti, and Simone D'Amico. New state transition matrices for relative motion of spacecraft formations in perturbed orbits. 09 2016.

[12] Parvez S.A. Xing, G.Q. and Folta D. Design and implementation of synchronized autonomous orbit and attitude control for multiple spacecraft formation usinggps measurement feedback. *AAS/AAIA Spaceflight Mech. Mtg.*, pages 115–134, 2000.

[13] Yuri Ulybyshev. Long-term formation keeping of satellite constellation using linear-quadratic controller. *Journal of Guidance Control and Dynamics - J GUID CONTROL DYNAM*, 21:109–115, 01 1998.

[14] Girish Joshi and R. Padhi. Robust satellite formation flying through online trajectory optimization using lqr and neural networks. *IFAC Proceedings Volumes (IFAC-PapersOnline)*, 3:135–141, 12 2014.

[15] Marcio Queiroz, Vikram Kapila, and Qiguo Yan. Adaptive nonlinear control of multiple spacecraft formation flying. *Journal of Guidance Control and Dynamics - J GUID CONTROL DYNAM*, 23:385–390, 05 2000.

[16] Lukas Steindorf, Simone D'Amico, Julian Scharnagl, Florian Kempf, and Klaus Schilling. Constrained low-thrust satellite formation-flying using relative orbit elements. 01 2017.

[17] Daniel Bock, Alexander Kramer, Philip Bangert, Klaus Schilling, and Martin Tajmar. Nanofeep on uwe platform - formation flying of cubesats using miniaturized field emission electric propulsion thrusters. 07 2015.

[18] Klaus Schilling, Philip Bangert, Stephan Busch, Slavi Dombrovski, Andreas Freimann, Alexander Kleinschrodt, Alexander Kramer, Tiago Nogueira, Dmitry Ris, Julian Scharnagl, and Tristan Tzschichholz. Netsat: a four pico/nano-satellite mission for demonstration of autonomous formation flying. 10 2015.

[19] Samuel Schweighart and Raymond Sedwick. High-fidelity linearized j model for satellite formation flight. *Journal of Guidance Control and Dynamics - J GUID CONTROL DYNAM*, 25, 11 2002.

[20] D.R. Izzo. Formation flying linear modeling. *Dynamics and Control Systems and Structures in Space*, 2002.

[21] Koji Yamanaka and Finn Ankersen. New state transition matrix for relative motion on an arbitrary elliptical orbit. *Journal of Guidance Control and Dynamics - J GUID CONTROL DYNAM*, 25:60–66, 01 2002.

[22] Dong-Woo Gim and Kyle Alfriend. State transition matrix of relative motion for the perturbed noncircular reference orbit. *Journal of Guidance Control and Dynamics - J GUID CONTROL DYNAM*, 26:956–971, 11 2003.

[23] Gabriella Gaias, Jean-Sbastien Ardaens, and Oliver Montenbruck. Model of j2 perturbed satellite relative motion with time-varying differential drag. *Celestial Mechanics and Dynamical Astronomy*, 123, 08 2015.

[24] Rajasingh C. K. Eckstein, M. C. and P. Blumer. Collocation strategy and collision avoidance for the geostationary satellites at 19 degrees west. *International Symposium on Space Flight Dynamics*, 1989.

[25] Simone D'Amico and O. Montenbruck. Proximity operations of formation flying spacecraft using an eccentricity/inclination vector separation. *AIAA Journal of Guidance, Control and Dynamics*, 01 2005.

[26] Michelle Chernick and Simone D'Amico. New closed-form solutions for optimal impulsive control of spacecraft relative motion. 09 2016.

[27] Vrabie D. Syrmos V. L. Lewis, F. L. Optimal control. *John Wiley and Sons*, 1986.

[28] Hugo Leiva and Stefan Siegmund. A necessary algebraic condition for controllability and observability of linear time-varying systems. *Automatic Control, IEEE Transactions on*, 48:2229 – 2232, 01 2004.

[29] Marco Nicotra, Mihovil Bartulovic, Emanuele Garone, and Bruno Sinopoli. A distributed explicit reference governor for constrained control of multiple uavs. *IFAC-PapersOnLine*, 48:156–161, 12 2015.

[30] Craig Underwood, Sergio Pellegrino, Vaios Lappas, Christopher Bridges, and John Baker. Using cubesat/micro-satellite technology to demonstrate the autonomous assembly of a reconfigurable space telescope (aarest). *Acta Astronautica*, 114, 04 2015.